CENTRAL INTELLIGENCE AGENCY

50X1

S-E-C-R-E-T

COUNTRY Germany, Soviet Zone

REPORT

SUBJECT Technical Examination of East German Semi-Conductor, Diodes and Transistors

DATE DISTR. 7 April 1959

NO. PAGES 43

50X1

REFERENCES

DATE OF INFO.

PLACE & DATE ACQ.

50X1-HUM

THIS IS UNEVALUATED INFORMATION

1. These semi-conductors are believed to have been produced for the East German "Office of Technology" and for the East German NVA. 1/ 50X1-HUM

b. MCN 15914 - Two high frequency, high-voltage (150 V), miniature diodes produced as for MCN 15913.

c. MCN 15915 - Two high-frequency, high-voltage (110 V), miniature diodes produced as for MCN 15913.

d. MCN 15916 - Two high-frequency, high-voltage (160 V), miniature diodes produced as for MCN 15913.

e. MCN 15932 - A box received from the field containing 30 devices which could not be associated with any description. Upon inspection, it was determined that the box contained semi-conductors of six general types as follows: (For equivalent West-German type designations, see Table I)

(1) Sub-miniature diodes (numbered 1 and 2 for identification in this report).

(2) Small diodes (numbered 3 through 10 for identification in this report).

(3) Small, all-glass diodes (numbered 11 and 12 for identification in this report).

(4) Flat diodes (numbered 14 through 21 for identification in this report).

(5) Glass-envelope transistors (numbered T-1,T-4,T-5, and T-13 for identification in this report).

50X1-HUM

(6) Metal-envelope transistors (numbered T-2,T-3,T-9 and T-12 for identification in this report).

STATE | ARMY | NAVY | AIR | FBI | AEC | ED/OSI | ESV

S-E-C-R-E-T

f. MCN 15933 - One germanium, power transistor, reported to be a copy of the West German "Tekade, Type GFT 2006". The producers are reported to claim that this is a very high-power transistor for D.C. voltage and conversion applications, that it is used to replace mechanical choppers, that it meets all requirements for [illegible] ship-borne applications, and that it will sustain a 50 percent overload at 50° C without damage or impairment.

g. MCN 15934 - Two germanium, power transistors of recent (March 1958) development to which it is reported the East Germans had not yet assigned type designations. It is further reported that tests at VEB RFT Werk fur Fernmeldwesen, Berlin-Oberschoenweide show very good ratings.

50X1-HUM

2. [redacted] items [redacted] comprising eight germanium, point-contact, glass-envelope, double-end, miniature diodes are treated together here because of their structural and electrical similarity. For identification, the samples will be referred to as follows: [redacted] MCN 15914 (diodes C and D), MCN 15915 (diodes E and F) and MCN 15916 (diodes G and H):

50X1-HUM

50X1-HUM

50X1-HUM

50X1-HUM

[redacted]

c. Forward and reverse voltage-current characteristics were photographed on the curve tracer. No drift at turn-on was visible in the forward curves at the sensitivities shown. Diode C shows somewhat more than usual thermal effect in the forward direction as evidenced by the fact that the sweeps to 10 ma and 30 ma peak forward current do not overlap. This diode also shows a greater thermal effect in its reverse characteristic than the remainder of the group, or for that matter than the miniature Diodes 1 and 2 of MCN 15932 as shown by the hysteresis effect in the reverse characteristic curve. No drift was observed in the reverse characteristic curves for any of the eight diodes. (See Table II)

50X1

(1) The diodes show good forward characteristics. The statement that the pellets are germanium is based on the start of significant conduction at about 0.3 v forward voltage as shown in these curves. (No analyses of the pellets have been made.) At one volt, forward current characteristics in general are like the miniature diode No. 1 of MCN 15932 and better than No. 2. They are as good as, or better than, the larger point contact diodes of MCN 15932, except for the best of those which is No. 6.

(2) In the reverse direction, the characteristics are also very good. Since these diodes can be expected to have high thermal resistances of about 1.0°C/mw, the curves were not carried out to a peak inverse voltage as defined in MIL-specifications for fear of thermal damage during these preliminary measurements. Instead a peak permissible power of about 58 mw was chosen as a limit, based on a maximum safe junction temperature of 85°C.

50X1-HUM

(b) MCN 15914 - (C and D) are reported to have maximum voltages of 130 v. At the power limit, Diode C reached 126 v while Diode D reached 134 v. The peak inverse voltage of Diode C would exceed 130 v, but operation should probably be well below this since Diode C is beginning to show hysteresis effects while swept to 126 volts; dc operation would be more demanding.

(c) MCN 15915 - (E and F) are reported to have maximum voltages of 110 v. This is easily met by both diodes. At 110 v, reverse current is only 100μA or less. At the power limit, both diodes reached 140 v.

(d) MCN 15916 - (G and H) are reported to have maximum voltages of 160 v. At the power limit, Diode G reached 140 v, while Diode H reached 136 v. Neither shows evidence of maintaining a peak inverse voltage of 160 v dc. A momentary check of Diode G showed that a reverse current considerably in excess of 1.0 ma would be required to reach 160 v, with a consequent dissipation of the order of 200 mw. Diode B of MCN 15913 actually comes closest to being a 160 v diode.

d. These diodes have better reverse characteristics on the average than the miniature diodes Nos. 1 and 2 of MCN 15932, but the maximum voltages at the power limit for all of the 10 miniature diodes falls in the range from about 120 v to 140 v, except for Diode B at 150 v. Some of the other diodes of MCN 15932 such as Nos. 3,4, and 9 are competitive with these.

50X1-HUM

50X1

e. The capacitance of Diode A was measured at a small-signal frequency of one megacycle at two values of reverse voltage bias. At 0.5 v, the capacitance was 0.40 μμf, and at 25.0 v, it was 0.30 μμf. This variation is within the measurement tolerance of 0.1 μμf. This independence of voltage on the part of the capacitance is typical of point contact units where the capacitance is due primarily to the leads and encapsulation rather than to the junction. The remaining diodes were measured only at 0.5 v dc reverse bias and ambient temperature 27.8°C with the following results:

Item	Diode	Capacitance
[redacted]		
MCN 15914	C	0.50
	D	0.45
MCN 15915	E	0.45
	F	0.45
MCN 15916	G	0.65
	H	0.50

50X1-HUM

f. These [redacted] diodes may be compared with the JAN-1N127A (MIL-E-1/157C), which is of comparable size and peak inverse voltage rating. This diode is rated at 100 v maximum reverse voltage, with a peak inverse voltage of 125 v. All of these diodes will meet the P.I.V. rating; some with a few tens of volts to spare. The forward current of these diodes at 1.0 v falls within the specified range of 3.0 to 25.0 ma, the measured range being 7.0 to 12.5 ma. The reverse current specification of this JAN type calls for a maximum of 300 μA at a reverse voltage of 50 v. All eight of these diodes are far superior to this, even though they were measured at up to 2.8°C above the 25°C test temperature of the specifications. (MIL specifications permit a test temperature of 25 ± 3°C) The poorest diode shows 35 μA reverse current at 50 v. Similarly, the specified maximum reverse current at 10 v is 25.0 μA. The poorest diode shows 5.5 μA, well within the specification.

50X1-HUM

g. As a check on the high frequency capabilities of these devices, the reverse recovery time was measured. In the discussion of MCN 15932, it is explained that recovery measurements were made under two sets of conditions:

(1) At a forward current of 20 ma and a reverse voltage of 25 v with a loop resistance of 750 ohms and,

(2) At a forward current of 30 ma and a reverse voltage of 35 v with a loop resistance of 2500 ohms.

(a) In case (2) the total reverse current was measured as a function of time while in case (1) the current in excess of steady state was measured. Case (2) allows direct comparison with the specifications of a switching diode of MCN 15932 and is similar to commonly used Western conditions. Case (1) avoids the difference in results which occur due to differing steady-state, reverse-leakage current, and separates out the transition current. It also permits comparison with results obtained earlier with a number of USA point-contact diodes.

h. The results of the recovery measurements for these eight diodes are shown in Tables III and IV. Considering first the conditions of case (1), these diodes appear to fall in that category of the miniature diodes of MCN 15932, together with the other units of

50X1

h. (continued)
that item, which comprise the slower group. This group is comparable to the poor 10% of 182 USA point-contact diodes tested and reported in 1954. On the other hand, because of the very good reverse voltage-current characteristics, the recovery characteristics measured under the conditions of case (2) appear to be a little better. At 3.5 usec, all of these eight diodes meet the requirement of the VALVO OA87 specifications This is not true of the slower group of MCN 15932. At 0.5 usec, one-half of these diodes exceed the maximum current specified by as much as 36%. The average time for the diodes to recover to 0 5 ma reverse current is 0.76 usec. This is essentially the same as the 0.79 usec required for the slower diodes (Nos. 1 through 6 and 8). A check on two sample diodes under the bias conditions and loop resistance, called for in the specifications of the only JAN computer germanium diode, the JAN-1N276, indicates that all of these diodes would probably meet the JAN specifications for recovery.

3. The semi-conductors identified as MCN 15932 are discussed in succeeding sub-paragraphs. The individual devices and their West-German equivalents are listed in Table I.

a. Subminiature diodes 1 and 2:

(1) Diode No. 1 was compared with the VALVO OA95, specifications dated 1.2.56. There it is listed as a general-purpose, all-glass germanium diode with a peak reverse voltage of 115v. Dimensionally, No. 1 meets the OA95 specifications; it is approximately 6mm long by 2.5mm O.D. and is shaped like the OA95. No. 1 is a double ended diode of all glass construction, hermetically sealed by a Dumet-to-soft-glass type of seal at each end. At the cathode end, a tinned copper wire is butt welded to the rod supporting the semi-conductor chip. The glass-metal seals on No. 1 have been somewhat overheated; most of the copper-cladding is no longer visible. The curves are generally typical of point-contact types, the reverse break being sharper than usual. Data from these curves are tabulated together with VALVO characteristics (only nominal values, without limits, are specified for this type.) Measured values are close to those specified except at the higher reverse voltage and forward current points. Here the diode is poorer than the given values. Note, however, that where limits are given in the case of other VALVO types (see Table VI) the ratios of maximum to nominal to minimum values would suggest limits for the OA95 readily covering the observed values for No. 1 No drift of the characteristic curves was observed

(a) Assuming a thermal resistance of 1°C/mw and a maximum safe junction temperature of 85°C (10°C above the specified value for the OA95), a maximum safe dissipation at 25°C is 58 mw. The reverse curve for No. 1 reaches this dissipation at 122v, before the 10K ohm slope point. Breakdown is above this value

(b) Over the range of voltage from 0.5v to 25.0v, the capacitance was constant within the measurement tolerance at an average value of 0.42 mf. This characteristic, too, is typical of a point-contact type where the capacitance is due primarily to encapsulation and leads and so is voltage independent. For this reason, no plot is attached.

(c) No specification for reverse recovery time is given for the 0A95. However, it was measured for Diode No. 1, for comparison with the others and the data are discussed under Small Metal-Ceramic Diodes, for some of which such measurements were required.

(d) This diode may be compared with the JAN-1N127A (MIL-E-1/157C). In so far as the measurements made are concerned, and in consideration of dimensions, this diode will meet this specification. However, certain ratings for the 1N127A exceed those of the 0A95 (e.g. Max. E_b, Max. T). These cannot be checked on a single sample under room temperature conditions. The JAN-1N70 (MIL-E-1/154C) and JAN-1N38B (MIL-E-1/492B) specifications can be met by measurements made and those diodes are rated at Max. T. = 70°C which the 0A95 is reported to meet. The 0A95 ratings do not quite meet the dc voltage rating of these types (90 v vs 100 v) or the peak inverse voltage (115 v vs 120 or 125 v) but the measured sample does meet the peak inverse voltage requirement. These two JAN types are in a larger case size than Diode No. 1.

(2) Diode No. 2 was compared with the VALVO 0A91 specification sheet dated 1.2.56. The statements made for Diode No. 1, as to application and structure, both specified and observed, apply to this unit also. Again, VALVO gives only nominal data for this type. Both the forward and reverse characteristics of this diode are below the quality level of the specified nominal values, this is particularly true of the reverse current at high reverse voltage. The reverse curve is more typical of a point contact than No. 1, but it does not hold up so well or break as sharply as No. 1. Again, however, attention is called to the fact that where VALVO (or Phillips which is essentially the same organization) gives limits as well as nominal values, the maximum leakage current at high reverse voltage is several times the nominal value. Thus, the measured value of 200 ma at 100 v might well be within limits, even though the nominal value is only 75 ma. No drift of the characteristic curves was observed. As for Diode No. 1, a safe dissipation limit was reached before the reverse curve reached a slope as low as 10K ohms. The reverse voltage at the 58 mw point was 135 v; this exceeds the 115 v breakdown limit given for the 0A91. Over the range of reverse voltage from 0.5 to 25 v, capacitance remained constant at 0.45 $\mu\mu$f. Like Diode No. 1, this represents encapsulation and lead capacitance. The effect is typical of a point contact diode.

(a) No specification for reverse recovery time is given for the 0A91. However, it was measured for Diode No. 2 for comparison with the others and the data are discussed under Small Metal-Ceramic Diodes, for some of which such measurements were required.

(b) The comments made in regard to equivalent JAN types under Diode No. 1 apply to Diode No. 2 as well.

b. Small Metal-Ceramic Diodes (Nos. 3 through 10)

(1) None of these double-ended diodes have been opened to determine internal structure, but externally they show the use of a right-cylinder of a hard, dense, white ceramic (similar to an aluminum oxide in appearance) which is sealed at each end by a smoothly formed soft solder cap. This is a relatively expensive structure, generally replaced in the U.S.A. for non-microwave types by some other form such as glass for good quality units or plastic for lower quality units. The solder seal provides a chance for flux to be present inside the encapsulation, which may degrade reliability unless some other internal

(1)(continued)

seal is present which can only be determined by opening the unit. This is unlikely, however. One of these units, No. 8, showed a drift in reverse current of about 15 sec. duration. No. 7 had no drift, but did display a small (0.5μA) reverse current jitter in the 10v range. Another, No. 6, shows two reverse characteristics, either one of which it may follow arbitrarily when it is turned on.

(a) None of these diodes is equivalent in mechanical structure to the comparable VALVO types listed in the "General" discussion above. All of the types OA70, 73, 81, 85, and 87 are all glass diodes in contrast to the structure described for Nos. 3-10. The overall length varied from 13.3mm (No.6) to 15.2mm (No.10). Maximum diameter was 4.35mm. All exceed the maximum length specification of 12.7mm for the "equivalent types", but meet the specification for maximum diameter of 5mm. The units are reasonably uniform in shape, although the solder seal shape varies somewhat from unit to unit.

(b) For all of these units, a thermal resistance of about 0.7°C/mw was assumed, together with a maximum junction temperature of 85°C, to calculate a safe dissipation limit of 82 mw at 25°C. In all cases, this dissipation limit was reached before a reverse characteristic slope of 10K ohms was reached. Thus where "breakdown" voltage is quoted, it represents the value at this dissipation.

(c) Before treating the diodes individually, some general comments should be made. The first of these refer to the capacitance versus voltage measurements. These measurements were made at reverse dc bias voltages of 0.5v to 25v. In general, capacitance was low and largely independent of voltage, characteristic of point-contact types. Some diodes showed a distinct increase in capacitance at low voltages. Note that No.3 and No. 5 are reported to be the same type (OA70), but Nos. 3 and 4 have similar C vs V curves, showing the most pronounced increased in capacitance at low voltages. It will be seen later that this similarity applies to other characteristics also. Neither have slopes high enough to suggest purposely diffused or alloyed junctions. Results are shown in Table V together with the limits observed for the plotted data and specifications for capacitance where given in the equivalent type data sheets. VALVO does not state the bias voltage used for their capacitance measurement.

(d) In general, the forward characteristics of all of these diodes are representative of typical point-contact units not of bonded or plated point (very low impedance) types.

(e) Two diodes in this class (Nos. 8 and 9) were reported to correspond to the OA87 for which reverse recovery measurements are specified. All of the diodes of MCN 15932 were measured, however, as a check on their suitability at high frequencies (especially since high frequency rectification efficiency measurements could not be made). Measurements were made under two sets of conditions. For comparison with previous diodes tested reverse recovery was measured with a loop resistance of 750 ohms, a forward current 20 ma, and a reverse (continued on next page)

(e) (continued)
voltage of 25 v. The reverse current in excess of steady-state current is recorded during recovery as a function of time. This has the advantage of showing recovery speed unaffected by the steady-state reverse leakage current which varies from diode to diode. The second set of conditions called for a loop resistance of 2500 ohms, a forward current of 30 ma, and a reverse voltage of 35 v. Total reverse current is shown as a function of time. This was done to correspond to the specifications for recovery measurement of the 0A87 to which Nos. 8 and 9 are reportedly equivalent. Also, this corresponds closely to conditions of 256 - JAN and frequent USA practice. Its advantage is that the rectifier resistance as a function of time during recovery is obtained by simply dividing the constant reverse voltage by the observed current. Tables of results therefrom, are attached. Those for selenium diodes, which are limited to low frequency applications are not shown. Of the others Nos. 1 through 4,9,10,and 12 were within the maximum limits for the 0A87. These specifications are 0.30 ma maximum at 3.5 μsec. A very rough comparison may be made with the only JAN computer germanian diode (JAN-1N276). At the same loop resistance but at a much lower forward current (5 ma) and slightly higher reverse voltage (40 v), the JAN-1N276 is required to have less than 0.5 ma at 0.3 μsec. These bias conditions would cause a substantial reduction in current at 0.3 μsec. over that measured in this evaluation. However, the time required for the diodes in this group to reach 0.5 ma is shown in Table XI for the conditions of loop resistance equal to 2500 ohms. Using the JAN loop resistance and bias conditions, a check on the two slowest diodes of the group (No. 4 and No. 8) showed that all of the diodes in this group would meet the 1N276 recovery time requirement if correlation between the different test sets is assumed. A comparison of these twelve diodes can be made with 182 domestic point-contact germanium of various manufacture as tested and reported in 1954.

(f) The 750 ohm loop resistance and corresponding biases were closely matched in both cases. With the exception of Nos. 2 and 6 at 0.1 μsec, and No. 2 at 0.3 μsec., the group 1,2,3,4,5,6,8, would fall with the poor 10% of the 182 USA units in reverse recovery time. Nos. 7,9,10,11 and 12 would be in the top 50%.

(g) Looking now at the tabulated recovery times for 750 ohm loop resistance and ignoring momentarily the "equivalent types", these diodes seem to fall naturally into several groups. (See Table VIII)

(1) Nos. 1,2,3,4,5,6 and 8 have very similar recovery rates. Nos. 7,9 and 10 are much faster and are similar to each other. Nos. 11 and 12 are quite similar to each other, and comprise the fastest group. Nos. 1,2,11 and 12 will be excluded from this discussion since they have different encapsulations.

(2) On the basis of similarity of forward and reverse characteristics the first group splits into two. Nos. 3 and 4 are much alike and Nos. 5 and 6 form a pair of similar units. Nos. 7,9 and 10 are much alike. No.8 has a rather a typical reverse curve beyond a reverse voltage of 10 to 20 v which excludes it

(2) (continued)
from matching others. Of these groups, Nos. 3 and 4 have the best overall characteristics. Of the remaining groups, Nos. 5 and 6 have the better forward characteristics and Nos. 7,9, and 10 have the better high-voltage reverse characteristics. At low reverse voltages, Nos. 7 and 9 have somewhat poorer leakage characteristics.

(h) In Table VI, the data for these diodes are compared with the specifications for the equivalent types listed earlier. In many cases it will be evident that the measured values do not meet the electrical specifications. Other equivalences are suggested by the comments made above.

(1) Nos. 7,9 and 10 might well be compared with the OA87, since high reverse voltage characteristics are suitable and speed is high as required for the electronic switching applications suggested for this type. These units would not meet the computer application requirements of the MIL-E-1/1025 (JAN-1N276), which calls for a much higher forward conductance (Maximum of 1.0v at 40ma). These diodes give only 4 to 5 ma 1.0v. The difference lies in the gold-bonding employed in the 1N276. They would probably meet MIL specifications for some of the general purpose diodes such as the 1N38B (MIL-E-1/492B), 1N69A (MIL-E-1/142D) or the 1N70 (MIL-E-1/154C).

(2) Nos. 3 and 4 are comparable with the OA81 or 85 which are all-purpose diodes with a peak reverse voltage of 115v. Among the JAN types, these may be compared with the 1N38B (MIL-E-1/492B) and so far as they have been tested, they would appear to compare very favorably with these specifications. Again No. 5 and No. 6, though similar to each other, seem to correspond to difference VALVO types. No. 5 is comparable to the OA70 as suggested but No. 6 is better than the diodes covered by this type and corresponds more nearly to a very good OA70 or OA72, or possibly an OA73 when allowance is made for the different temperatures at which the measurements were made. These diodes may be compared on the basis of measurements made with the JAN 1N69A (MIL-E-1/142D) or the JAN-1N81A (MIL-E-1/155D).

c. Small All-Glass Diodes (Nos. 11 and 12)

(1) Diode No. 11 was compared with the VALVO OA72 specification sheets dated 29.11.54 and 9.12.54. There the OA72 is described as an all-glass germanium diode for use singly in a high-resistance rectifier or demodulator circuit, or in pairs in ratio-detector and discriminator circuits. Diode No. 11 is a point-contact diode in an all-glass envelope 12.2mm long and approximately 4.3mm O.D. This size is within the specified 12.7mm by 5mm O.D. maximum dimensions. No. 11 is a double-ended, hermetically-sealed unit, apparently closed at each end by a hard glass to metal seal. The seals show light metal, not the usual Kovar mouse-gray, but the lead

50X1

(1) (continued)
metal is magnetic and stiff as is Kovar. This is a high quality sealing technique. The diode shows a considerable amount of dirt on the interior of the glass encapsulation. Data from these curves are tabulated together with VALVO's nominal values for the OA72. (See Table IV) A small drift in reverse characteristics appears on first operation after several days shelf life, but the drift ends too rapidly to permit photographing it. Forward characteristics are close to the nominal specified values. Reverse current is considerably poorer than the specified values, even at low voltages. This unit shows the highest low-voltage saturation current of any diode in MCN 15932 higher by a factor greater than two than the next lower (No.7). These values would probably exceed limits estimated on the basis of other VALVO types. The OA72 is a low voltage unit, with a maximum peak voltage of 45v specified. The maximum estimated safe dissipation limit was reached at an estimated reverse voltage of 62 before the 10K ohm slope resistance was reached. Specifications call for a capacitance of "about" 1 μμf. The measured values, at 1 Mcps, were 0.55 μμf at 0.5v reverse bias and 0.45 μμf at 25v reverse bias. This diode and No. 12 are almost identical in reverse recovery characteristics and they are the best in this item.

(a) This diode can only be compared with the lowest voltage rating JAN type, the 1N81A (MIL-E-1/155D), and even then it will fail to meet the specification. Although the forward characteristics are satisfactory, and the peak inverse voltage specification can be met, No. 11 would fail by a large margin to meet the requirement of 0.010 ma reverse current at 10v.

(2) Diode No. 12 was compared with the VALVO OA79 specification sheets, dated 15.2.56 and 15.12.56. There the OA79 is described as an all-glass-enclosed germanium diode for the same applications as the OA72. It is evidently a higher quality version of the OA72, since the data sheets show very slightly poorer forward conduction characteristics but appreciably lower reverse leakage. Diode No. 12 is an all-glass-enclosed, point-contact diode appearing to be essentially identical to No. 11 in construction and size. There is somewhat more dirt visible within the encapsulation. From the tabulated data, it appears to have very slightly poorer forward conduction characteristics than No. 11, slightly better than the nominal values for the OA79. In its reverse characteristics, it is very much better than No. 11, and is within the specified values for the OA79. The maximum safe dissipation limit (82mw) was estimated to be reached at 95v. No specification is given for capacitance. It has the same values at the limits of reverse bias that were observed for No. 11. This is typical of a point-contact unit. This diode, with No. 11 had the best reverse recovery time of the diodes in this item.

(a) This diode should probably be compared with the JAN-1N69A (MIL-E-1/142D). However, its forward current fails very slightly to meet this specification, although its reverse characteristics are superior to those required. It could very readily meet the requirements of the JAN 1N81A (MIL-E-1/155D) in so far as measurements made are concerned.

d. Flat Diodes (Nos. 14 through 21)

(1) These units are all selenium rectifiers. Forward and reverse voltage-current characteristics suggested that this is so, and flame and X-ray spectrographic analysis confirmed it.

(a) What appears to be an identifying letter (like an H) is seen on No. 16. A similar letter is on No.14. The remainder have had the black paint scraped away in the region where the letter appears on Nos.14 and 16. The condition of No.15 in this respect is not known, since it was spectro-analyzed before this identification was observed. As a result of disassembly of No.17, and analysis of No.15, the internal structure of the unit appears to be what might be expected for a small selenium rectifier, although the external appearance is not typical of USA selenium units. 6/

(b) In the sample analyzed, the base plate was found to be a stainless steel comprising Fe (major), Ni, Co, Mn, and Cr. It was nickel plated. The rectifier material is, of course, selenium. With the selenium were found bismuth, nickel, tin, and cadmium with none of these as a major constituent. This is in agreement with materials expected in USA practice. One lead with its eyelet makes contact to the selenium by means of a composite solder-like material which is insulated from the selenium by a fiber pad except at the center of the structure where a small hole in the fiber permits the contact. This solder contains bismuth as a major constituent, tin in nearly the same proportion, and cadmium as a lesser, but still major constituent. An adhesive layer holds the fiber to the selenium layer. The other eyelet with its lead contacts the base plate. The entire structure is coated with a thick, soft, black layer of insulating paint. It was not identified, but was easily removed with amyl acetate. The selenium covers the entire base plate, which is typically 14 mm long, 5 mm wide, with half circle ends and with two 3 mm diameter holes for the eyelets. This gives an area of approximately 0.57 cm^2. 6/

6/ A typical USA selenium rectifier is constructed as follows: A base plate of aluminum or steel plated with nickel is roughened and bismuth or other material which makes a non-rectifying contact to selenium is added. Then one or more layers of selenium are deposited (possibly with chlorine or bromine in combination) and processed. A layer of selenium oxide, cadmium selenide, cadmium sulfide, shellac, or varnish is added. Finally a layer of inert metal or of cadmium, bismuth, or tin is laid down. To this layer one of the electrical contacts is made, while the other is made to the base plate.

50X1

(2) The East-German diodes were tested first at a 26 v peak reverse voltage and to approximately a 1.0 v peak forward voltage. Data from these curves are tabulated and calculations of forward current density at 1.0 v, on the basis of 0.57 cm^2 active area, are shown. (See Table XII Reverse-to-forward-resistance ratio at 20 v reverse, 1.0v forward is also shown. Note that the resistance values are based on the average value in the hysteresis loop at 20 v. These values may be compared with the typical Western values. They are very low. They could be expected to increase at higher ambient temperatures, higher duty cycle or higher forward peak voltages, but not by the two orders of magnitude required to reach typical values. 7/

(a) Diodes No. 20 and 21 have relatively poor reverse characteristics, the remainder fall in a reasonably close grouping of about 7 to 20 megohm reverse resistance at 20 v. The forward characteristics, exclusive of No. 21 seem to fall in two distinct groups.

(3) Capacitance as a function of reverse bias at a one megacycle small signal test frequency was measured early in the analysis before it was established that the units were selenium. The values obtained were very low for selenium. As a check on these values, measurements at a frequency of one kilocycle were made on samples of these units and on a single plate of a typical USA rectifier stack (Federal 1004A, 17911CX). The active area of the Federal unit was estimated at 7.7 cm^2. Table X shows the results on a per square centimeter basis. Resistance values were such that the domestic unit could not be measured on the one megacycle bridge. Nor could the unknown units be measured on the one kilocycle bridge except at zero bias. Zero bias measurements could not be made for these on the one megacycle bridge. The tabulated values do, however, give an overlap that allows a conclusion to be drawn. All measurements were made in the order of decreasing bias.

(a) It is quite apparent that the flat diodes have capacitance per square centimeter which is significantly lower than common USA rectifier stacks. Evidently, high forward conductance has been traded for this characteristic.

(b) As a check on this possibility, a very rough test of the frequency characteristics of the flat diodes was made. There is evidence that a given forward to reverse current ratio, of say ten to one, is maintained to a frequency of perhaps an order of magnitude higher than is the case for the USA single-plate low-frequency unit, for the same total forward current.

7/ Published Western data on selenium rectifiers give various AC voltage ratings, ranging usually from about 26 v rms reverse voltage to 26 v peak reverse voltage. Some companies may give a higher figure. Beyond about 40 v damage will occur. Forward-current densities can be expected to be about 50 ma/cm^2 at 1.0 v, although at least one company (Sarkes Tarzian) quotes a lower figure as a safe rating and one reference shows 50 ma/cm^2 at about 0.6 v dc. A ratio of forward resistance measured at 1.0 v to reverse resistance measured at 20 v ranges from a common 100 to 1 to the order of 1000 to 1 for special applications such as magnetic amplifiers. These values are generally given for a 35°C ambient.

(4) All but No. 20 have high reverse-to-forward resistance ratios, comparing favorably with the requirements listed above as typical for magnetic amplifier applications. Note that these measurements were made in an air ambient of 28.6 to 28.9°C with a half-sine-wave sweep applied 120 times per second. At the higher temperature of 35°C usually assumed as an ambient temperature, the forward currents would be higher and reverse resistances lower, but the changes should not be very great. 8/

e. Glass Envelope Transistors (T-1, T-4, T-5, and T-13)

(1) These transistors were reported to be possibly equivalent to the Intermetall types OC 33,34,40 or 41. These types have been replaced by the OC 303, 304, 400, and 410 which the manufacturer claims to differ only in mechanical dimensions. None of these correspond mechanically to the transistors under test. The earlier models of the OC 33, 34 series were flat-sided structures while the later models are cylindrical with flat ends and triangular lead patterns. The OC-400-410 series have the same shape but an in-line lead structure. Maximum dimensions of the recent models of both series are 5.0 mm o.d. with a 5.6 mm seal diameter, and 8.0 mm in length. T-1 and T-13 are cylindrical with one rounded end and are typically 14.0 mm long, 4.6mm in o.d., with a seal diameter of 5.2mm. T-5 is 15.2mm long and 5.1mm in o.d. with negligible seal bulge. All have in-line lead patterns. Lead diameters are 0.4mm for T-1, T-5, and T-13, but 0.3mm for T-4.

(a) Nevertheless, since preliminary alpha-cutoff measurements for the four units suggested agreement with the equivalent types, they were measured for comparison with these types where possible. After the electrical measurements for this report were completed, the paint was removed from these units to observe the internal structures. A brief description is given before the electrical results are presented.

(b) Transistor T-4, in common with the other three, appears structurally to be an alloy type, with a large collector dot visible and a smaller emitter dot on the reverse side of the rectangular semiconductor block. This block is soldered to a metal tab which in turn is spot-welded to a wire lead. The lead is one of three Dumet-like wires sealed into a soft glass bead. The other two have spot-welded to them the leads (of undetermined material) which contact the emitter and collector dots. This structure is sealed into a soft glass tube, using as a stem a second bead sealed to the Dumet-like wires. A true hermetic seal results. The structure appears to have been torch-sealed at both ends and the internal atmosphere is probably close to atmospheric pressure. There is no silicone grease, dissicant or other protective device visible inside. The semiconductor has been etched to a smooth shiny surface, but it is not completely free of stains. There are no obvious signs of dirt or extraneous particles on the interior of the tube, aside from a glass chip.

8/ Note also that steady state values are discussed. Initial reverse currents were as much as three times as great as that when the units were first turned on, but they all stabilized in less than 30 seconds. Forming time is normally required for selenium rectifiers, 3 to 5 minutes being permitted in some cases, so that this is not excessive. With the exception of #15 the diodes were remeasured at a higher reverse voltage, corresponding to 26v rms or approximately 38v peak. The average reverse resistance and current at 20v is tabulated for comparison with the lower peak voltage case. Drift or forming times were much longer in these cases.

50X1

(c) Transistor T-13 uses the three Dumet-like leads sealed into a bead as a starting point, but thereafter the structure differs from T-4. The tube is molded soft glass, and the mode line is directly visible at the rounded end, and indirectly visible down the side facing the viewer through the optical distortion of the internal center lead. A base molded from powdered glass is used to seal hermetically to the lead wires. It has a flat bottom with a step and a pedestal on top. The step receives the bottle and its presence is visible as a transverse line near the flat base of the tube. The inner pedestal is also visible; it produces the raised central portion from which the three internal leads rise. Sealing is probably not done with a torch in order to avoid distortion of the stem. On completion of the seal, the outside of the glass base region is ground to produce a nearly uniform outer diameter of the entire bottle below the hemispherical top. The reason for this apparently excessive effort toward a smooth outer wall was not evident until the "metal envelope transistors" described in the next section were investigated structrually after preliminary electrical measurements. It will be described in that section.

(d) Transistor T-13, and also T-1 which is similar use a small circular semi-conductor disk as the base of an alloy type unit. Two smaller diameter wires, which appear to be gold, are spot-welded to the larger Dumet-like leads at one end, and at the other they contact the emitter and collector dots at right angles to the plane of the disk. A third small diameter wire (apparently not gold) is bent to form a loop in one end. The loop has a diameter of about 2/3 the diameter of the disk. The loop is soldered on one side of the disk and the lead extends to the remaining Dumet-like support wire where it is spot-welded. The entire upper half of the envelope is filled with a material which is probably silicone grease. This may both stabilize surface conditions and improve heat dissipation Excessive oxidation of the internal lead wires has produced black particles which are free inside the encapsulation. None seem to have penetrated appreciably into the silicone. The smaller disk and dot sizes (to minimize capacitance values) and the wire loop base connection (to reduce base spreading resistance) may be expected to contribute to the higher frequency capabilities observed for T-1 and T-13. It appears probable that the disk and, therefore, the base region is thinner in T-1 and T-13 than the other two units. This would also raise frequency response by reducing base transit time.

(e) T-5 uses a molded glass stem similar in principle to that of T-13 though with a much higher pedestal A torched bulb and seal similar to T-4 is used, again giving a hermetic seal. No bead structure is necessary. A formed, perforated, metal frame is spot-welded to the center lead and a semi-conductor die is soldered to it. The die has an orange peel surface. A large collector dot is alloyed to the uncovered side of the die, while a smaller emitter dot is alloyed on the opposite side. The remaining two lead wires make soldered contact to these dots; access to the emitter is through the perforation in the frame. It seems surprising that the lead wire is found suitable for soldering directly to the dots, for example mechanical strains might result. This structure appears to be clean inside. From the standpoint of ruggedness and reduced thermal resistance, this unit is probably superior to T-4. Base spreading resistance may also be better.

(2) Alpha-cutoff measurements showed that the glass transistors were divisible into a lower frequency group (T-4 and T-5) and a higher frequency group (T-1 and T-13) which could be compared with the OC 302 to 304 series and the OC 390 to 410 series respectively. The lower frequency pair is considered first. 11/ 50X1

(a) Under the bias conditions V_{CB} = -5.0 v at I_E = 1.0 ma, alpha-cutoff is given in the following table. Measurements were made with the Transalyzer, based on low frequency values of alpha observed on the Baird GP-4.

Unit	Alpha Cutoff Frequency (megacycles)
T-4	1.1
T-5	1.4
OC304	.90
OC303	.75
OC302	.60

(b) The measured cutoff values lie between the most accurate ranges of the Baird and Transalyzer instruments, but the units clearly fall in the range of the OC 304 rather than the OC 302 or 303.

(c) Small-signal h-parameters in the common emitter configuration at a bias of V_{CE} = -5v, I_E = 1.0 ma, measured at 1000 cps ($T_{AMB} \sim 27°C$), are given in the following table, using April 1957 Intermetall data for comparison. No drift was observed in these measurements.

Unit	h_{21e}	h_{22e} (μmho)	h_{11e} (K ohms)	h_{12e}
T-4	124	38.7	4.55	9.8×10^{-4}
T-5	148	43.5	4.65	10.8×10^{-4}
OC304	32	45	1.80	11.0×10^{-4}
OC303	16-32 12/	25	1.00	6. $\times 10^{-4}$
OC320	9-16	15	0.60	3.8×10^{-4}

12/ 32 to 120 in March 1958 specification.

(d) Again, the two units compare well with the OC 304, although the input impedance is rather high. T-4 and T-5 are very high B(or h_{21e}) units.

11/ Electrical analysis of these transistors began before knowledge of probable equivalent types was received. After establishment of polarity type, which was found to be PNP, the first step was to sweep a family of curves through the region in which h-parameters were to be measured. This covered the bias conditions common in the USA (V_{CB}=5v, I_E=1 ma), and those required for previous measurements made here on Soviet transistors V_{CB}=10v, I_E=1ma). Since no excessive drift, hysteresis nor alpha crowding were observed, nor was breakdown seen, measurements of h-parameters were made under these bias conditions. Subsequently, they were also made under conditions of V_C=5v and 10v with I_B as required for I_C equivalent to that in common base. This is about one milliampere. All units stabilized in five minutes or less but one. T-13 was still very slowly drifting during common emitter voltage feedback (h_{21e}) measurements at both 5v and 10v bias conditions. Later it was learned that some of these units probably are equivalent electrically to the Intermetall OC 390,400,410 series which have voltage ratings of V_{CB} = 10v, V_{CE} - 5v (March 1958) or V_{CE} =3v (OC410, April 1957). A repeat of common base h-parameter measurements at 5v was made to see if damage had been done by the 10v common emitter bias but there had been no appreciable change caused by the high common bias measurement. This repeat was made for T-1 and T-13 which are the high frequency units probably corresponding to the OC390 to 410 series. These comments are included for completeness to cover conditions of treatment accorded these units and their reaction.

(e) Measurements of I_{CBO} show results well within the specifications for the OC 302 to 304 types. The specified maximum at T=25°C is 15 uA at V_{CB}= -5v. Steady state measured values at this voltage and at TAMB about 26± .7°C are 5.8 and 4.8 μA for T-4 and T-5 respectively. Measurements at three voltages are shown below. The values are indicative of clean surfaces, especially in the case of T-5. Even T-4 shows a surface leakage of the order of 15 to 30 megohms. 50X1

Unit	Steady State I_{CBO} at V_{CB} Of:		
	-2v	-5v	-10v
T-4	5.6μA	5.8μA	5.9μA
T-5	4.7 (5)	4.8	4.8

(f) Drift characteristics were measured with I_{CBO} vs time at constant V_{CB} values of -5v and -15v. The high sensitive of 1.0μA per inch should be considered in interpreting these plots, since a 0.1°C temperature change causes approximately a 1% change in I_{CBO}. The downward drift of T-4 is small and in a safe direction, but is evidence of a surface which not quite as clean or stable as T-5.

(g) Curves were run for common-base output. Here the locus of end points of sweeps represents a load line maintaining operation within power limits based on the published thermal resistance (2.25°C/mw), and maximum junction temperature (75°C), with a supply voltage equal to the published rating for V_{CB} (-15v). These are based on the OC302 to 304 series. This corresponds to roughly optimum conditions for maximum power output, giving a voltage swing of one-half of the rated collector voltage. T-4 oscillated under these conditions. T-5 operated normally.

(h) Additional curves were run to show the input characteristics for operation along the load line just described. Again the oscillation of T-4, unless drive is reduced, is apparent.

(i) Additional curves were made of output and input characteristics for similar load-line conditions but in the common emitter configuration. Again T-4 cannot operate at rated conditions. In this case it drifts toward runaway conditions. The curves show large signal current gain for operation along this load line. Current gain is non-linear for these conditions.

(j) Curves showing collector-voltage saturation characteristics were run. No specifications for saturation voltage are given for these devices.

(k) Upon comparison with the emitter-output curves for a typical OC304 the high-current gain characteristics of T-4 and T-5 are immediately evident. Relative non-linearity or current gain at constant collector voltage (B crowding) is also evident.

(l) The tenth and eleventh sets of c... show V_{CBO} vs I_{CBO} and V_{EBO} vs I_{EBC} for a determination of collector breakdown voltages. Breakdown voltages, it will be recalled, are determined for this report by the lowest voltage at which (1) the slope of the curve reaches a value of 10 k ohms or (2) the maximum permissible dissipation is reached. The slope limit applied for common base breakdown for all transistors of MCN 15932 which were tested. It also applied for common emitter breakdown except for T-5 which reached the power limit first. The curves are all run out to a dissipation of about 100 mw. The breakdown voltages are as follows:

50X1

Unit	BV_{CBO}	B_{VCEO}
T-4	-144v	-15v 13/
T-5	-172v	-24.0v

Ratings for the OC 302-304 series are V_{CB} max = -15v, V_{CE} max = -15v.

(m) The twelfth set of curve traces shows the output characteristics of T-5 in the common emitter configuration. These duplicate the conditions shown before except that these were taken after breakdown measurements. This could not be done for T-4 because the small lead to the emitter broke off during repeated handling in these measurements.

(n) In the final graphs for these units is shown output capacitance versus collector-to-base reverse bias. These curves show the operating output capacitence, and in addition provide a check on junction type and quality. Throughout the bias range used, the slope remained constant and close to measured value for typical Western alloy junction transistors, in agreement with the visual evidence that the units are alloy-junction types.

(o) For general information and for comparison with other units Table XIII showing common-base characteristics of all of the MCN 15932 transistors is included in this report, although there are no values given for these characteristics for the OC 304 in the data sheets attached. In addition, a B-cutoff frequency of about 9.6 kcps was measured for T-5. The broken emitter lead precluded a similar measurement for T-4 .

f. Metal Envelope Transistors (T-2, T-3, and T-9 through T-12)

(1) These transistors were reported to be possibly equivalent to the Intermetall types Oc 33, 34, 40, or 41. Preliminary alpha-cutoff measurements put them in the general OC 33, 34, or 303, 304 category. Externally, however, they differ considerably from the encapsulation shown by Intermetall for these equivalents. Removal of the black paint disclosed a metal envelope apparently with a glass plug in the base through which the leads passed. A red dot found under the black paint and on the metal case denoted the collector lead. The leads were placed in an in-line pattern. Dimensions of the case are typically 15.2 to 15.5mm in length and 5.6 to 5.9mm o.d. near the closed metal end, flaring to 5.9 to 6.0mm o.d. at the lead end. Lead wires were about 0.4mm o.d. Except for the lead pattern, the metal closure and physical dimensions agree perfectly with the description of the Intermetall OC 307 and 308.

13/ Excessive drift set in at V_{CEO} well below -15v for T-4

f.(1) continued

50X1

Because of the structural similarities to the CC [illegible] series, the units were tested for comparison with these as well as the OC 302 to 304 series.

(2) After the analysis, and because T-2 suffered an overvoltage which impared its characteristics, T-2 was opened to determine its internal structure. This turned out to be unique. Evidently, a molded glass stem, similar to those described for T-13 and T-5, together with a molded glass bottle, such as the one used for T-13, form the basic hermetically-sealed encapsulation. In this there is spot-welded to the central lead a perforated nickel plate, different in shape from those previously described. A germanium die is soldered to the plate. The die bears well-formed, alloyed dots; a large collector dot on the uncovered side of the plate and a smaller emitter dot accessible through the perforation in the plate. These are indium with gallium present. A basically-tin solder joins these dots to their respective leads which are of a high-chrome nickel. These in turn are spot-welded to the stem leads. The analysis of the material mentioned here was made spectrochemically. Grease (probably silicone since it was not readily dissolved by common organic solvents) fills most of the glass enclosure.

(a) The unique features of the structure are the close dimensional tolerances on the glass case and the reason for them; the basic glass encapsulation is inserted in a metal enclosure and cemented in place. The metal is copper, plated presumably with nickel. Evidently this is done in an effort to achieve a lower thermal resistance and hence to increase the permissible power dissipation. The metal cover, in the case of the OC 307 and 308, is intended to be inserted in a metal heat sink which is presumably to be bolted to a chassis, further increasing the dissipation capabilities. This transistor structure seems like a stop-gap method of providing increased dissipation without the effort required for a better, all-metal encapsulation with lower thermal resistance.

(b) Why the units were painted black is not known. Certainly the paint would only reduce the poor thermal path which now includes grease, glass, cement, metal case and external sink before reaching the chassis. And it hid the collector color code dot. Perhaps the units are experimental for determination of low-power, small-signal operation rather than high power capabilities, but if so, the metal envelope would have a negligible value.

(c) Electrical analysis of these transistors began before knowledge of probable equivalent types was received. The same initial measurements of h-parameters at collector voltages of 5v and 10v as described under Section 3e were made for these units and the same comments apply in general. All of the units in the metal envelope group stabilized quickly except T-11. It required three minutes to stabilize at $V_{CB} = -10v$ for an h_{22b} measurement. During this time about a 10% change in h_{22b} occurred. No excessive drift or instability was observed in initial common emitter measurements which followed the common base measurements.

(d) Alpha cutoff measurements placed all of these units in the range near one megacycle, excluding them from similarity to the OC 390 to 410 series, and analysis proceeded based on comparison with the OC 302 to 304 series. With a basis of V_{CB} = -5.0v, I_E = 1.0ma the following values were measured with the Baird GP-4, based on the low frequency (1 Kc) alpha values shown. 14/ 50X1

Unit	Alpha At 1 Kc	Alpha Cutoff Frequency
T-2	0.974	0.73 Mc
T-3	0.988	1.02
T-9	0.988	1.02
T-10	0.960	0.53
T-11	0.991	0.78
T-12	0.989	0.63
OC304		0.90
OC303		0.75
OC302		0.60

(e) Small signal h-parameters in the common emitter configuration at bias values of V_{CE} = -5v, I_E = 1.0ma, measured at 1000 cps ($T_{AMB} \approx 27^{\circ}C$), are given in the following table. Intermetall data of April 1957 are given for comparison. 15/

Unit	h_{21e}	h_{22e} (umho)	h_{11e} (K ohms)	h_{12e}
T-2	44	18.2	1.46	4.3×10^{-4}
T-3	111	32.5	3.72	8.7×10^{-4}
T-9	108	29.3	3.75	8.2×10^{-4}
T-10	93	26.2	3.35	7.5×10^{-4}
T-11	185	43.5	6.50	13.9×10^{-4}
T-12	118	30.5	4.15	9.3×10^{-4}
OC304	32	45	1.80	11.0×10^{-4}
OC303	16-32	25	1.00	$6. \times 10^{-4}$
OC302	9-16	15	0.60	3.8×10^{-4}

(f) Measurement of I_{CBO} show results well within the specifications for the OC302 to 304 types. The specified maximum value at T = 25°C is 15uA for V_{CB} = - 5v. Steady state values at three voltages are shown below for an ambient temperature of 26 ± 0.7°C. These values are low and the small change with voltage indicates high surface leakage resistance; even for the poorest one (T-11) it is of the order of 7 megohms.

14/ This table initially places T-3 and T-9 in the OC304 class, T-2 and T-11 in the OC303 class, and T-10 and T-12 in the OC302 class.

15/ All of these are high-B units, h_{21e} in one case even exceeding the March 1958 upper limit for the OC304. All surpass the minimum values for this type. The poorest output impedance is shown by T-11, but even it is close to the typical value for OC304. T-11 also has the poorest value of h_{12e} and the highest input impedance, it will be seen later that it also has poor breakdown characteristics. The other units fall in the acceptable range of h_{12e}, but in general they show high values of h_{11e}, as did T-4 and T-5, the other low frequency alloy units. These high values of h_{11e} may be expected to cause errors in measurement h_{21e} (B) and h_{11e} with the Baird GP-4. About 1% of error is introduced per 1000 ohms of true h_{11e}, and the error is in the direction of too-low readings of h_{11e} and h_{21e}. Thus, the true values of h_{11e} and h_{21e} are probably a few percent higher than the table indicates.

Unit	Steady State I_{CBO} at V_{CB} of:		
	-2v	-5v	-10v
T-2	4.1uA	4.1uA	4.3uA
T-3	5.2	5.4	5.7
T-9	1.8	1.8	1.9
T-10	2.3	2.3	2.4
T-11	2.0	2.1	2.8
T-12	2.1	2.2	2.2

50X1

(g) Drift characteristics were measured at constant V_{CB} values of -5v and -15v. With the exception of T-11 which becomes relatively very poor at V_{CB} = -15v, the metal envelope units show very good stability. If it is assumed that all of these units have grease-stabilized surfaces as T-2 proved to have on opening it, the grease is doing an effective job. However, its sensitivity to the effects of atomic radiation should be noted. Later, these devices are compared with the OC307 and 308, drift at V_{CB} = -30v after shelf life and the above results are further supported.

(h) Common-base output characteristics where the locus of endpoints of sweeps represent a load line maintaining operation within power limits based on the published thermal resistance (2.25°C/mw) and maximum junction temperature (75°C), with a supply voltage equal to the published rating for V_{CB} (-15v) are good, with no alpha-crowding to contribute to non-linearity. In measurements of output and input characteristics for similar conditions, but in the common emitter configuration the end points of the output family define an approximately optimum power output condition. T-2 shows a relatively low current gain.

(i) Measurements at a typical small-signal bias condition (V_{CE} = -5v) show considerable non-linearity for large swings in I_B. 16/

(j) All of the metal-covered transistors broke down before the thermal dissipation limit (of roughly 100 mw) was reached. The measured values are shown in the following table. 19/

Unit	B_{VCBO}	B_{VCEB}
T-3	121 v	37.5 v
T-9	118	35.5
T-10	116	40.5 17/
T-11	97	9.0 18/
T-12	87	30.0 17/

16/ Transistor T-2 suffered a damaging momentary overvoltage of about 150v during the course of these measurements, before the input characteristics at constant V_{CE} were taken. Of course, input data is derivable from the voltage transfer curves as noted under T-1 and T-13. This data will correspond more closely to the published curves in principle.

17/ Measured at lowest current portion of hysteresis loop.

18/ Measured at middle of blur.

19/ Ratings for the OC302 to 304 series are V_{CB} max = -15v, V_{CE} max = -15v. T-11, which has shown relatively poor collector characteristics from the start, fails to meet the V_{CE} requirements.

(k) Output capacitance vs collector to base, reverse bias with emitter open circuited was measured. These measurements show normal or better capacitance values for a one-megacycle alloy unit of this power rating. The 50X1 slopes, ranging from 0.43 to 0.45, are typical of a good alloy unit as has been previously mentioned. No specification for capacitance is stated in the OC302 to 304 specifications.

(l) For general information and for comparison with other units evaluated a table of common base characteristics of these units is included in Table XII. There are no specifications for these values given for the equivalent types.

(m) For the analysis comparing these units with types OC307 and OC308, the paint was removed and the units were inserted in a heat sink made following the dimensions shown on the Intermetall sheet. The heat sink was bolted to a heavy copper plate. "Ambient temperature" in the case of the measurements for this analysis is considered to be the temperature of the heat sink. For these measurements, a thermocouple was soldered to the cylindrical part of the heat sink at a position about midway along the length of the transistor. Because of the relatively incomplete description of these units in the March 1958 table of characteristics for the OC307, 308, the April 1957 data is used for comparison purposes for all characteristics not appearing in the later data. Evidently the OC307 and OC308 are essentially the same device, with different applications in mind calling for control of different parameters. Both call for current, voltage, and dissipation characteristics considerably in excess of the OC302 to 304 series. For example, I_C max is five times as great, V_{CB} max is twice as great. The OC307 is intended for use as a dc amplifier at powers up to one watt in push-pull operation, or in a multivibrator or electronic switching circuit. This requires control of the current and voltage saturation regions primarily. On the other hand, the OC308 is intended for use in a class-B push-pull output stage of a low frequency amplifier. Operation between the saturation regions must, therefore, be controlled as well, and this is apparent in the specification sheets.

(1) To make this comparison, two additional sets of measurements were taken for the metal envelope transistors. These show (1) the output characteristics in the common emitter configuration under low voltage high current conditions and (2) the input characteristics in the common emitter configuration at constant V_{CE} = -0.7v. With these data and those taken earlier, most of the required data could be determined.

(2) Using DC betas calculated at I_C = 10ma and V_{CE} = -5.4v and at I_C = 80ma and V_{CE} = -0.7v, I_E was calculated and data obtained to compare the specified current gain with that observed. The values are shown in the tables following.

(a) Bias Conditions: V_{CE} = -5.4v, I_E = 10 ma

Unit	I_B
T-3	95 μA
T-9	74
T-10	70
T-11	45 19/
T-12	75
OC308	75 to 140

50X1

(b) Bias Conditions: V_{CE} = -0.7v, I_E = 80 ma

Unit	I_B
T-3	1.1 ma
T-9	1.0
T-10	1.3
T-11	0.8 20/
T-12	1.3
OC308	1.0 to 3.3

(3) Using the values of I_B shown in (b), the input resistance was found from the input characteristics at V_{CE} = -0.7v and is presented hereunder:

(a) Bias Conditions: V_{CE} = -0.7v, I_E = 80 ma

Unit	$-V_{BE}$
T-3	0.37
T-9	0.36
T-10	0.38
T-11	0.30
T-12	0.38
OC308	0.60 max.

(4) Saturation voltage is poorly specified on the OC 308 sheet. Since the conditions for the OC307 evidently apply to the same measurement, it may be assumed that the same specifications should apply to both. From the output curves at high current and low voltage were taken the data in the following table, which apply to this specification.

(a) Bias Conditions: I_C = 125 ma, I_B = 6.5 ma

Unit	$-V_{CE}$
T-3	0.165v
T-9	0.180
T-10	0.175
T-11	0.150
T-12	0.185
OC308 and OC307	0.35 max.

19/ T-11 falls far out of the limits and T-10 is too low but marginally. Low values here correspond to higher than normal current gains. The remaining values are within specifications, falling nearer the high gain limit.

20/ These values are with one exception within the specified range, and near the lower limit which represents highest gain. The exception is T-11 which has a gain exceeding the specified limit.

(5) Collector saturation current in the common base configuration (I_{CBO}) is specified at V_{CB} = -10v to be 10μA or less. The values of I_{CBO} under these conditions have been tabulated earlier, in the OC 302 to 304 analysis. The highest value (5.7 μA for T-3) is well below the specified maximum. 50X1

(6) Collector saturation current in the common emitter configuration, after one minute of stabilization, is shown in the table below. Measurement temperature is 25.6±0.2°C, requiring a reduction in the tabulated values of four to eight percent or less for comparison with 25°C data as specified.

(a) Bias Conditions: V_{CE} = -6.0v, I_B = 0. ma 21/

Unit	I_{CE}
T-3	375 μA
T-9	175
T-10	140
T-11	310
T-12	130
OC308 and OC307	300 max.

(7) A very rough estimate of beta cutoff can be made from measured values of beta(h_{21e}) and alpha cutoff. The bias conditions (V_{CB} = -5.0v, I_E = 1.0ma) do not correspond to those specified however.

Rough Estimate of Beta Cutoff $(\frac{FA}{B})$

Unit	Value
T-2	16.8 kc 22/
T-3	9.2
T-9	9.4
T-10	5.7
T-11	4.2 23/
T-12	5.3

21/ These values are high, because I_{CEO} is approximately equal to DC beta times I_{CBO}. Thus a high-gain unit, such as these all are, suffers by comparison with a low-gain unit, other things (e.g., junction quality) being equal. The gain of T-3 although high, is not greatly different from the other units, but its low voltage I_{CBO} is relatively high as shown in earlier table. Hence, it is out of the specified limit. T-11 is high and drifting very slowly up (about 10μA in one minute). The other units were stable within their 5μA tolerance of the reading.

22/ Comparison of the previously tabulated values of alpha cutoff and h_{21e} for these units shows immediately that high values of beta lead to the low beta cutoff frequencies shown here. Only T-2, the lowest beta unit, is in the specified region.

23/ All of the units have open circuit input, common base collector breakdown voltages (B V_{CBO}) considerably in excess of the rated value of 30v. All but T-11 have open circuit input, common emitter breakdown voltages (B V_{CEO}) in excess of the rated value of 18 v. B V_{CBO} and B V_{CEO} are tabulated in the OC302 to 304 analysis.

(8) Turning now to the OC307, it is found that the controlled values are I_B and V_{BE} measured at I_C = 125 ma and V_{CE} = -0.7v. Data from the common emitter output and input families for the metal covered transistors taken at these points are shown in the following table: 50X1

(a) Bias Conditions: I_C = 125 ma, V_{CE} = -0.7

Unit	I_B	$-V_{BE}$
T-3	2.0	0.44
T-9	1.8	0.47
T-10	2.7	0.45
T-11	1.6	0.40
T-12	2.7	0.47
OC307	5.8 max.	0.70 max.

(9) The "knee-voltage" or voltage saturation requirements for the OC307 have been discussed above in connection with 3f(2)(m)(7)(a) where the measured values are compared with the specifications. All of the transistors met the specifications, with measured values close to half the maximum permitted value.

(10) Common base collector saturation current at V_{CBO} = -30v has been measured as a function of time to determine collector quality at this voltage, which is twice the rated value of the OC302 to 304 series. T-3, T-9 and T-10 are very stable; T-12 shows some drift, but it is in a favorable direction. T-11, however, shows an initial high leakage and then after a momentary drop its current rises rapidly. As indicated in previous measurements, its low breakdown voltage and other characteristics mark it as far below the quality and capabilities of the rest.

(11) Values of I_{CBO} measured after one minute of stabilization are shown in the following table for comparison with the OC307 specifications. Values are read to the nearest half-microampere. Temperature was 24.2°C during measurement.

(a) Bias Conditions: V_{CB} = -30v, I_E = 0 ma

Unit	I_{CBO}
T-3	5.0 μA
T-9	3.0
T-10	7.0
T-11	14.0 24/
T-12	4.0
OC307 (25°C)	15.0 max.

24/ Compensation for the temperature difference between conditions of measurement and specification would increase the measured values by about 8% or possibly less. T-11 had drifted out of specifications at about one minute and was still rising steadily. The other units are well within the specified value.

(12) Common emitter collector current under reversed bias conditions was measured at 25.7 ± 0.1°C, for comparison with the OC307 specifications. Tabulated below are the data after one minute of stabilization. 50X1

(a) Bias Conditions: V_{CE} = -30v, V_{BE} = ± 0.1v 25/

Unit	I_C
T-3	5.4 uA
T-9	3.2
T-10	2.5
T-11	14.
T-12	3.6
OC307	15. max.

(13) The emitter junction quality is indicated by the measured values of I_{EBO}, the reverse biased emitter saturation current with collector open circuited. Measured values taken at a temperature of 25.3 to 25.8°C after one minute of stabilization are tabulated below.

(a) Bias Conditions: V_{EB} = -6.0v, I_C = 0 ma 26/

Unit	I_{EBO}
T-3	2.6 uA
T-9	1.4
T-10	1.5
T-11	1.1
T-12	1.1
OC307	4.5 max.

(14) A value of saturation resistance is specified for the OC307. Data from the common emitter output curves has been used to calculate this resistance for the five samples, and the values are shown in the following table.

(a) Bias Conditions: I_C = 125 ma, I_B = 6.5 ma

Unit	Saturation Resistance
T-3	1.3 ohms
T-9	1.4
T-10	1.4
T-11	1.2
T-12	1.5
OC307	2.8 max.

25/ T-3, T-9 and T-10 were stable. T-11 drifted up from an initial value below 6 μA to the value given. It went out of specifications at 70 sec. T-12 drifted downwards from an initial value of 4.7 μA. All but T-11 are therefore satisfactory and previous comments about their junction quality describe these measurements as well.

26/ All units but T-11 appeared to be stable within the measurement tolerance. T-11 drifted from 1.2 to 1.1 μA in one minute, a favorable direction of drift. Evidently the difficulty with T-11 lies in its collector junction. This is in agreement with its relatively low collector breakdown voltage.

(15) One other brief comparison may be made with an Intermetall type having the same overall appearance as the OC307 and OC308. It is the OC309, and the only data available for this report is that in the March 1958 sheet. Only two points of comparison will be made. The first is that common base breakdown voltage, B V_{CBO} has already been shown to be greater than the V_{CB} max. of 60 v specified for OC309. The second is a measurement of I_{CBO} taken in a temperature range of 25.7 to 26.0°C, under bias conditions specified for OC309 as shown in the following table. The recorded data were taken after one minute of stabilization. 50X1

(a) Bias Conditions: V_{CB} = -60.0v, I_E = 0 27/

Unit	I_{CBO}
T-3	6.6uA
T-9	3.7
T-10	21.7
T-11	18.5
T-12	19.5
OC309	30 max.

4. Testing of MCN 15933 and MCN 15934 has yielded the values set forth in Tables XIV, XV , and XVI. By gross inspection, measurement, and X-ray inspection these transistors appear identical.

a. MCN 15933 T-6 appears from electrical measurements to be an hermetically sealed, stud-mounted, germanium, PNP, alloy-junction, medium-power transistor with collector connected to the stud; it will meet the specifications for the West German "Telcade GFT 2006/30" or the USA "2N156" but will not meet the specifications for the "GFT 2006/60 or 90" or the USA type "2N158. 28/

(1) Higher leakage currents and lower saturation voltages were found than would be expected from silicone.

(2) A slope of the curve of capacitance vs V_{CB} or V_{EB} of approximately 0.45, close to the theoretical 0.5 for abrupt junctions, is observed for the major part of the curve at higher voltages.

27/ T-3 and T-9 stabilized in a few seconds; T-10 drifted downwards, the favorable direction, very slightly in one minute (0.3μA); T-11 as usual drifted upwards from an initial value of 7.5μA until at 3 minutes it reached 30μA and went out of specifications, still rising. T-12 drifted more than usual but still in a favorable direction and most of the substantial drift (from 70μA to about 30μA) was over in a few seconds. T-10 now shows a relatively high leakage for the group which differs from low voltage data. This could be anticipated from the breakdown characteristics which show a distinct bend in the V_{CBO} vs I_{CBO} curve for T-10 at about 50v. Again all but T-11 are within specifications.

28/ Note that the 2N158 at 8.5 watts and V_{CB} = -60 v is the lower-rating power transistor on the list of approved military types, the other one (2N174) being rated at 75 watts and V_{CB} = -80 v. Externally, the unit appears to be well constructed, and similar in design to the 2N174 though smaller in size; the overall diameter being about three-quarters of the 2N174. This suggests a lower power rating due to reduced dissipation area, but not so low as the GFT 2006/30, 60, 90 series actually has. This is apparently lower due to (1) lower maximum junction temperature (2) higher thermal resistance as well as (3) lower heat sink contact area. Thermal resistance should be measured. The specified maximum value of 5°C/W is high by comparison with high quality USA types.

(3) At low voltages (less than about one) a slope value approximating the theoretical one-third for diffused junction appears, showing a slight diffusion close to the alloy junction. 50X1

(4) The appearance of the device externally and its measured characteristics as shown in Table XIV, suggest compliance with the GFT 2006/30 design, and the electrical similarity to the 2N156. Polarities indicate PNP construction. Color coding of the emitter is blue, the base white, and the collector is electrically connected to the stud. The encapsulation is all metal and soft-solder sealed; the cap is probably steel and the base is copper. Except for the fact that resistance welding may be preferable to solder sealing, the unit appears to be well made.

(5) There is initial drift observed in the dc characteristics, mostly over in a few seconds but lasting over a minute for some. Oscilloscope traces are generally steady after such a stabilizing period. All drifts are in a favorable direction when measurments are within the limits of the assumed specifications.

(6) The unit is unusual in showing a higher emitter breakdown voltage (over 70 v) than collector breakdown voltage. A check was made to ensure that the emitter and base color code was properly interpreted. This gave a much lower α when collector and emitter were interchanged, indicating that the direction used throughout the tests, and the color code, are correct.

b. MCN 15934 (T-7 and T-8)

(1) T-7 came close to meeting the GFT 2006/30 specifications as measured on a curve tracer, but not as made by dc methods. This may be due to a damaged emitter since the greatest deviations from the specifications occur for the emitter-quality dependent measurements. Similarly except for a dc measurement of I_{CEO}, T-7 meets the specifications for the 2N156. It cannot meet the specifications for the 2N158, neither the collector nor emitter junctions being adequate. 29/

(2) T-8 was out of its class in being compared to the 2N174. It clearly was not designed to handle such high voltage, current, or power, nor even the percentage of these values that might be deduced from heat sink size. It stood remarkably well a current greatly in excess of its rated value. And even after damage which occurred during the high V_{CEO} measurements, it can qualify for the GFT 2006/60 type on all points except for an I_{CEO} at V_{CEO} = 16v which is 7% out of specifications. Prior to the damage it certainly could have so qualified, and very possibly as a GFT 2006/90. The unit does not seem to stand excess power without showing hysteresis effects.

(3) In so far as initial 25°C measurements are concerned, the GFT 2006 falls far short of the capabilities of the USA MIL-T-19500/13A type, even when allowance is made for heat sink size. The high voltage units are probably marginal in comparison with the 2N158.

29/ T-7 was received with the external emitter lead cut off almost completely.

c. Common measurements for MCN 15933 and MCN 15934 include the following:

(1) DC measurements were made of I_{CBO} and I_{CEO} at a low voltage to check saturation current; and of I_{CBO} at a typical low operation point at 25.6°C with no heat sink. The results follow: 50X1

Unit	V_{CBO}	I_{CBO}	V_{CEO}	I_{CEO}
MCN 15933 (T-6)	1.0v	16. μA	1.0v	0.15 m
	6.0	23.		
MCN 15934 (T-7)	1.0	7.0	1.0	0.60
	6.0	17.		
MCN 15934 (T-8)	1.0	32.	1.0	0.60
	6.0	48.		

(2) Voltage breakdown figures were measured next on the curve tracer with T-8 on a heat sink at 25°C to 26°C. With a resistor limiting peak instantaneous dissipation to 10 w, there was a distinct change in the V_{CEO} vs I_{CEO} curve. V_{CEO} dropped from 50v to 30v(approx.) for the same I_{CEO}. While a 2N174A should stand $V_{CBO} > 60$v, T-8 could not tolerate 50v. A recheck of leakage currents at low voltages show a small change as follows (T-25.6 to 25.8°C, air ambient no heat sink) 30/

Unit	V_{CBO}	I_{CBO}	V_{CEO}	I_{CEO}
T-8	1.0v	33μA	1.0v	0.60 MA
	6.0v	53μA		

30/ Since the 1.0 volt values are essentially unchanged, surface-condition changes probably caused the observed effect.

50X1

TABLE I

West German Semi-Conductor Devices roughly equivalent to those here designated as MCN 15932.

Diode Number	Equivalent West German Type	Structure
1	OA95	Ge diode
2	OA91	Ge diode
3	OA73	Ge Point-Contact Diode
4	OA70	Ge Point-Contact Diode
5	OA73	Ge Point-Contact Diode
6	OA85	Ge Point-Contact Diode
7	OA81	Ge Point-Contact Diode
8	OA87	Ge Point-Contact Diode
9	OA87	Ge Point-Contact Diode
10	None	----------
11	OA72	Ge Point-Contact Diode
12	OA79	Ge Point-Contact Diode
13 2/	OA31	Si Power Diode Rectifier
14	None	Si Wafer Diode
15	None	Si Wafer Diode
16	None	Si Wafer Diode
17	None	Selenium Diode (?)
18-21	--	

Equivalent types for the transistors were reported to be OC33, OC34, OC41, or OC410, manufactured by Intermetall, Dusseldorf.

2/ No diode No. 13 was received.

TABLE II

MCN 15913-16, Diodes A-H

Summary of Measured Forward and Reverse Characteristics

		Forward Characteristics			Reverse Characteristics		
Diode		Current (ma)	Measured Voltage (volts)	Measured Temp (°C)	Voltage (volts)	Measured Current (μA)	Measured Temp (°C)
MCN 15913	A	0.1	0.17	26.4	1.5	2.0	27.8
		10	0.97	26.4	10	3.0	27.8
		30	1.65	26.4	60	25.0	27.2
					132	4400	27.2
	B	0.1	0.16	26.4	1.5	4.0	27.8
		10	1.15	26.4	10	5.0	27.8
		30	2.10	26.4	60	45.0	27.2
					150	3850	27.2
MCN 15914	C	0.1	0.175	26.4	1.5	1.0	27.8
		10	1.23	26.4	10	5.0	27.8
		30	2.35	26.4	60	45.0	28.1
					126	4700	28.1
	D	0.1	0.175	26.4	1.5	1.0	27.8
		10	0.98	26.4	10	1.5	27.8
		30	1.83	26.4	60	15.0	28.1
					124	4300	28.1
MCN 15915	E	0.1	0.165	26.7	1.5	1.5	26.4-26.1
		10	1.00	26.7	10	2.0	26.4-26.1
		30	1.80	26.7	60	18.0	27.8
					139.5	4150	27.8
	F	0.1	0.172	26.7	1.5	1.5	26.4-26.1
		10	1.00	26.7	10	2.0	26.4-26.1
		30	2.00	26.7	60	18.0	27.8
					139.5	4150	27.8

(continued on next page)

TABLE II
(continued)

50X1

Diode		Current (ma)	Measured Voltage (volts)	Measured Temp (°C)	Voltage (volts)	Measured Current (μA)	Measured Temp (°C)
MCN 15916	G	0.1	0.165	26.6	1.5	3.0	27.6
		10	1.15	26.6	10	4.5	27.6
		30	2.28	26.6	60	30.0	25.9
					140	4150	25.9
	H	0.1	0.170	26.6	1.5	1.5	27.6
		10	0.93	26.6	10	3.0	27.6
		30	1.72	26.6	60	10.0	25.9
					136	4300	25.9

TABLE III

MCN 15913-16, Diodes A-H

Diode Reverse Recovery Time

Reverse current in excess of steady state vs time.

Conditions: Forward Current 20 ma. Reverse V - 25 v. Loop Resistance = 750 ohms.

	Excess Current At Peak	Excess Current At 0.1 μsec.	Excess Current At 0.3 μsec.	Excess Current At 0.5 μsec.	Excess Current At 1.0 μsec.
MCN 15913					
A	5.5 ma	0.8 ma	0.6 ma	0.5 ma	0.3 ma
B	5.3	0.9	0.5	0.4	0.3
MCN 15914					
C	4.5	0.8	0.4	0.3	0.2
D	4.9	1.0	0.5	0.4	0.3
MCN 15915					
E	4.6	0.8	0.3	0.2	0.1
F	4.7	1.1	0.7	0.5	0.3
MCN 15916					
G	4.7	0.9	0.4	0.3	0.2
H	5.4	1.3	0.7	0.5	0.3

TABLE IV

MCN 15913-16, Diodes A through H 50X1

Reverse Recovery Measurements: Reverse Current Above Zero vs Time

Conditions: Forward Current = 30 ma, Reverse volts = 35 v, Loop Resistance = 2500 ohms

Diode	Current At Peak	Current At 0.3 μsec.	Current At 0.5 μsec.	Current At 3.5 μsec.	Time for Current of 0.5 ma.
MCN 15913					
A	3.3 ma	1.4 ma	1.1 ma	0.1 ma	1.2 ma
B	2.45	1.0	0.75	0.05	0.9
MCN 15914					
C	1.9	0.6	0.35	0	0.4
D	2.55	1.1	0.8	0.05	0.9
MCN 15915					
E	2.1	0.5	0.3	0.05	0.3
F	2.9	1.3	0.95	0.05	1.0
MCN 15916					
G	1.85	0.6	0.4	0	0.4
H	3.0	1.3	0.95	0.1	1.0
OA87 Nominal			0.38	0.036	
Specs. Maximum			0.70	0.175	

TABLE V

Capacitance Vs Voltage 3/

Diode Number	Equivalent Type	Specified Max. C.	C Measured at V = 0.5V.	C Measured at V = 25 V.
3	OA73	1 μuf	1.00 μuf	0.60 μuf
4	OA70	1	1.10	0.65
5	OA73	1	0.70	0.60
6	OA85	1	0.70	0.50
7	OA81	1	0.55	0.50
8	OA87	No Spec.	0.70	0.65
9	OA87	No Spec.	0.60	0.55
10	None	--------	0.60	0.45

3/ Relative values of measured capacitance are estimated to be accurate to less than approximately - 0.1 μuf.

TABLE VI

MCN 15932, Diodes No. 1 through No. 12

Comparison of Measured Values With "Equivalent Type" Specifications

Diode And Equiv. Type	Forward Characteristics: Current (ma)	Measured Voltage (volts)	Measured Temp (°C)	Specified Voltage at 25°C Min(v)	Norm(v)	Max(v)	Reverse Characteristics: Voltage (volts)	Measured Current (uA)	Measured Temp (°C)	Specified Current at 25°C Min(uA)	Norm(uA)	Max(uA)
1	0.1	0.185	27.2		0.18		1.5	2.5	26.1		1.2	
0A95	10	1.00	27.2		1.05		10	4.0	26.1		2.5	
	30	1.63	27.2		1.85		75	34	26.1		35	
							100	130	26.1		80	
2	0.1	0.19	27.2-27.5		0.18		10	4.5	26.4		4	
0A91	10	1.36	27.2-27.5		1.2		75	95	26.4		40	
	30	2.26	27.2-27.5		2.1		100	200	26.4		75	
3	0.1	0.14	27.5	0.1	0.13	0.2	1.5	4.0	26.4	1	5	18
0A73	10	1.00	27.5	0.6	0.8	1.1	10	6.0	26.4	8	30	100
	30	1.80	27.5	1.5	1.7	2.3	20	15	26.4	25	120	400
							30	20.0	26.4	45	275	1200
4	0.1	0.145	27.2	0.10	0.15	0.25	1.5	4.0	26.4	1.0	5	30
0A70	10	1.00	27.2	0.55	1.05	2.0	10	6.0	26.4	5.5	30	180
	30	1.78	27.2	0.80	1.7	3.2	15	16.0	26.4	10.5	65	350
							22.5	17.0	26.4	23	145	800
5	0.1	0.177	27.8	0.1	0.13	0.2	1.5	1.5	26.6	1	5	18
0A73	10	1.00	27.8	0.6	0.8	1.1	10	8.0	26.6	8	30	100
	30	1.71	27.8	1.5	1.7	2.3	20	40	26.6	25	120	400
							30	80	26.6	45	275	1200
6	0.1	0.185	26.9	0.1	0.195	0.25	1.5	1.5	26.6	0.4	1.2	4.5
0A85	10	0.84	26.9	0.65	1.15	1.5	10	6.5	26.6	0.8	2.5	7
	30	1.3	26.9	1.0	2.05	2.6	75	*	26.6	5.7	35	110
							100	**	26.6	10	75	250

* Double-valued reverse curve. Highest voltage curve 720 uA
Lowest voltage curve 670 uA

** Double-valued reverse curve. Highest voltage curve 770 uA
Lowest voltage curve 720 uA

TABLE V.I
(Continued)

Diode And Equiv.Type	Forward Characteristics: Current (ma)	Measured Voltage (volts)	Measured Temp (°C)	Specified Voltage at 25°C: Min(v)	Norm(v)	Max(v)	Reverse Characteristics: Voltage (volts)	Measured Current (uA)	Measured Temp (°C)	Specified Current at 25°C: Min(uA)	Norm(uA)	Max(uA)
7+	0.1	0.185	26.6	0.10	0.20	0.25	1.5	6	26.9	0.3	1.5	7
0A81	10	1.67	26.6	0.65	1.4	1.9	10	15	26.9	0.5	4	11
	30	2.95	26.6	1.0	2.45	3.3	75	105	26.9	5.5	40	180
							100	205	26.9	10.0	75	275
8++	0.1	0.185	26.6		0.18		1.5	1.5	26.9		1.3	
0A87	5	0.95	26.6		0.78		10	3.0	26.9		2.5	
	10	1.35	26.6		1.12		60avg.	240	26.9		34	
	30	2.46	26.6		2.15		90avg.	390	26.9		130	
9	0.1	0.19	25.8		0.18		1.5	5.0	26.9		1.3	
0A87	5	1.14	25.8		0.78		10	9.5	26.9		2.5	
	10	1.65	25.8		1.12		60	45	26.9		34	
	30	3.05	25.8		2.15		90	95	26.9		130	
10	0.1	0.189	25.6				1.5	2.0	26.9			
None	5	1.00	25.6				10	4.0	26.9			
	10	1.40	25.6				60	40.	26.9			
	30	2.45	25.6				90	110	26.9			
11++	0.1	0.23	25.6		0.20		1.5	13	27.8		0.8	
0A72	10	1.37	25.6		1.4		10	55	27.8		4.5	
	30	2.20	25.6		2.5		30	220	27.8		50	
							45	490	27.8		130	
12	0.1	0.23	25.8	0.15	0.23	0.30	0.1	1.0	27.8	-	0.35	1.0
0A79	10	1.48	25.8	0.8	1.5	2.2	1.5	1.5	27.8	0.1	0.8	2.8
	30	2.43	25.8	1.4	2.8	4.0	10	8.0	27.8	0.4	4.5	18
							30	11.0	27.8	1.5	35	150
							45	25.0	27.8	4	90	350

+ Very slight reverse current jitter (0.5μA), but no drift
++ Drifts, (for #11 duration too short to photograph).

TABLE VII

MCN 15932, Diodes 1-12

Reverse Breakdown Voltage

Diode	Equivalent Type	Specified Peak Reverse Voltage At 25°C (v)	Measured Reverse Breakdown Voltage 4/ (v)	Meas. Temp. °C
1	0A95	115	122	26.1
2	91	115	135	26.4
3	73	30	151	26.4
4	70	22.5	166	26.4
5	73	30	95	26.6
6	85	115	5/	26.6
7	81	115	134	26.9
8	87	90	125	26.9
9	87	90	138	26.9
10	None		132	26.9
11	72	45	62	27.8
12	79	None	95	27.8

4/ All diodes except No. 12 reached an estimated maximum safe power dissipation before the slope impedance of the reverse curve became as low as 10,000 ohms. Breakdown is defined as the voltage at this dissipation: 58 mw for Nos. 1-2, 82 mw for Nos. 3-12. For the exception, breakdown voltage at which slope of reverse curve is 10K ohm and maximum dissipation is reached is essentially the same.

5/ Double valued reverse curve:
Highest voltage curve ------ 106v.
Lowest voltage curve-------- 110v.

TABLE VIII

MCN 15932, Diodes Nos. 1-12

Diode Reverse Recovery Time

Reverse current in excess of steady state vs time.

Conditions: Forward Current 20 ma. Reverse V=25 v. Loop Resistance=750ohms

Diode	Excess Current At Peak	Excess Current At 0.1 μsec.	Excess Current At 0.3 μsec.	Excess Current At 0.5 μsec.	Excess Current At 1.0 μsec.
1	4.2 ma	0.9 ma	0.5 ma	0.4 ma	0.3 ma
2	3.8	0.8	0.4	0.4	0.3
3	6.1	1.1	0.5	0.4	0.3
4	6.0	1.0	0.5	0.4	0.3
5	4.9	0.9	0.5	0.4	0.3
6	4.1	0.8	0.5	0.4	0.3
7	3.3	0.4	0.2	0.2	0.1
8	4.7	1.2	0.5	0.4	0.3
9	3.6	0.4	0.2	0.2	0.1
10	3.6	0.5	0.2	0.2	0.1
11	1.8	0.3	0.1	0.1	0.1
12	2.4	0.3	0.1	0.1	0.1

TABLE X

Unit	Capacitance per cm^2 at 1 KC ($\mu\mu f$)				
Bias:	0.0 v	1.2 v	1.5 v	2.0 v	2.3 v
USA #16	4550	2530	2320	2150	2080
#16	250				
#21	480				

TABLE XI

Diode	Time After Turn-On Drift Apparently Stopped
14	4 to 5 minutes
16	4 to 5
17	5.
18	4.5
19	4
20	5
21	6

TABLE XII

MCN 15932 "Flat Diodes" Selenium Rectifiers Nos. 14-21

Diode	Forward Current At 1.0v (ma)	10/ Forward Current Density at 1.0v (ma/cm^2)	Forward Resistance at 1.0v (K Ω)	Data for 26v Peak Sweep: Reverse Current at 20v (μA) 9/	Reverse Resistance at 20v (MEG Ω)	Ratio Reverse to Forward Resistance	Data for 37v Sweep: Reverse Current at 20v (uA) 9/	Reverse Resistance at 20v (MEG Ω)	Breakdown Voltage (10K slope Resistance) (volts)
14	0.27	.47	3.7	1.0	20.	5400	1.0	20	75
15	0.29	.51	3.4	3.0	6.7	2000			
16	0.27	.47	3.6	2.0	10.	2800	1.5	13	67
17	0.44	.77	2.3	2.5	8.	3500	2.0	10	61
18	0.43	.76	2.3	2.0	10.	4300	1.5	13	64
19	0.48	.84	2.1	1.0	20	10000	1.0	20	66
20	0.42	.74	2.4	18.0	1.1	460	15.0	1.3	71
21	0.68	1.19	1.5	7.5	2.7	1800	16.0	1.2	36

9/ Reverse current is average value of hystersis loop.

10/ Based on estimated area of conduction equal to 0.57 cm^2.

50X1

TABLE XIII

COMMON BASE h-PARAMETERS
MCN 15932 T-1 to 5, 9 to 13

Conditions of Measurement: V_{CB} = See Table, I_E = 1.0 ma, f = 1000 cps, T_{AMB} = 23.3 -25.6°C

Unit	$-V_{CB}$ (volts)	h_{11b} (ohms)	h_{12b}	h_{21b}	h_{22b} (umho)	$(h_{22b})^{-1}$ (megohms)
T-1	5.0	27.8	9.5×10^{-4}	.974	1.22	.820
T-1	10.0	27.7	10.5	.978	1.27	.787
T-13	5.0	27.4	7.6	.979	.710	1.41
T-13	10.0	27.3	6.8	.982	.995	1.00
T-4	5.0	25.0	6.3	.989	.328	3.05
T-4	10.0	34.5	4.8	.990	.233	4.29
T-5	5.0	30.5	5.8	.995	.308	3.25
T-5	10.0	30.5	4.7	.995	.214	4.67
T-2	5.0	31.2	2.8	.976	.405	2.47
T-2	10.0	31.0	1.5	.977	.291	3.44
T-3	5.0	31.2	3.3	.988	.300	3.33
T-3	10.0	31.0	2.4	.989	.215	4.66
T-9	5.0	30.6	2.6	.987	.285	3.51
T-9	10.0	30.8	2.0	.988	.204	4.90
T-10	5.0	31.2	1.7	.986	.291	3.44
T-10	10.0	31.2	1.3	.986	.208	4.81
T-11	5.0	30.2	2.2	.995	.266	3.76
T-11	10.0	30.2	1.7	.995	*	*
T-12	5.0	30.8	1.7	.988	.269	3.72
T-12	10.0	30.1	1.3	.989	.202	4.95

*Unstable; change in measured value of ± 0.010 μmho. Value initially is 0.285 μmho, drifting to 0.320 μmho in 3 min. at which time drift has ended.

TABLE [illegible]

SUMMARY OF SPECIFICATIONS AND MEASURED VALUES [illegible] 2N1223 (T-1)

CHARACTERISTIC OR RATING (25°C)	SPECIFIED VALUES 2N1502	2N[illegible]	GE [illegible]	GE [illegible]	[illegible]	MEASURED FOR [illegible] 2N1223 ([illegible] to stabilize)	COMMENTS
1. Max. V_{CB} (v)	-30	-30				Rating	See Number [illegible]
2. Max. V_{EB} (v)	-30	-15				Rating	See Number 6
3. Max. P_t (w)	8.5	8.5	10	[illegible]		[illegible]	[illegible] is conservative: 0 and [illegible] would give 20 w.
4. Max. T_J (°C)	85	85	75	[illegible]	[illegible]	[illegible]	Rating included to compare with PT,C.
5. Max. I_C (A)	- 3	- 3	- 2	-	-	[illegible]ing	
6. I_{EBO} (MA)							
a. V_{EB} = -30v	- 0.5					-.25	Initial 3 sec surge to 0.1
b. V_{EB} = -15v		≦ - 0.5				-.[illegible]	Initial 3 sec surge to 0.04
7. h_{FE}							
a. V_{CE} = -2v, I_C = [illegible]	[illegible] 20 - 60	≧ 2[illegible]	-------35 ([illegible])--------			[illegible]	Curve Tracer Measurement
b. V_{CE} = -6v, I_C [illegible]						[illegible]	Curve Tracer Measurement
8. V_{BE}(v)							
a. V_{CE} = -2v, I_C = 0.5A	_0.85	≦0.70				0.28	Curve Tracer Measurement
9. $V_{CE}SAT$ (v)							
a. I_C = 1.0A	≤0.75	≤0.60				0.17	I_B - 120 MA, Curve Tracer Measurement
10. V_{EBF}(v)							
a. V_{CB} = -60v	[illegible].30					0.095	
11. I_{CB} (MA)							
a. V_{CB} = -30v, R_{EB} = 00		≦1.5				-0.11	
b. V_{CB} = -30v, R_{EB} = 0			≦-5			-0.1	Initial Value 0.15
c. V_{CB} = -60v, R_{EB} = 00	≦1.5					-10.1	

50X1

TABLE XII
(continued)

CHARACTERISTIC OR RATING (25°C)	SPECIFIED VALUES 2N1581	2N1562	GFT 2006/303	GFT 2006/603	GFT 2006/903	MEASURED FOR ITEM MCN 15933 (After 1 min. to stabilize[4])	COMMENTS
11.d. V_{CB} = 60v, R_{EB}=0				-5		-10.1	Initial value ≈11.6, only small drift > 1 min.
e. V_{CB} = -90v R_{EB} =0					<-20	Note 5	
f. V_{CB} = -2v, R_{EB} =00						-0.012	
12.0 (°C/W) (Thermal Resistance)	3	3	5	5	5	To be measured	
13 fab (KC) a. V_{CE} = -2v, I_C = [illegible]							
14. fae (KC) a. V_{CE} = -6v, I_C = 500MA			12	12	12		Value 12KC is Typical
15. I_{CBO} (MA) a. V_{CE} = -[illegible]			≤ - 3	- - 3	. - 3	-0.48	

NOTES:

1. Specification MIL-T-19500/24 (SHIPS); measurements made accordingly except where noted.
2. Commercial specification, CBS Hytron.
3. Commercial specification, TEKADE.
4. In many cases dc stability was not reached completely in 1 min, but major drift was complete. A minimum off-time of 3 minutes preceded dc measurements.
5. V_{CB} not taken to -90v, but I_{CBO} [illegible] V_{CB} = -90v [illegible] .30 MA.

S-E-C-R-E-T

S E C R E T

50X1

Declassified in Part - Sanitized Copy Approved for Release @ 50-Yr 2013/12/11 : CIA-RDP81-01043R003300180006-6

TABLE XV

SUMMARY OF SPECIFICATIONS AND MEASURED VALUES - MCN 15934 (T-7)

CHARACTERISTICS OR RATING (25°C)	SPECIFIED VALUES 2N1581[1]	2N1562[2]	GFT 2006/30[3]	GFT 2006/60[3]	GFT 2006/90[3]	MEASURED FOR ITEM MCN 15934 (After 1 min. to stabilize)[4]	COMMENTS
1.Max. V_{CB}(v)	-60	-30				Rating	See Number 11
2.Max. V_{EB}(v)	-30	-15				Rating	See Number 6
3.Max. P_t(w)	8.5	8.5	10	10	10	Rating	8.5 is conservative; 0 and Tj give 20 w
4.Max.Tj (°C)	85	85	75	75	75	Rating	
5.Max I_C(A)	- 3	- 3	- 2	- 2	- 2	Rating	
6.I_{EBO}(ma)							
a.V_{EB} = -30v	$\geq$ - 0.5						
b.V_{EB} = -15v		$\geq$ - 0.5				0.28	Initial value 4.4ma. Drifts. (Tracer gives 0.24 ma)
7.h_{FE}							
a.V_{CE} = -2v,I_C =0.5A	21→60	$\geq$24				46	Curve Tracer Measurements
b.V_{CE} = -6v,I_B =16ma			---------35(25→50)--------			43	Curve Tracer Measurements
8.V_{BE}(v)							
a.V_{CE} = -2v,I_C=0.5A	$\leq$ 0.85	$\leq$0.70				0.42	Curve Tracer Measurements
9.V_{CE} SAT(v)							
a.I_C =1.0A	$\leq$0.75	$\leq$0.60				0.17	I_B = 120ma Curve Tracer Measuements
10.V_{EBF}(v)							
a.V_{CB} = -60v	$\leq$0.30						Cannot use 60v V_{EBF} = 0.08v @ V_{CB} = 30v.

50X1

TABLE XV
(continued)

CHARACTERISTICS OR RATING (25°C)	SPECIFIED VALUES 2N1581	2N1562	GFT 2006/303	GFT 2006/603	GFT 2006/903	MEASURED FOR ITEM MCN 15934 (After 1 min. to stabilize)4	COMMENTS
11. I_{CB} (ma)							
a. V_{CB} = -30v, R_{EB} = 00		≤-1.5				-1.4	Initial 2.3 ma Drops to<2 in.
b. V_{CB} = -30v, R_{EB} =0			≤-5			-1.0	2 or 3 sec. (Tracer gives 1.9 ma)
c. V_{CB} = -60v, R_{EB} =00	≤-1.5						Curve Tracer Measurement can't
d. V_{CB} = -60v, R_{EB} =0				≤-5			measure safely. Tracer gives 5ma@ 38v
e. V_{CB} = -90v, R_{EB} =0					≤-20		Breakdown< 60v
f. V_{CB} = - 2v, R_{EB} =00							Breakdown< 90v.
12.0 (°C/W) Thermal Resistance	≤3	≤3	≤5	≤5	≤5	-0.008	Stable
13.fab (KC) a. V_{CB} = -2v, I_C = 0.25A							
14.fae (KC) a. V_{CE} = -6v, I_C = 500ma			12	12	12		Value of 12 is typical.
15. I_{CEO} (ma) a. V_{CEO} = -16 v			≤3	≤3	≤3	6.5	(Tracer gives 1.9 ma) Initial 14 ma. Drops to 10 ma in 30 sec. I_{CEO} = 3 ma @ V_{CE} = 13 v.

NOTES: 1. Specification MIL-T-19500/24 (SHIPS): Measurements made accordingly except where noted.
2. Commercial specification, CBS Hytron.
3. Commercial specification, TEKADE
4. In many cases dc stability was not reached in 1 Min, but major drift was complete. A minimum off-time of 3 Min. preceded measurements.

TABLE XVI

SUMMARY OF SPECIFICATIONS AND MEASURED VALUES - MCN 15934 (T-8)

CHARACTERISTIC OR RATING (25°C)	2N1741,2	GFT 2006/30	GFT 2006/60	GFT 2006/90	MEASURED FOR ITEM MCN 15934 (After 1 min. to stabilize)[5]	COMMENTS
1. Max. V_{CB} (v)	-80					Rating of Number 11
2. Max. V_{EB} (v)	-60					Rating of Number 6
3. Max. Pt (w)	70	10	10	10		Rating
4. Max T_j (°C)	95	75	75	75		Rating
5. Max. I_C(A)	-15[3]	- 2	- 2	- 2		Rating
6. I_{EBO} (ma)						
a. V_{EB} = -2v	≤ -0.2				-0.021	Initial value 0.024 ma
b. V_{EB} = -60v	≤ -10.0				-1.15	Initial value 1.25 ma, Drifts to 1.0 ma in 2.5 min. Tracer shows 1.0 ma.
7. h_{FE}						
a. V_{CE} = -2v, I_C = -1.2A	40→80				24.5	Curve Tracer Measurement
b. V_{CE} = -2v, I_C = -5A	≥25				8.2	Curve Tracer Measurement
c. V_{CE} = -6v, I_B = 16ma		---------35 (25-50)------			32	Estimated from curve tracer. Note: At V_{CE}= -2v, I_C = .5A $h_{FE} \approx 33$
8. V_{BE} (v)						
a. V_{CE} = -2v, I_C = -1.2A	≤0.50				0.7	Curve Tracer Measurement
V_{CE} = -2v, I_C = -5 A	≤0.9				1.7	Curve Tracer Measurement
9. V_{CE} SAT (v)						
a. I_C = -12 A, I_B = -2A	≤0.7				→	I_C too great for MCN 15934, see report
10. V_{EBF} (v)						
a. V_{CB} = -80v	≤-1.0				-0.11	

S-E-C-R-E-T

S-E-C-R-E-T

50X1

TABLE XVI
(continued)

CHARACTERISTIC OR RATING (25°C)	2N174[1,2]	GFT 2006/30	GFT 2006/60	GFT 2006/90	MEASURED FOR ITEM MCN 15934 (After 1 min. to stabilize)[5]	COMMENTS
11. I_{CB}						
a. V_{CB} = -2v, R_{EB} = 00	≤-0.2				-0.030	Stable in <0.5 Min.
b. V_{CB} = -30v R_{EB} = 0		≤ -5				
c. V_{CB} = -60v R_{EB} = 0			≤-5		-0.46	
d. V_{CB} = -80v R_{EB} = 00	≤15.0				-5.8	Tracer shows 9.0 ma. Initial value 9.0 ma Drifting slowly at 1 Min.
e. V_{CB} = -90v, R_{EB} = 0				≤-20	-->	Ran away at 80< V_{CB}< 90v 15< I_{CB}< 20 ma. See report.
12.0 (°C/W) Thermal Resistance	≤ 1	≤ 5	≤ 5	≤ 5		
13. fab (Mc) a. V_{CB} = -12v, I_C = -1 A	≥0.1[3]					
14. I_{CEO} (ma) a. V_{CE} = -16v		≤ -3	≤ -3	≤ -3	3.2	Initial value 5.2 ma. Drifts to stable 3.2 ma in 0.5 Min.
15. I_B(ma) a. V_{CE} = -2v, I_C = -1.2A	15-30				49	Curve Tracer Measurement
16. I_B(ma) a. V_{CE} = -2v, I_C = -5A	≤200				612	Curve Tracer Measurement

NOTES:
1. Specification: MIL-T-19500/13A measurements made accordingly except where noted.
2. DELCO specs state 2N174A meets MIL-T-19500/13A, not the 2N174.
3. Not in MIL-T-19500/13A in this form through omission or error; Mfg's value for 2N174A.
4. Commercial specification, TEKADE.
5. Measurements made after change in V_{CE} vs I_C curve described in report

50X1-HUM

Next 214 Page(s) In Document Denied

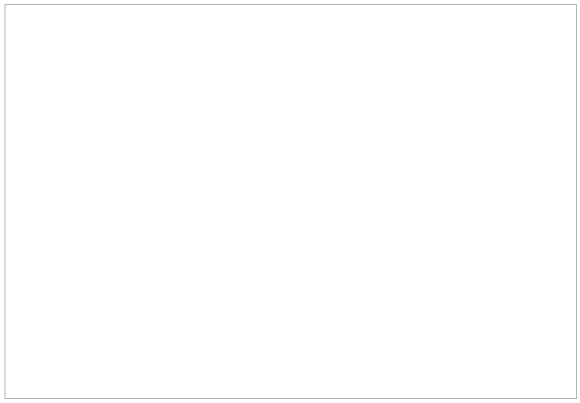

Confidential

GLOSSARY

AICBM	Anti-Intercontinental Ballistic Missile
AFCRC	Air Force Cambridge Research Center
ARDC	Air Research and Development Command
CAA	Civil Aeronautics Administration
DEW	Distant Early Warning
FGD	Fine-Grain Data
IFF	Identification, Friend or Foe
NWT	Northwest Territories
RADC	Rome Air Development Center
WADC	Wright Air Development Center

50X1-HUM

Declassified in Part - Sanitized Copy Approved for Release @ 50-Yr 2013/12/11 : CIA-RDP81-01043R003300180006-6

DESIGN ENGINEERING
GROUP 71

I INTRODUCTION

During the quarter the major effort of the Design Engineering Section of Group 71 continued to be the completion and activation of the mechanical components of the experimental radar Mk I at Boston Hill.

Other activities included some minor mechanical repair of the AN/FPS-31 radar at Jug Handle Hill; assistance to Group 76 in design of a 68-foot diameter foamed plastic radome; continued studies of large, mechanically phased arrays; studies leading to the conversion of Navy twin 5-inch shipboard gun mounts to land-based precision mounts for large antennas; firming-up of a test and development program to improve materials and methods for azimuth support of large rotating antenna systems; some assistance in the maser program; continued work on a mobile radiometer and servicing varied requests from groups in the Laboratory.

These activities are reported in some detail in the following sections.

II. EXPERIMENTAL RADAR MK I

A. Introduction

The Division 7 Quarterly Progress Report for 15 July 1958 stated that a full description of the activities on the experimental radar would not be given until this quarter, because of the intense preoccupation of the reporting personnel with erection problems. In addition to a brief review of previously reported progress, this report will include all activity through turn-on and early operation of the radar at Boston Hill.

B. Résumé

As of 31 March 1958, the status of the project was as follows:

(1) Engineering and design efforts on the reflector, feedhorn and their supporting structures were nearing completion.

(2) Erection and assembly of mechanical components atop the recently completed tower roof were well under way. The antenna pedestal was in place, ready for grouting to the roof, after achieving the desired degrees of roundness, flatness and levelness for it and for the installed large azimuth bearing.

(3) Planning was under way for structural and deflectional testing under calculated maximum operational conditions of the spider arms and reflector at the fabricator's facility.

(4) Fabrication was continuing at a rapid pace. The hub weldment had arrived at the site from the Watertown Arsenal where all machining had been completed. The reflector, its backup structure and support legs, and the spider arms were in the shop. Lofting and tooling for the feedhorn and its supporting structure had begun as a prelude to fabrication.

(5) Most of the remaining mechanical components had been procured and were at the site awaiting installation.

C. New Progress

Major efforts were directed toward completion of all engineering on the reflector, feedhorn and spider assemblies; and toward completion of a component test program to verify the structural performance of the reflector, its supports, and the spider arms, under simulated maximum operational loadings.

Other efforts included engineering liaison during fabrication of antenna components at the vendor's plant, and close supervision of all assembly and erection at the site.

Early in May 1958, the design phase came to a close as drawings of the feedhorn and its support were completed and delivered to the vendor for component fabrication. As with the other antenna components, the designs were analyzed for structural rigidity and stress levels under both operational and survival conditions.

D. Antenna Component Structural Testing

Concurrent with the design and fabrication of the antenna components, plans were made to undertake a test program at the fabricator's facility to verify the structural analysis and integrity of the various components. The tests themselves were performed on a concrete test pad which also served as part of an assembly jig for the complete reflector on its support legs. Static loads representing those computed for maximum operational conditions of 5 rpm, 1/2 inch of radial ice, and a wind velocity of 60 mph were applied to the reflector and to a representative spider arm. Deflections and critical member stress levels were observed and compared with the values allowed. Also included in this program was an investigation of the main vibrational characteristics of the reflector and spider arm. A detailed account of this program and the conclusions reached may be found in Lincoln Laboratory Engineering Report No. 71-47. A brief description of the tests and summary of the results follows.

Figure 71-1 shows the test pad with the assembled reflector being loaded at panel points through a cable and pulley system extending from an A-frame truss. Calibrated weights provided the required loading to simulate the operational condition under test. Deflections at various points on the reflector surface were measured, and stresses in selected truss members were recorded. Figure 71-2 shows the 60 strain-gage leads running from the reflector to a 60-gage switching unit and a 2-channel recorder under the reflector rear support leg The key results of this test were:

(1) The maximum tensile stress recorded in any strain-gaged member was 2620 psi, and the similar maximum compressive stress was 2500 psi.
(2) The maximum measured deflection at the reflector tip relative to the center was approximately 0.9 inch.

The measured stresses in the test concurred closely with the computed values and indicate that a conservatively safe stress level can be anticipated under survival conditions. Furthermore, the deflections fell well within the tolerances allowed for the reflector surface under maximum operational loads.

Although the reflector was assembled on the test pad, it was also decided to "pluck" the reflector tips and record natural frequencies. This was done by applying, and then swiftly releasing,

a 1000-lb load at one tip. Vibration pickups and strain gages supplied the information from which natural frequencies were obtained:

(1) The natural frequency of the reflector in a horizontal plane was 3.25 cps.
(2) The natural frequency in a vertical plane was 6.5 cps.

Experience leads to the conclusion that the above values lie in a band which may safely be exposed to the expected wind environment.

The next test consisted of determining stresses and deflection of the spider arms under the maximum operational loadings. Since the three arms supporting the reflector are identical, tests could be performed on any one. Figure 71-3 illustrates the spider test configuration, the two transits used for observing deflections, and some of the 30 strain gages used for measuring stress levels in the more critically loaded truss members. Figure 71-4 shows how the loads were applied. Since the spider must react to horizontal shear and vertical loads from the reflector, it was necessary to apply the computed loads simultaneously. Hydraulic jacks supplied the vertical loading and a Dillon dynamometer was used for horizontal loading.

Results of the most critical spider operational loading were:

(1) The maximum recorded tensile stress was 3374 psi and the similar compressive stress was 2374 psi.
(2) The maximum deflection horizontally or vertically, at the tip of the spider, was 1/8 inch.

As with the reflector, the test stresses agreed closely with the computed values, indicating a safe margin even under survival conditions. The deflections were low, as expected, and will contribute only slightly to reflector deformation under maximum operational conditions.

1. Azimuth Bearing Emplacement

In order that the installed bearing have the greatest chance of reaching computed life, under full static load the maximum radial and vertical excursions of the inner race shall not exceed 0.006 inch during 360° of rotation, nor shall the average slope in 7.5° exceed 0.001 inch. Despite the difficulties presented, this requirement must be met because the probability of achieving computed bearing life falls off rapidly if the noted values are exceeded. For example, the manufacturer indicates that an increase in the 7.5° slope will proportionately increase the load on all balls as they pass this sector. Since bearing computed life varies inversely as the cube of the load, a reduction to one-eighth of computed life becomes possible by allowing as little as 0.002 inch of slope in 7.5°.

In deference to the foregoing, all factors contributing to the precision of the installed bearing were carefully reviewed, resulting in the following considerations during design, fabrication and erection:

(a) The tower was configured in heavily reinforced concrete so that a rigid, stable platform was economically obtained.
(b) The bearing lower housing weldment, or pedestal, was designed for rigidity and then machined accurately for roundness, flatness and a close bearing fit. Furthermore, provisions were made to level the pedestal and correct for roundness at the bearing seat prior to grouting to the tower roof.

(c) Provisions were made to orient the bearing in the pedestal as necessary to compensate for, rather than to reinforce, radial variations between mating components.

(d) During bearing installation, instrumentation and procedures were devised to record accurately vertical and radial runouts of the bearing, correcting as required.

(e) The bearing upper housing weldment, or hub, was also carefully designed for strength and stiffness, and machined accurately for roundness, flatness and fit to the bearing. Furthermore, the configuration was chosen to accept the varying and concentrated loads from the antenna system and then to redistribute them as evenly as possible over the bearing, avoiding loading concentrations. Orientation of the hub relative to the bearing was made selective in order to favor roundness and inner race heat-treat gap location. After installation, provisions were made to record vertical and radial runouts, and make corrections if necessary.

(f) Finally, after the antenna installation was completed, provisions were made to carefully balance the load on the bearing statically, and to again record bearing runouts, correcting if necessary

In the Division 7 Quarterly Progress Report for 15 April 1958 it was reported that the pedestal and bearing were in place atop the tower, with the pedestal ready for grouting to the tower roof after achieving desired roundness, flatness and levelness. Figure 71-5 illustrates the "radius bar" that was used to determine values of these parameters for the bearing seat in the pedestal, and for the bearing itself. The oar is pivoted at one end for rotation in both horizontal and vertical planes as the seat and/or bearing are swept through 360° Mounted midway along the bar was a precision level calibrated to read to 0.0005 inch in 12 inches. By carefully centering the bubble before each reading of the dial gages at the bearing end of the bar, it was possible to work the level to many times its rated precision. Sweeping the seat or bearing with the radius-bar precision-level combination established a horizontal reference plane from which minute deviations were recorded at 7.5° increments along the circumference. Deviations from true roundness were simultaneously recorded from other dial gages at the bearing end of the bar. Since it was practically impossible to center the radius bar pivot exactly, the resultant eccentricity was canceled out by a procedure of subtracting the reflected sine curve from rectangular coordinate plots of roundness

In the process of bolting the outer race of the bearing to the pedestal, one of the bolts seized and then was sheared off in the process of removal. After replacement and retorquing of all bolts to the desired value, bearing level readings were taken, resulting in the plot shown in Fig. 71-6(a). At the location of the replaced bolt, a spike showed up on the plot. Torque on the bolts in this sector was increased from 250 to 450 ft-lb, with the results shown in Fig. 71-6(b). The spike remained, although the slopes were reduced. Increasing the torques in this vicinity to 1000 ft-lb resulted in the plot of Fig 71-6(c), indicating no further improvement. At this point the bearing was unbolted and jacked up out of the pedestal seat At the bolt location in question, it was found that a ridge approximately 1/64 inch high ringed the hole in the pedestal. The ridge was removed by filing and stoning; the bearing was reinstalled and torqued back up to 450 ft-lb New level readings were taken with the final results shown in Fig. 71-6(d). The total vertical excursion in 360° was 0.0029 inch with a maximum slope in 7 5° of 0.0009 inch

The radius bar was next used to check vertical and radial variations of the inner race of the bearing, with the results shown in Fig. 71-7. Both came out well within the prescribed limits. At this point the radius bar was removed, and the hub was lifted, oriented to favor the bearing inner race heat-treat gap and lowered into place on the inner race. After bolting and torquing to 450 ft-lb, indicators were mounted to the pedestal, and radial and vertical runouts were recorded as the hub was rotated by hand. The results are shown in Fig. 71-8, and are remarkably better than the prescribed values.

When the antenna structure was finally mounted on the hub, vertical and radial mounts of the inner race were again recorded as the hub was rotated by hand. The results are shown in Fig. 71-9 Although somewhat increased in magnitude over values with the hub alone (Fig. 71-8), the runouts were still, at most, only half of the allowable limits.

2. Fabrication

In the 6-month period covered by this report, antenna system components were being fabricated on a tight schedule at the General Bronze Corporation plant in Garden City, New York. The components included reflector panels, reflector backup truss, reflector support legs, spider arms, hog-horn feed, inner feedhorn, feed support structure and catwalks.

The 96 reflector panels were fabricated of 69 per cent open, 1.25 $inch^2$ perforations on 1.5 inch centers, from 1/8 inch thick aluminum-alloy sheet stock, and then spot-welded to formed-channel aluminum-alloy frames and ribs. Assembled in eight different contour jigs made from lofted coordinates, the panel surface tolerances were held to within 1/16 inch of true contour. After inspection the panels were iridite treated, primed with zinc chromate, and undersized holes were drilled in the mounting flanges for later use as pilot holes in assembly to the reflector truss mounting brackets.

The reflector truss subassemblies, consisting of vertical and horizontal tubular frames, diagonal members, upper and lower frame extensions, were fabricated of 6061-T6 aluminum-alloy tubing gussets, and then welded together in fixtures designed to function later as drill jigs The top and bottom horizontal frames, which included the chord members and their bolting flanges, were shipped to Portland Machine Tool Corporation, Portland, Maine, where they were held on a large planer bed and the flanges faced off by means of an adjustable index milling fixture to provide the necessary mitres between adjacent joints. After shipment back to General Bronze, holes were drilled in the flanges by means of autopneumatic drills mounted on the drill jigs. Dimensional checks were made and recorded for each truss frame. Preliminary assembly of horizontal top and bottom frames with the two adjacent vertical frames was made for each full bay of the reflector truss, using optical tooling to establish squareness while attaching diagonals and drilling of mating parts. After match-marking, each bay was dismantled, the outboard vertical frame then being used to start the next bay.

After each preassembly had been accomplished in the above manner, including that of the special center fitting for the rear support (Fig. 71-10), the frames were then re-assembled at the specially prepared test pad located outdoors at the vendor's facility. There, supported on temporary cribbing, the entire truss was assembled into three sections, mid and two tips (Fig. 71-11), and then checked for over-all dimensional conformity. Shims were provided where necessary to compensate for machining variations.

Meanwhile the three support legs had been fabricated, the outboard or forward legs of welded tubular 6061-T6 aluminum alloy (Fig. 71-12) and rear support of welded, tubular SAE1020 steel. The outboard legs were assembled to the male steel base fittings; and the rear support, after radiographing and some minor corrective rework, was assembled with the upper adjustable shim package and support fittings. The double clevis base support plate was bolted to the outboard assembly pad and the rear support leg base fittings made up to the clevises and pinned in place.

As the truss center section was raised by a crane, the SAE4140 rear support saddle and yokes were clamped to the truss as shown in Figs. 71-13 and 71-14, and the outboard legs were bolted to the truss and pinned to the base fittings as shown in Fig. 71-15. The outboard sections were then raised into position and bolted to the center section as shown in Figs. 71-16 and 71-17. By means of optical tooling erected on the assembly pad, rectangular coordinates were established and piano wires were erected at each truss station for use in aligning reflector panels to the desired contour. This proved to be an efficient, practical and accurate method for this phase of assembly.

In order to simulate the full static deflection of the truss while aligning the piano wires and then attaching the reflector panels, six sand bags simulating the weight of the six reflector panels of each bay were hung midway between all truss joints, as shown in Fig. 71-18. Then, as each panel was installed, one sand bag was removed (Fig. 71-19), resulting in very accurate reflector surface static conformity. With all panels installed, the entire surface was checked with the optical tooling on the pad. The early morning of 26 June 1958 was picked because of the occurrence of a very stable ambient temperature of 68°F as well as an overcast sky, precluding erroneous readings due to differential expansion over the rather large completed structure. Maximum contour deviation from the theoretical parabolic cylinder was found to be 1/4 inch.

The various catwalks, ladders and the cable pulling rigs (Fig. 71-20) were installed before the center-of-gravity, load and vibration tests were made under close direction of Lincoln Laboratory personnel.

Upon conclusion of the test programs, reflector panels were removed, pilot holes in the panels and mounting brackets were reamed to full size, and panels were then spray-painted and crated for shipment, three to a box. The catwalks, ladders and truss frames were match-marked, dismantled and loaded on truck trailers for shipment All steel parts were either cadmium-plated or primed with zinc chromate prior to shipment to the site where they eventually received a final coat of protective paint.

All 6061-T6 aluminum-alloy parts, except for reflector panels, were solvent cleansed and then shipped without further finishing treatment because of the material's exceptionally good long-term weathering characteristics

The spider arm trusses, welded together from 6061-T6 aluminum-alloy tubing and gusset plates, were confronted with particularly high-load carrying requirements. To attain this it was desirable to develop higher allowable stresses in critical welded areas. Consequently, the two welded vertical side trusses for each spider arm were shipped to the nearby Grumman Aircraft Engineering Corporation for heat treatment and aging before assembly with the horizontal or top and bottom members to complete the spider assemblies Next the spiders were shipped to

Botwinik Brothers, Incorporated, near Worcester, for machining of flange joint faces and template drilling of holes to match those of the flanges on the hub extensions.

Two of the three identical trusses were then shipped directly to the site (Fig. 71-21); the third was returned to the test pad at Garden City for load, deflection and stress level testing by Lincoln Laboratory personnel.

The configuration of the hog-horn feed was developed by the Radiation Engineering Laboratory, Maynard, Massachusetts, whose staff conducted microwave model studies of the entire antenna system. Subsequent development of the full-scale structural design called for stiffness without the use of heavy sections The horn sides were limited to a maximum thickness of 2 inches. The use of high-strength aluminum-alloy sheet for horn side corrugations and the flat inner skin was able to satisfy the stiffness requirement for relatively little weight.

The detail layout and subassembly work on the hog horn were carried out directly on full-scale loft lines laid out on a large layout table, permitting close dimensional control of the back reflecting surface, the sides, side support points and adjusting pivot points. It became necessary to develop special techniques for forming, spot-welding, straightening and riveting of the large, stiff side panels, particularly in the region of the transition sections on either side of the lower aperture area. These sections, which reduce the inside width of the hog horn from 25 inches to 17-1/2 inches, required development of tapering standoffs for support of the inner skin from the corrugated side panels. Subassembly drilling and use of blind rivets for fastening made possible the required assembly. Because the valleys between corrugations were only 1 inch wide, special right-angle pneumatic drill heads and expansion devices were employed in corrugation splice and standoff member assembly development.

The dielectric window covering the vertical aperture was fabricated of 1/8 inch thick silicone-fiberglass laminate, the apertures at the top and bottom of the horn consisted of similar material with the thickness increased to 1/2 inch. The horn upper-side supports, pivot arms and adjusting mechanism were welded up of aluminum-alloy tubing and sheet stock, after which preassembly was accomplished.

The horn support spider arm, consisting of five welded aluminum-alloy tubular truss modules, was shipped to the Portland Machine Tool Company for chord flange machining after fabrication, and then returned to the General Bronze facility for assembly to the hog horn and upper supports Alignment and radial positioning of the horn was accurately established, shims were provided and holes for mounting on the hub extensions were template drilled. This procedure proved to be both practical and expedient as confirmed by later experience during site erection. Shipment of the horn and its upper supports was by flat-bed trailer as shown in Fig. 71-22, and the spider arm came on another low-bed trailer with other components.

The inner feedhorn, designed from information also provided by the Radiation Engineering Laboratory, consisted of three box sections of rectangular cross section having 1/4 inch thick sides of aluminum-alloy plate. The throat area contained two parabolic ridges into which a tuning line was inserted The inner horn aperture was covered with a 1/16 inch thick silicone-fiberglass window and the other end was flanged for waveguide attachment. Upon completion the horn was shipped to Radiation Engineering Laboratory for installation of special irises and ridges

prior to final electrical matching with the hog horn at the site. Mounting brackets were provided for adjusting and securing it in position within the hog horn.

Some of the final items of the antenna system to be fabricated were the ladders, catwalks, CAA obstruction light supports and the IFF support provisions. All support spiders were furnished with catwalks extending from the hub to the tips for access to reflector and horn mounting and adjusting provisions. A center ladder was provided for access from the hub to the midheight reflector catwalk and the IFF access catwalk. At the outboard tips of the main catwalk, ladders extended up to the top of the reflector where small platforms were installed for obstruction light access and servicing. Trial preassembly was accomplished for most of these items at the General Bronze plant before their shipment to the site, with final components arriving during the first week in August.

3. Study of Wind-Induced Vibrations

During erection of the reflector backup truss at the vendor's plant, an investigation into the effect of wind toward inducing vibration in slender exposed tubular members similar to those used throughout the reflector backup structure was being carried on The investigation was primarily an analytical one supported by some wind tunnel testing. The result was determination of critical wind velocities, at the level of vortex shedding, for all members in the reflector truss in the operational regime of the antenna up to 130 mph. In addition, the maximum theoretical vibration-induced stresses in critical truss members were analytically computed. Most importantly, the various methods of best suppressing vibrations in the critical members were considered and evaluated. A full description of this investigation may be found in Lincoln Laboratory Engineering Report No. 75-2 dated 15 August 1958. A brief summary of the conclusions follows:

(a) The developed charts indicate that it is possible for most of the truss members to set up some form of vibration in the zero to 130-mph wind range.

(b) The stresses in the vibrating members can, in time, exceed the fatigue limits of the material However, fatigue failure is dependent on a great many (or else extremely long duration steady state) applications of the critical velocity for each member. In the actual environment this could take forever, but action should be considered for members having very low critical velocities.

(c) Methods of suppressing vibrations by increasing member cross sections or by shortening lengths were considered impractical but a recommendation to increase stiffness in a very simple fashion was made and adopted.

The method employed and installed before erection on top of the tower is illustrated in Fig. 71-23. Simple V-shaped, light-weight tubes were fabricated to clamp together the diagonal of each lower horizontal truss at its midpoint to the lower diagonals of the front and back vertical K-frames at their midpoints. This was done for the second, third, fourth and fifth bays from each tip and at the top as well as at the bottom of the main truss. By serving as column breaks for the members in question, the critical ranges were changed to new ones either outside of the survival limit, or in ranges where long fatigue life can be expected in the installed wind environment.

Lincoln Laboratory Engineering Report No. 75-3 dated 19 August 1958 discussed the preliminary wind tunnel investigation into wind-induced vibrations on slender tubular members

The most significant finding was that use of simple spirally wound spoilers on critical members may prove effective in removing affected members from the critical ranges of vibration amplitude and low fatigue life. Studies will continue to further verify this approach as to its effectiveness relative to that now in use on the reflector.

As the antenna stands, its structural rigidity and integrity in the present environment, up to survival limits, are believed to be at least fairly well confirmed analytically. Operational experience of some duration is required for further confirmation.

4. Erection and Assembly at Boston Hill

As summarized earlier in this report, the erection and assembly of components at the site had progressed to the point of grouting the pedestal to the tower roof. Grouting was readily accomplished and after curing, the roundness, levelness and race runouts of the bearing as well as the eccentricity of the large gear cut on the inner bearing race were once again checked and the results recorded:

(a) The bearing radial and vertical excursions remained as illustrated in Fig. 71-7.

(b) The maximum tilt of the bearing from a true horizontal plane was 0.015 inch in 160 inches.

(c) The eccentricity of the bull gear pitch diameter was found to total 0 0093 inch.

With these measurements considered satisfactory, the four drive pinions, which had been preassembled in their pillow block supports, were mounted onto the pads on the pedestal inner wall as shown in Fig 71-24. By means of adjusting shims between the pillow blocks and the mounting pads, each pinion was adjusted and temporarily secured with a minimum tooth clearance of 0.006 inch when the bull gear was rotated to the position of tightest gear mesh with that pinion. Couplings were then installed between the shaft end of the drive pinions and the right-angle speed reducers, with shaft alignment made good to 0.002 inch. The reducers were then secured to their foundations.

The next operation in the erection schedule was installation of the 42,000-lb hub onto the bearing inner race, and the preparations made were:

(a) Three centering guides, shown in Fig. 71-24, were first installed in the pedestal.

(b) Two accurately machined and ground guide pins were mounted 180° apart, protruding from inner race mounting bolt holes approximately 8 inches. These would provide the precision centering as the hub approached the bearing.

(c) Eight 35-ton hydraulic jacks were placed on the pedestal jack pads to use for fine control of the last few inches of lowering the hub into the bearing.

The hub was than rigged and elevated by the roof-top derrick to a height about 5 feet off the ground. The bearing engagement surfaces were cleaned and the load was leveled and balanced as shown in Fig 71-25. The lift began and the hub is shown arriving at the roof level in Fig. 71-26. The derrick was then boomed in and the hub positioned over the rough guides, as illustrated in Fig. 71-27, which also shows the jacks and one guide pin in place. At this position

it was necessary to orient the hub a certain way over the bearing before lowering for the following reasons:

(a) The bore of the bearing inner race and the hub pilot diameter were to be matched in such a way as to minimize or compensate for detail out-of-roundness.

(b) Proper orientation also permitted the reflector loads transmitted through the hub to be applied to the bearing inner race so that its heat-treat gap is always on or very close to the neutral axis for tilting.

After achieving the desired hub orientation, the hub was lowered to partial engagement with the guide pins, at which time the load was transferred from the derrick to the eight hydraulic jacks. From this stage on, the jacks were carefully operated to lower the hub evenly and slowly over the guide pins onto the bearing, as shown in Fig. 71-28. With the hub home the 48 bolts attaching it to the inner race of the bearing were torqued to 450 ft-lb. The radial and vertical runouts of the manually rotated inner race were recorded and are illustrated in Fig. 71-8. The values were far better than required, so erection to this point was considered eminently successful.

Next the 18-foot long torque tube, used for support and rotation of the upper half of the RF rotary joint, was lifted and set in place supported by the hub.

The rotary joint and slip-ring assembly were then installed as shown in Fig 71-29 The joint was secured after runout between the stationary and rotating portions was reduced to 0.003 inch. The basket truss shown is used to support the stationary half of the joint. The synchro data gear box, previously assembled to the rotary joint, can also be seen in Fig. 71-29.

While the rotary joint installation was being made, the four drive motors were raised and lowered into position on their foundations on the roof outside the pedestal. The motor shafts were then aligned with the speed reducer input shafts to within 0 002 inch, after which the couplings were installed. The motor brake assemblies were installed and aligned with the extended motor shafts

The bearing lubricating system, consisting of a topside spraying system and a lower collecting system was now installed. The spraying system, some of which is shown in Fig. 71-30, consists of a circulating positive displacement pump of 7- to 11-gpm capacity, a 4-way valve for selection of either of two 5-micron filters, a Shur-Flo valve to throttle down the oil flow, and a spray ring (not shown) around the top gap between the bearing inner and outer races. Oil is supplied from a sump built into the pedestal outboard of the two filters. The collecting system, partly illustrated in Fig. 71-31, consists of a scavenger pump, two electromagnetic filters for removal of any magnetic material particles showing up in the oil, a 4-way valve for selection of either filter, and a collecting trough to catch oil dripping from the bearing before its recycling.

The hurricane or survival rail, fabricated by Bethlehem Steel from a heavy-duty flat-topped crane rail section, was shipped to the site early in May and its installation was begun immediately. The rail was placed in position (Fig. 71-32) on small A-frames stabilized by welding to the steel reinforcing rods protruding from the roof. The holes in the sole plates welded to the bottom of the rail sections served as a template to locate the supporting anchor bolts With the rail in position, it was checked for roundness and flatness by the device shown in Fig 71-33, an arm supported by and rotated with the hub. Concentricity with the azimuth bearing was achieved by

adjusting the rail inboard by use of turnbuckles (Fig. 71-33) and outboard by means of jacks. Leveling nuts on the anchor bolts under the sole plates were used to achieve the level adjustment. The rail was made level to within 1/32 inch and concentric, for its complete circumference, within 1/8 inch. Next, forms were placed and the concrete parapet, enclosing the rail anchor bolts, was poured. After curing, the forms were removed and the rail position and accuracy were rechecked. No change from the former values was noted. Figure 71-34 is an aerial view of the tower and roof-top details at this stage of erection.

The auxiliary lubrication system was next installed. This system provides azimuth bearing lubrication even in the event of power failure and becomes necessary if high winds tend to drive the antenna. Two aircraft emergency ram-air-driven hydraulic pumps supplied by Aeroproducts supply the oil pressure, one mounted diagonally opposite the other on the roof corners outside the parapet, as shown in Fig 71-35. Flow begins at wind speeds in the vicinity of 30 mph, and if one pump is blanketed from the wind the other will do the job. Hydraulic lines from these pumps are routed into the pedestal where they tie into the regular lubrication system. However, when the auxiliary system is operating, the normal circulating and scavenger pumps, as well as their valves and filters, are all bypassed to spray the bearing directly, after which the drippings are collected and returned to the sump by gravity. The system is simple, reliable, provides extra bearing protection, and eliminates the complexity of auxiliary power packages and associated involved wiring and switching.

During the first week in July erection of the spider arms was accomplished. Lifts were made with a 25-ton, 130-foot boom truck crane. Figure 71-36 shows a reflector spider on the way, and Fig. 71-37 shows the same spider suspended in final position while the special very-high-strength bolts were installed, securing it to the hub extensions. High-strength self-locking nuts were used and special preload indicating washers permitted accurate torquing of all bolts. The remaining reflector spiders were similarly installed, until all three were in place on the hub (Fig. 71-38).

Next, the two survival locks were assembled and mounted on each spider arm (Fig. 71-39). The locks were positioned to provide, when opened, a minimum clearance of 1/2 inch with the survival rail, which by now had been grouted to the parapet. The 1/2 inch was calculated to provide rail clearance despite spider operational deflections. Interlock switches on the locks prevent antenna rotation unless each lock is fully open.

The installation of the reflector was begun by centering a transit on the hub to measure the variations and alignment of the mounting pads on each spider, first without load and then with loads simulating the static reflector weight. Dimensions between predrilled mounting holes in the pads on each spider were checked by means of a calibrated steel tape. These were checked against the values determined during initial assembly at General Bronze. Variations were slight enough to require no readjustment. It was also determined that the reflector when mounted would come within 1/8 inch of its theoretical position from the center of rotation and be level to within 1/32 inch in 120 feet of span. Figure 71-38 illustrates the two opposite spiders under simulated loads for determination of the shim requirements necessary to provide a common plane for mounting of the rear and outboard support legs. Shim thicknesses varied from 1/16 to 1/4 inch.

Beginning the week of 15 July 1958, reflector trusses were assembled on the ground in three sections for ease of handling and for minimizing roof-top assembly. Figure 71-40 shows the bare center section truss assembly and one of the outboard truss and panel assemblies. Panels were left off the center section during lifting because the safe handling capacity of the 35-ton, 160-foot boom crawler crane would be strained at the boom angle required during placement.

On 28 July 1958 with the survival locks engaged, the reflector rear support leg was raised into position on the aft spider arm as shown in Figs. 71-41 and 71-42. A jury strut held the support in position until the center section was installed. The shim package on the rear leg was adjusted to accept the center section in an untilted position. Figure 71-43 shows all the topside componentry ready to accept the center section.

On 8 August the stripped center section, weighing 16,800 lb, was lifted (Fig. 71-44), amid rain, wind and electrical activity, onto the rear support and spiders (Fig 71-45), and secured by bolting (Fig. 71-46). With the center section in place, the two reflector tips (Fig. 71-47) were readied for erection. The right tip was raised first, as shown in Figs. 71-48 and 71-49. With the crane holding the tip in position, attachment to the center section by bolting was accomplished as shown in Fig 71-50. This procedure was repeated with the left-hand tip.

Next, the center section panels were installed (Figs. 71-51, 52 and 53). The panels fitted into place, and bolts slipped easily into the predrilled holes, so no adjusting was found necessary at the site.

With the reflector now assembled as a section of a cylinder in a vertical position, its curvature and contour were next subjected to checks of their conformity with the theoretical values and for later accurate relative positioning of the feedhorn. The checks were performed by projecting selected discrete points along the contour onto a level rectangular coordinate grid system which had previously been laid out on the ground to a precision of 1 part in 50,000. The grid was 220.000 by 462.405 feet with its origin of axes at the projected center of rotation of the antenna. The projected points were then compared with theoretical values. The actual measurements were obtained as follows:

(a) The vertical piano wires which were used for contour control during preliminary reflector assembly at Garden City were reinstalled on the erected reflector.

(b) Two theodolites, accurate to one second of arc, were stationed along the grid base lines at the coordinates of each point to be checked. The coordinates were projected to their rectangular intersection which was then marked on a copper plate mounted on a 4 × 4-inch beam driven into the ground.

(c) With the theodolites still at the coordinate base lines, lines of sight were taken along the selected piano wire and projected down onto the copper plates. For each wire the process was repeated until all projected values were available for comparison with theoretical values.

The maximum recorded deviation from the true parabola was found to be just under 1/4 inch, and this occurred at one point only, with the majority of check points found to be less than 1/8 inch off.

While the reflector was being erected, pattern measurements were being taken of the feedhorn assembly lying flat on a wooden fixture on the ground (Fig 71-54). Upon completion of

these tests, which confirmed relationship of the inner feedhorn to the hog horn, the entire assembly was further assembled with its supporting structure onto its spider arm and prepared for lifting (Fig. 71-55). The assembly, which weighed approximately 8000 lb, was raised off the ground, carefully leveled and then hoisted to roof level (Fig. 71-56) for final installation. Prior to final attachment of the horn assembly, shims were attached to the hub extension to locate the axis of the feedhorn relative to the centerline of the reflector. The shim thicknesses were computed from the reflector support location as determined at General Bronze, and from the mounting hole locations on the spider assembly on top of the tower. With the crane steadying the load, the horn spider was made fast to the hub, using the same type of high-strength fasteners as for the other spiders.

The horn location was checked for precision by use again of the rectangular coordinate grid system and the theodolites. For some reason that was unaccountable, although all other dimensions were in almost exact agreement with theoretical values, the distance from the reflector was off by one inch. Even though the correction could then have been made through use of the provisions made in the design, because theoretical location was not precisely known, it was decided to wait for the results of pattern measurements before position correction was attempted. Figure 71-57 shows the feedhorn installed.

With the reflector and feedhorn in place and now tilted to the desired angles, one important final operation was carried out. A counterweight totaling 1400 lb was installed at the base of the rear support leg, bringing the entire rotating mass as close to static balance as possible. This was another in the long list of requirements established to favor load distribution on the azimuth bearing.

In Fig. 71-58 the waveguide run from the hatch on the hub to the feedhorn may be traced. Careful examination will reveal two flexible sections inserted to accommodate detail misalignment and/or differential expansion. A 4-step, 90° transition may also be noted. Figure 71-59 is a view showing the waveguide path up through the torque tube toward the hub hatch. Figure 71-29 shows the waveguide coming up to the stationary half of the rotary joint, and Fig. 71-60 shows the location of the RF switch on the sixth floor of the tower, with one run into a dummy load and the other upward toward the rotary joint The lower run is from the transmitter on the floor below

Simultaneous with all of the foregoing installation, the operator's control panels for the master drive system and the data-recording equipment was installed on the fourth floor, as shown in Fig. 71-61. The drive system panels contain controls not only for the antenna drive switch gear, but also for:

(a) An interlock system to interrupt antenna rotation for protection of personnel thoughtlessly passing through hatches into areas of moving machinery or equipment,

(b) Another interlock system preventing mechanical operation of the antenna before bearing lubrication is turned on, or before all survival locks are released,

(c) An RF interlock normally de-energizing the antenna when rotation is stopped, and additionally an RF shutoff key that may be taken with personnel on their way to topside areas of possible radiation exposure,

(d) A selector switch for activating any of three remote stations for antenna rotation control,

(e) Antenna rotational speed and azimuth position indicators,

(f) Wind velocity and direction indicators,

(g) An antenna revolutions counter and a meter for recording accumulated hours of antenna rotation.

Figure 71-62 shows a typical remote control station, this one inside the antenna support pedestal. For further personnel protection, this remote station cannot be operated before selecting it at the master panel, removing the locking key therefrom, and using this key to activate this remote station. The other remote stations are at the receiver and the transmitter.

Power control and instrument wiring was another activity that transpired while the foregoing phases were completed.

The point was reached where the antenna was in place, the drive system was completely installed, and only checkout remained before mechanical turnon of the system. The drive system was checked out by dropping the drive pinion couplings, energizing the motors and then checking: direction of rotation, motor voltages at the master panel, voltages at the motor terminals and over-all steadiness. Where necessary, adjusting and trimming were accomplished, and then the motor brakes were set to hold 450 ft-lb of torque each when applied. The bearing lubrication system was checked out, the open lube greasing of the bull gear and pinions was completed, and the pinions were recoupled.

5. Powered Mechanical Operation

On 19 August the antenna was rotated under power for the first time. Control was from the remote station inside the pedestal and speed was limited to 1 rpm to permit unhurried observation of bearing runouts, bearing lubrication, apparent load sharing among the pinions and gear tooth contact. The procedure was repeated at 2 rpm and then after a time, 5 rpm were attempted. At this speed, bearing runouts showed no change over previous values, bearing oil temperature rose to and stayed at only 4°C over ambient, there was but slight hunting of the motor voltages, and better than 75 per cent tooth contact was observed between bull gear and pinions. One brake was found to be dragging during this run, however, and required readjusting. The antenna was now operational, except for some additional cleanup and completion of painting of the tower and exposed steel components. The latter was completed over the next 2-week period, and Figs. 71-63, 71-64 and 71-65 show several aspects of the system as it appeared near the close of the quarter.

The short period remaining was consumed by a myriad of various tasks while the as-yet-limited running time was being shared by Divisions 4 and 7 in efforts to discover and compare operational characteristics with those expected Details of early operational experience and preliminary findings from the system's instrumentation should be available in the next quarter

S. J. Acquaviva
F. A. Folino
P. G Knowles
C. A. Pappas
D. A. Regillo
M. A. Brown (Group 75)
J. B. Paddleford (Group 75)
J. N. Scott (Group 75)
P. Stetson (Group 75)

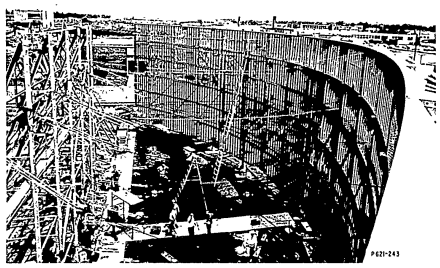

Fig. 71-1. Over-all view of static load test on reflector with pulley and weight system simulating maximum operational loads of 60 mph, 1/2 inch ice and antenna rotation of 5 rpm. Test was conducted on 1, 2 and 3 July 1958.

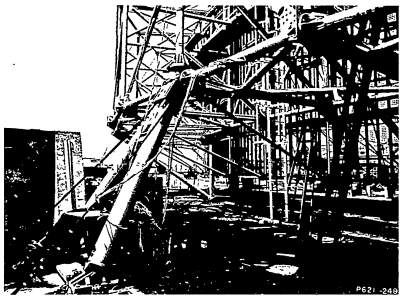

Fig. 71-2. Reflector rear support leg showing strain gage wiring terminating at instrument panel.

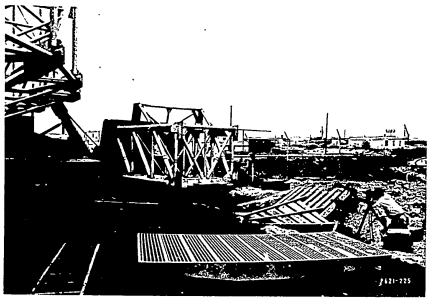

Fig. 71-3. Load test being performed on a typical reflector spider arm to measure deflections and stresses in the critically loaded members. Instrument panel to measure stresses in the truss members is seen in the background, with transits set up in three locations to measure deflections. Test was conducted on 17 and 18 June 1958.

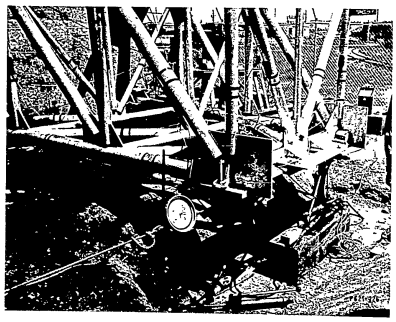

Fig. 71-4. Close-up view of loading with Dillon dynamometer applying simulated horizontal wind force and hydraulic jacks applying the resulting overturning wind moment; strain gages are visible on the critically loaded members.

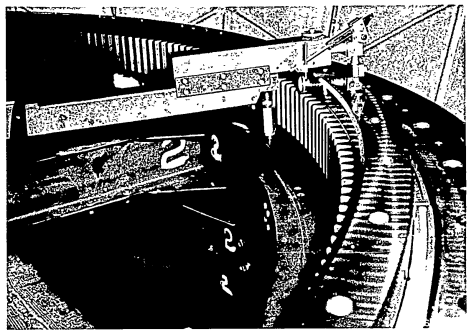

Fig. 71-5. Radius bar in operation during runout measurements of bearing. Indicator is set up to read radial deviations of bearing.

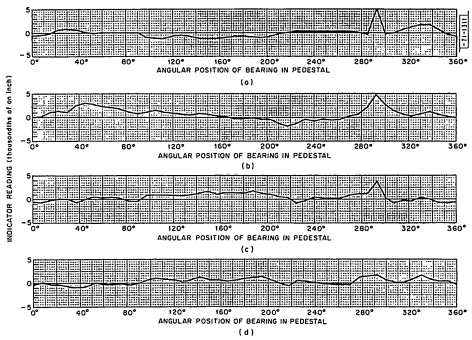

Fig. 71-6(a-d). Vertical excursion of bearing outer race after bolting to pedestal.

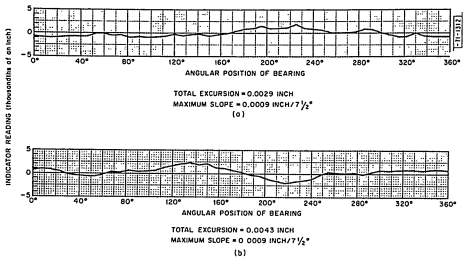

Fig. 71-7(a-b). Bearing excursions with radial arm sweep after bearing was assembled to pedestal with hold-down bolts torqued to 450 ft-lb.

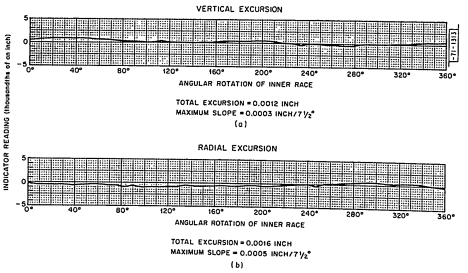

Fig. 71-8(a-b). Bearing excursions rotating inner race after assembling hub to bearing with hold-down bolts torqued to 450 ft-lb.

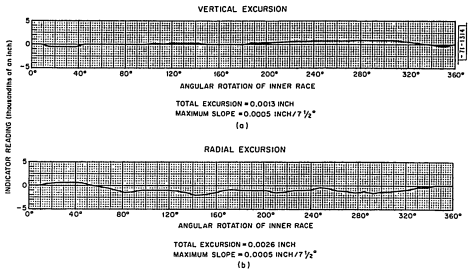

Fig. 71-9(a-b). Bearing excursions rotating inner race after assembling spider arms, reflector, feedhorn support, feedhorn and counterweights. Complete rotating assembly on bearing.

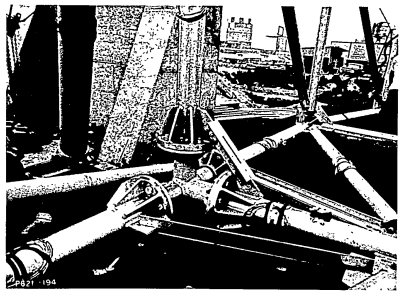

Fig. 71-10. Rear support fitting shown assembled with chord and vertical frame members of reflector truss. Note strain-gage leads and their protective covers on tubular members.

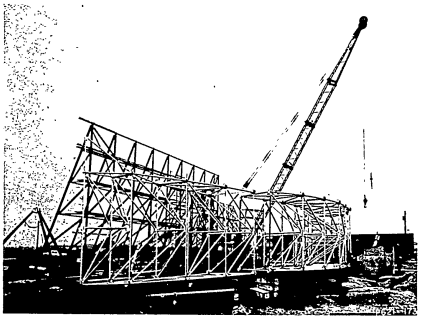

Fig. 71-11. Subassemblies of center and two end sections of reflector truss. Rear support leg being raised into position prior to lifting center section.

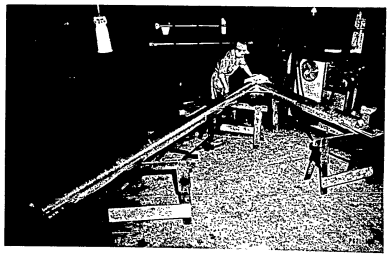

Fig. 71-12. One of front support legs tack-welded during fabrication.

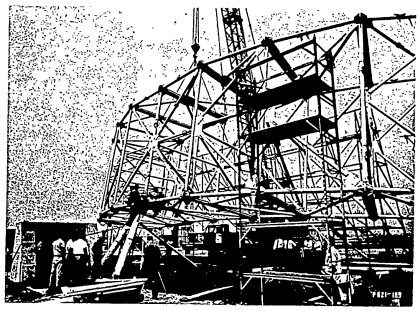

Fig. 71-13. Center section of reflector truss held by crane while attaching rear support saddle yokes to the truss. Rigging jury strut also in place, forming tripod with rear support leg.

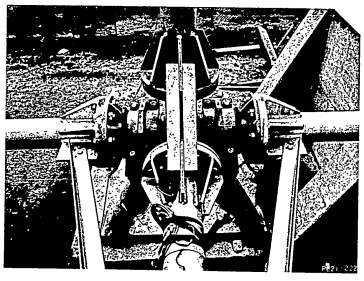

Fig. 71-14. Rear support fitting shown made up with yokes bolted to saddle. Steel cables are temporary rigging.

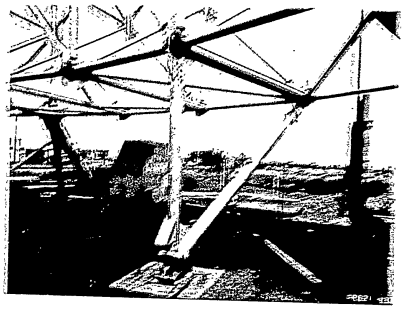

Fig. 71-15. (Front support leg locked in place, showing base fitting and locking pin. Rear support leg in background beyond antenna test mount.

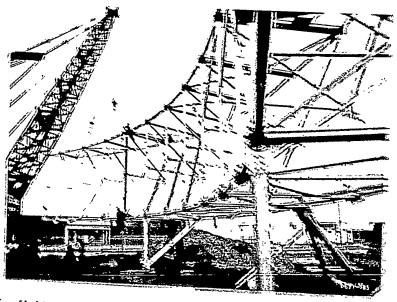

Fig. 71-16. Left dissection of reflector truss being bolted to the center section.

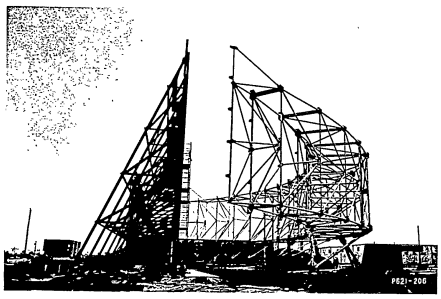

Fig. 71-17. Skeleton truss completed except for top vertical frame extensions.

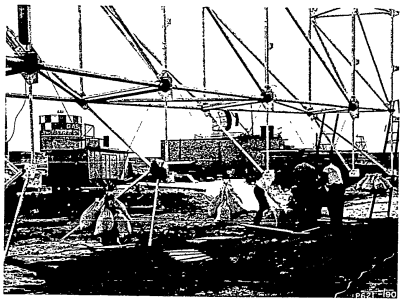

Fig. 71-18. Attaching sandbags to front of each bay to simulate weights of panels to be installed.

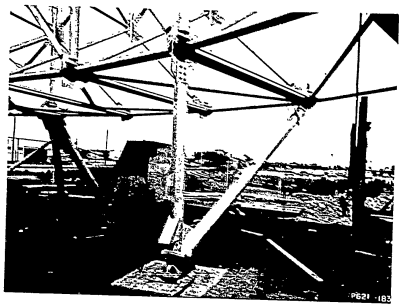

Fig. 71-15. Front support leg bolted in place, showing base fitting and jacking pad. Rear support leg in background beyond spider arm rest mount.

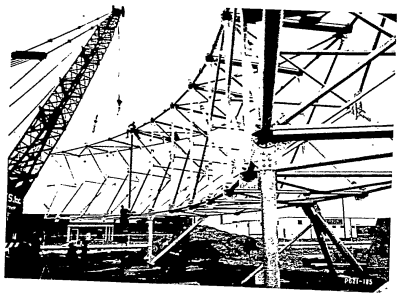

Fig. 71-16. Left tipsection of reflector truss being bolted to the center section.

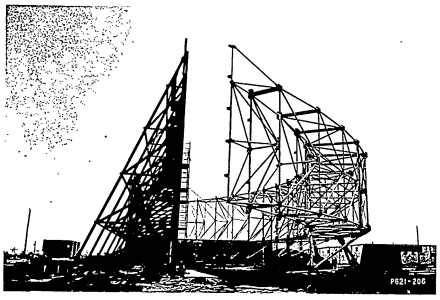

Fig. 71-17. Skeleton truss completed except for top vertical frame extensions.

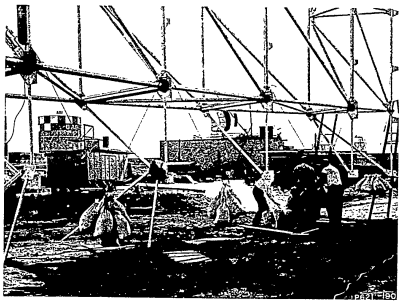

Fig. 71-18. Attaching sandbags to front of each bay to simulate weights of panels to be installed.

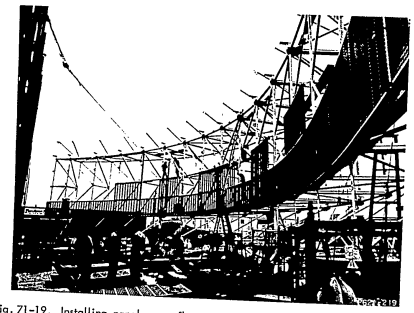

Fig. 71-19. Installing panels on reflector truss. Alignment was made with piano wires and optical tooling.

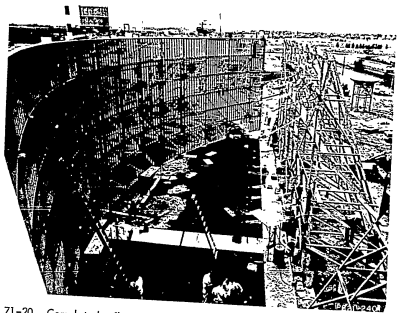

Fig. 71-20. Completed reflector screen surface showing piano wire clips projecting from surface. Also shown are pull rigs for static load test, and optical tooling being used to check contour.

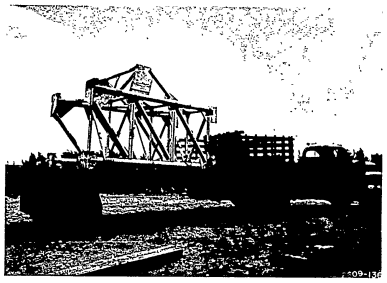

Fig. 71-21. Spider support arm loaded upside down, showing holes in mounting flanges, and brackets for survival locks.

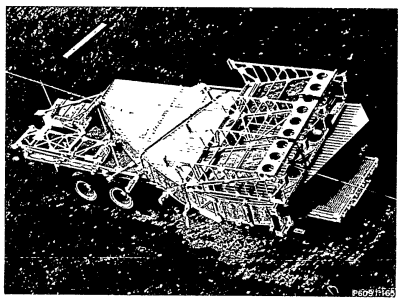

Fig. 71-22. Hog horn, upper supports, rear support and pivot arms as shipped from the fabricator required special road escorts because of 15-foot width.

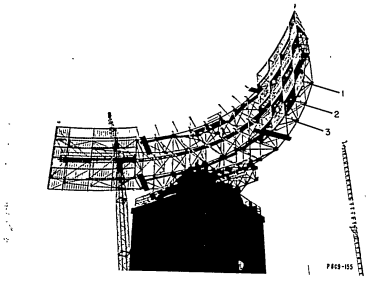

Fig. 71-23. Reflector tips in place, indicating method of suppressing wind-induced vibration in truss member of three outboard bays of reflector truss. Fourth set was not installed until board platforms were removed.

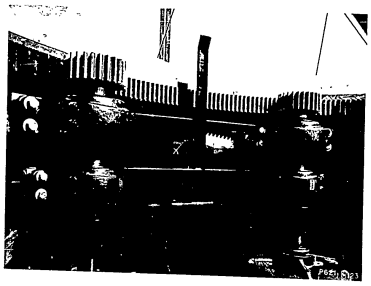

Fig. 71-24. Two of the four power pinions meshing with the internal spur bull gear. Also shown is one of the four reducers coupled to its pinion shaft.

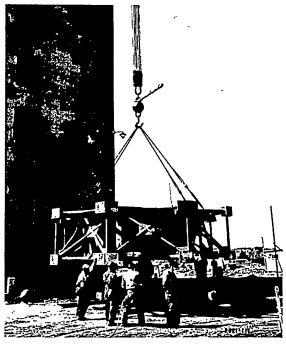

Fig. 71-25. The hub weldment, which weighs 42,000 lb, is balanced and tagged prior to lifting to the tower roof.

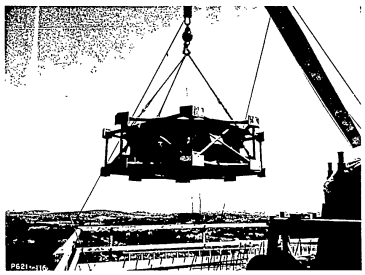

Fig. 71-26. Hub arriving at tower roof, with the boom of the derrick ready to swing it in over the pedestal.

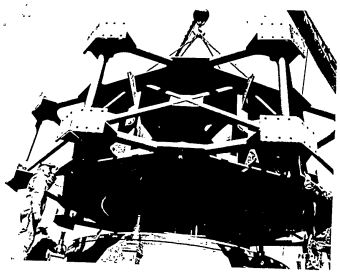

Fig. 71-27. Hub being lowered by the derrick onto the light jacks in place on the pedestal jacking pads. Guides can be seen in place for centering the hub on the way down. Also seen in the foreground is one of the two guide pins used for precision guiding of the hub onto the bearing.

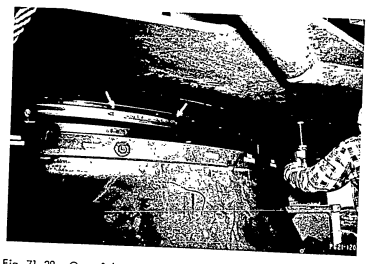

Fig. 71-28. One of the guide pins accurately locating the hub before it was finally lowered into the bearing by the jacks, one of which can be seen being operated. The arrows show a chatter mark on the bearing pilot diameter of the hub. This in no way affected the bearing quality or installation.

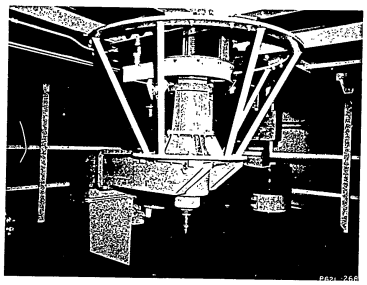

Fig. 71-29. The RF rotary joint with the waveguide on its way down to the transmitter. The slip ring and synchro data box assembly are also shown.

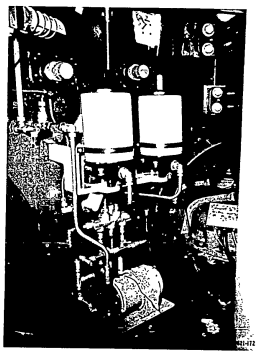

Fig. 71-30. The delivery side of the circulating oil lubrication system, including a gear pump, a solenoid operated selector valve, a filter bank, float switches and a level gage.

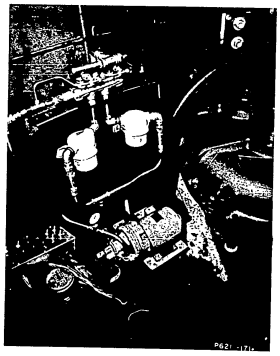

Fig. 71-31. The return side of the lubrication system which includes a suction pump, a solenoid operated selector valve and a bank of electromagnetic filters.

Fig. 71-32. Installation of survival rail showing A-frames supporting the rail, anchor bolts suspended from the rail sole plates and reinforcing rods protruding from tower roof.

Fig. 71-33. Checking concentricity of survival rail with respect to the bearing. Turnbuckle is being adjusted to round out this portion of the rail.

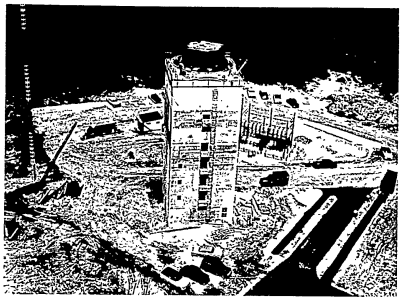

Fig. 71-34. Aerial view of tower and roof taken after the concrete parapet was poured, and showing status of project on 23 May 1958.

Fig. 71-35. One of the air-driven hydraulic pumps used in the auxiliary lubrication system. A wind vane is attached to the assembly to bring the propeller into the wind at all times. Hydraulic rotary joints on the top and bottom accommodate the flow to and from the pump.

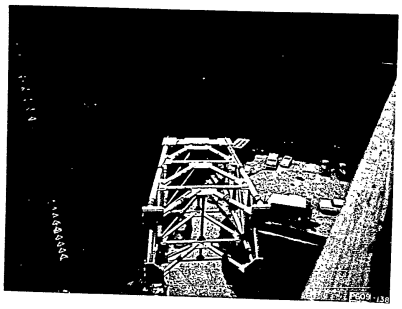

Fig. 71-36. One of the reflector spider arms in transit to the tower roof.

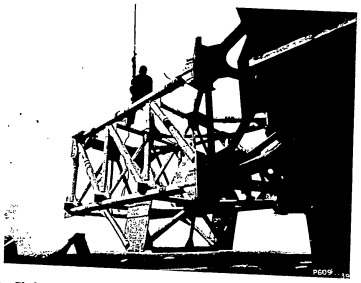

Fig. 71-37. A reflector spider arm in the process of assembly to the hub with special high-strength bolts.

Fig. 71-38. The three reflector spider arms are shown here assembled to the hub. The right- and left-hand spiders were under a load deflector test at the time.

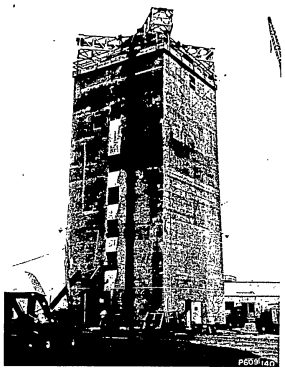

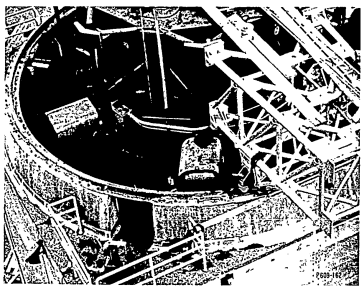

Fig. 71-39. One of the hurricane locks just after attachment to a reflector spider arm. Also visible are two of the drive motors and one of two air-driven hydraulic pumps.

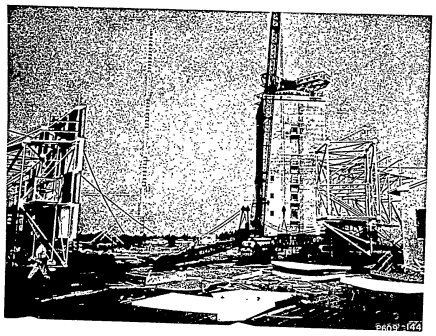

Fig. 71-40. Ground assembly completed on the 16,800-lb center section of the reflector truss, ready for lifting to the tower roof.

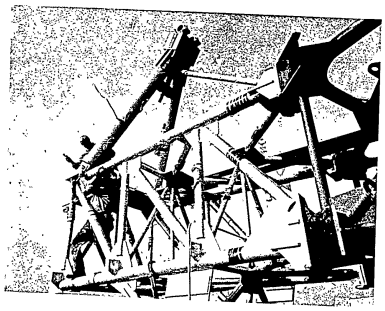

Fig. 71-41. Installation of the 4800-lb steel, adjustable, rear support leg assembly for the reflector. A jury strut is used to hold the rear support leg in place until assembly of center section of reflector truss is installed.

Fig. 71-42. Another view of the rear support leg installation, showing the jury strut attached to the hub, and the shim package and saddle in place to accept the reflector.

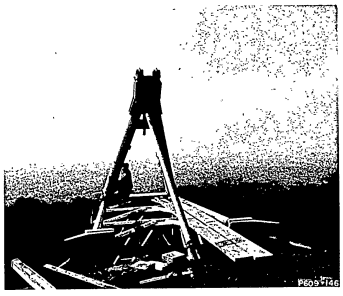

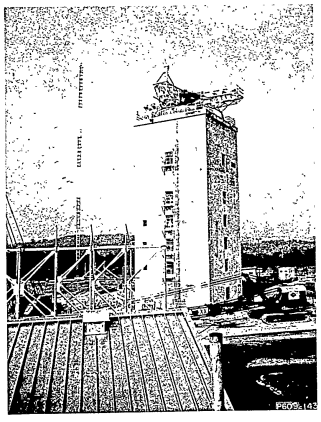

Fig. 71-43. The tower roof ready to accept the center section of the reflector truss, shown in the foreground. Also visible is the 35-ton crawler crane in position for lifting the truss.

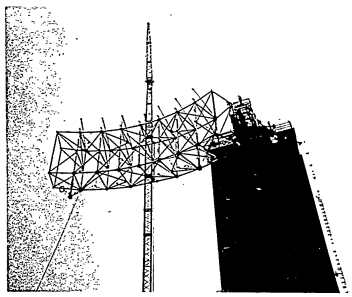

Fig. 71-44. The center section of the reflector truss in transit to the tower roof. A 160-foot boom was required to allow for enough drift when booming the load in over the tower. Also visible are two tag lines to stabilize the truss during the lift.

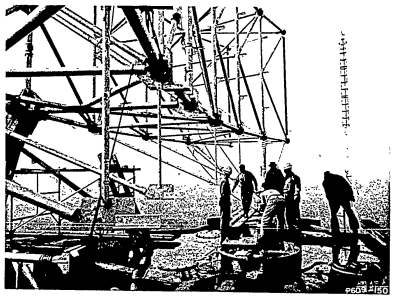

Fig. 71-45. Center section immediately after landing on the hub. Crew is in the process of securing the structure before final bolting operation.

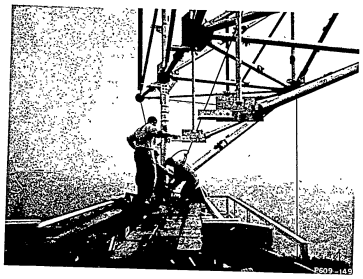

Fig. 71-46. Installing special high-strength bolts at attachment of reflector outboard support legs to spider arms.

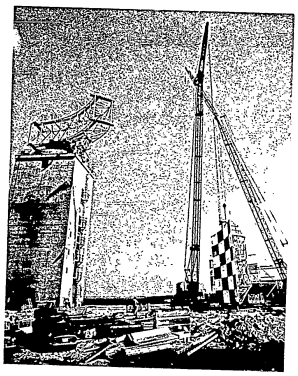

Fig. 71-47. Preparing one of the fully assembled 8000-lb reflector tips for lifting and installation to center section.

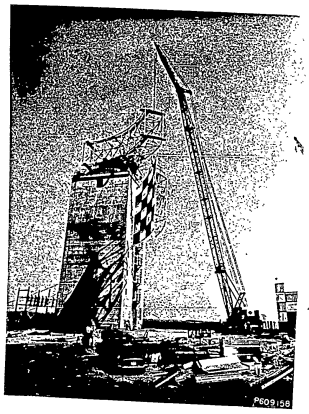

Fig. 71-48. A reflector tip in transit to the tower roof via the 160-ft 35-ton crawler crane.

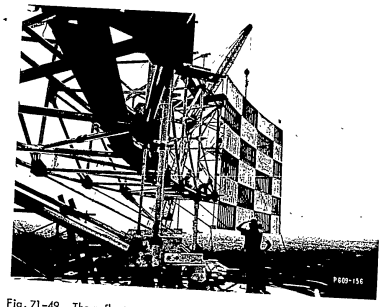

Fig. 71-49. The reflector tip being supported in place by the crane while crew men are attaching it to the center section.

Fig. 71-50. Ground view of the reflector tip during emplacement. Three tag lines, shown here, were necessary to stabilize the structure during the lifting operations and emplacement.

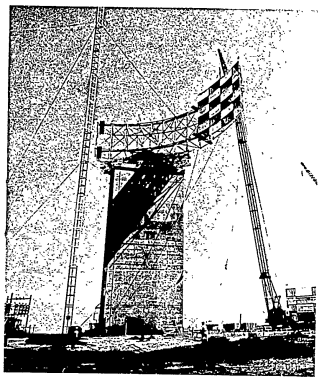

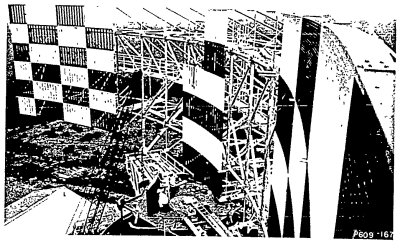

Fig. 71-51. View from one of the reflector tips, showing the other tip assembled and the installation of the remaining reflector panels.

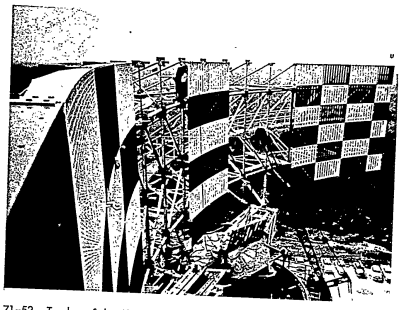

Fig. 71-52. Twelve of the 48 panels of the center section shown in place. Total time required to install all 48 panels of the center section was 2-1/2 days. Panels weighed approximately 100 lb each, were all 5 feet tall and varied from 8 to 9 feet in width.

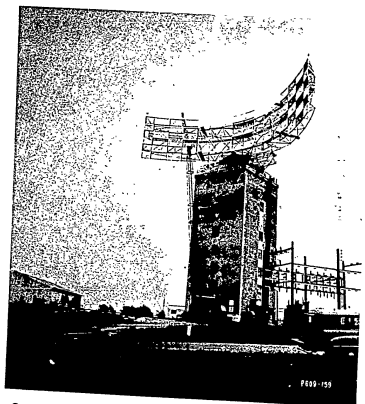

Fig. 71-53. Ground view showing over-all operation during installation of reflector panels.

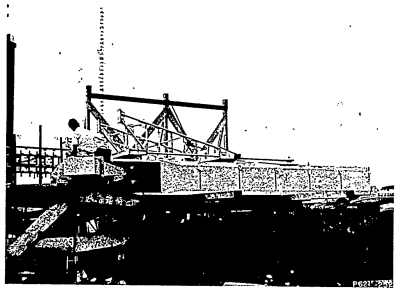

Fig. 71-54. Pattern measurement being taken on the feedhorn assembly. The inner horn can be seen in place, as can the silicone fiberglass dielectric aperture covering. The horn was tested in a horizontal position for ease of handling.

Fig. 71-55. The feedhorn and spider assembly in position off the ground being balanced and leveled prior to lifting to the tower roof. The entire assembly weighed approximately 8000 lb.

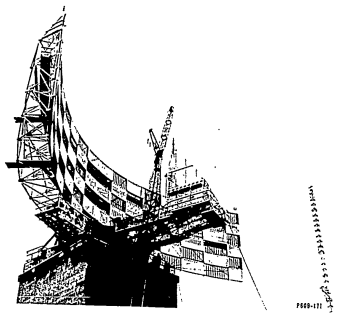

Fig. 71-56. The feedhorn assembly, after arrival on the roof, being supported by the crane while special high-strength bolts are installed to attach it to the hub.

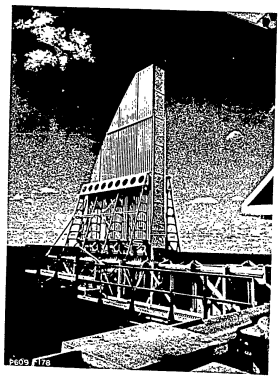

Fig. 71-57. Installed feedhorn assembly, showing waveguide within the spider arm and the catwalk for access.

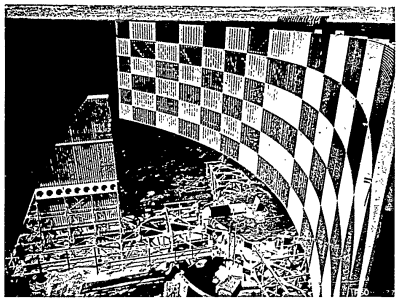

Fig. 71-58. Completed antenna assembly. Waveguide is shown coming up through the torque tube hatch and connected to the feedhorn.

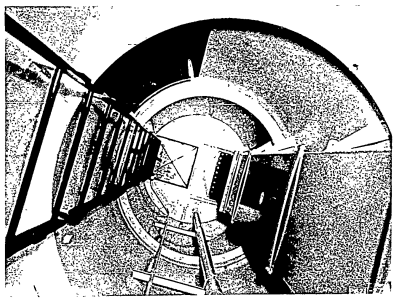

Fig. 71-59. Looking up the torque tube from the rotary joint, showing waveguide going through torque tube hatch and ladder for access between pedestal and outside top of hub.

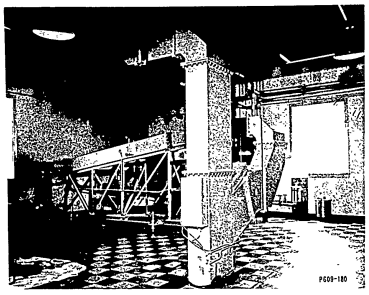

Fig. 71-60. Sixth floor in the tower, showing waveguide being fed down from rotary joint into an RF switch. In the background is the dummy load used to absorb RF energy when the antenna is not being energized.

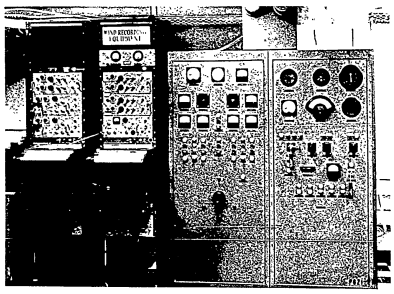

Fig. 71-61. Main control panel for operating the antenna. The two cabinets of recording equipment will be used to simultaneously record wind data, power consumption, strain gage readings, angular speed, azimuth position and vibrations at the reflector tip.

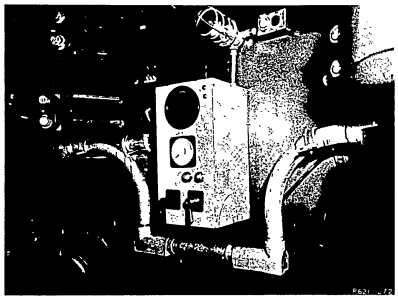

Fig. 71-62. Remote control station, located in the pedestal, from which the antenna can be operated. Panel contains speed and angular position indicators as well as slow-fast and forward-reverse controls.

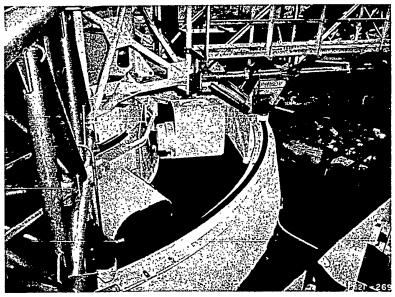

Fig. 71-63. Completed tower roof, showing motors and brakes, survival rail and locks, as well as auxiliary air-driven lubrication pump. Tower and equipment were painted white to minimize the effects of heating due to the sun.

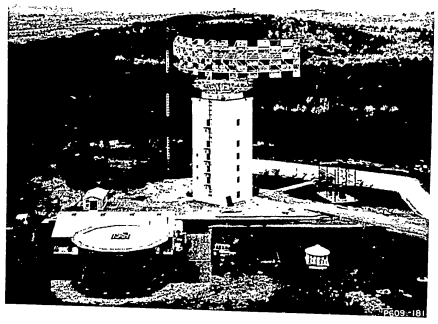

Fig. 71-64. Aerial view of antenna and tower showing a rear view of the reflector.

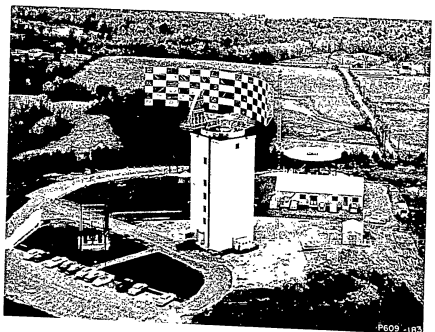

Fig. 71-65. Aerial view of completed antenna and tower during operation at 5 rpm.

III. MINOR REPAIR TO THE AN/FPS-31 RADAR AZIMUTH BEARING

On 17 and 18 September 1958, a minor repair operation was concluded on the azimuth bearing of the FPS-31 radar at Jug Handle Hill. It will be recalled that the subject bearing is the same one that was reactivated in Janaury 1957 after partial repair of extensive race damage, and replacement of the ball complement. The new damage consisted of a spalled area about 5/8 inch^2 located at the 340° position on the upper race of the inner bearing ring, and was believed to have resulted from growth of some microscopic subsurface damage remaining after the original repair operation. It was first noticed during the week of 11 August and study of photographs taken on 18 and 27 August and 9 September revealed the extent of damage but indicated no appreciable growth between photographs.

Nevertheless, it was decided to attempt repair as soon as preparations could be made, resulting in shutdown from noon 17 September through the evening of 18 September. The repair operation, performed by Laboratory personnel, followed closely that of 5 August 1957, which was reported in the Division 7 Quarterly Progress Report for 15 October 1957, with the following exceptions:

(a) An S.S. White right angle "A" hand piece was used to reach the damaged area more readily.

(b) A single mirror was used to view the work area instead of the rather complicated multiple mirror and borescope setup required for the earlier repair to the outer race

A complete visual inspection of the bearing at this time revealed no further new damage to races or balls, and particularly no change to the spot repaired in August 1957.

The newly repaired spot will be inspected frequently to observe the success of the operation Figures 71-66 and 71-67 show the affected area before and after the repair was accomplished

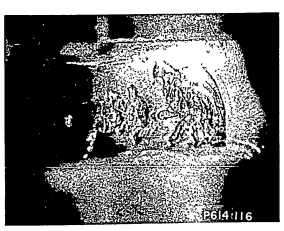

Fig. 71-66. Enlarged view (approximately 3X) of upper race on inner rotating bearing ring prior to repair, showing spalled area.

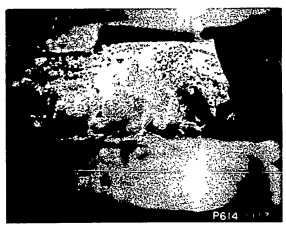

Fig. 71-67. Enlarged view (approximately 3X) of same area as in Fig. 71-66 after repair was completed, on 17 September 1958, by relieving spalled area with grinding wheels on dental drills. Shadow to left is one of the 2-inch balls.

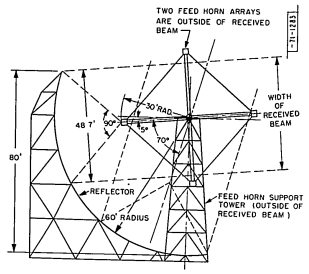

Fig. 71-68. Quadruple feed array.

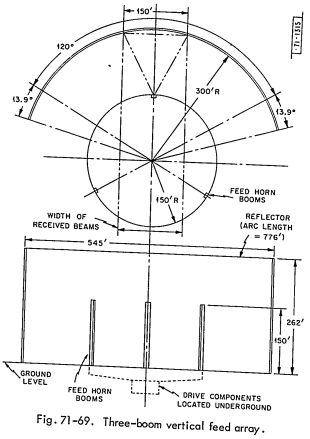

Fig. 71-69. Three-boom vertical feed array.

A representative of the bearing manufacturer (Kaydon Engineering) was present and witnessed the entire operation.

At shutdown on 17 September the azimuth bearing had operated for 3224 hours and 959,987 revolutions since reinstallation in January 1957. As the quarter closed, accumulated hours stood at 3278, an increase of 313 hours since conclusion of the preceding quarter.

D. A. Regillo

IV. LARGE MECHANICALLY PHASED-ARRAY SURVEILLANCE RADAR

A feasibility study for the design and construction of a phased-array radar was compiled in cooperation with Group 31 (Special Radar Systems). The Division 7 Quarterly Progress Report for 15 July 1958 explained several preliminary design concepts that were studied in arriving at the arrangement described in that report. This arrangement (Fig. 71-68) provided a cylindrical reflector of 60-foot radius and a length of 85 feet. The chordal length was 90 feet. Rotating on a 30-foot radius about the horizontal axis of this reflector were four feedhorn booms spaced 90° apart. The booms were 60 feet long and the rotating array was supported from two towers 60 feet high and spaced 140 feet apart. Although this arrangement appeared feasible, as shown in the report, it was felt that the coverage of 70° in elevation and 45° in azimuth, as well as the range, could be greatly improved by further study.

Data supplied by Group 31 for phased-array systems of various frequencies provided the basis for several additional design investigations. Although each design was primarily the same arrangement as described above, the physical size tended toward extremely large proportions, a typical configuration's being a 4-boom array rotating on a 71-foot radius, with each boom 94 feet long. The reflector was 194 feet long with a 148-foot radius. Distance between tower supports had increased to 294 feet. This arrangement proposed a rotational speed of 3.75 rpm.

Investigations were also made of several single-boom configurations that varied in size up to the point where the boom became 293 feet long and traveled along an arc of 240-foot radius. The reflector was 549 feet long with a 461-foot radius of curvature. Vertical height of the reflector was approximately 504 feet.

These large horizontal axis types of arrays did not appear too feasible from many points of view. It was at this stage that an investigation of the feasibility of a vertical axis array was initiated. The arrangement now under study (Fig. 71-69) proposes a reflector of 300-foot radius (arc length of 776 feet) and approximately 260 feet in height. About the vertical axis of the reflector and on a 150-foot radius, an array of three vertical horn towers will rotate, 150 feet high and spaced 120° apart, at a speed of 1 rpm. The three towers will be supported by a triangular or other suitably shaped spider connected to a central hub. The hub will be mounted on a roller bearing on the order of 30 to 40 feet in diameter. A torque tube connected to the hub and passing through the bearing will provide the means for transmitting the driving force through a 20-foot diameter bull gear to the rotating assembly. Suitable motors, gear reductions and pinions will provide the necessary power to actuate the array. All components below the top spider level will be located below ground level in an effort to attain minimum blockage.

Unclassified

A vertical array has the following advantages over a horizontal array of equivalent proportions:

(a) Greater azimuth coverage is available,
(b) Less power is required to rotate the array,
(c) Minimum blockage is achieved,
(d) Lack of towers to support array,
(e) Lack of a long central shaft necessary to keep support towers out of blockage area,
(f) Location of drive components at or below ground level, rather than high on a tower,
(g) Smaller vertical height of reflector is required,
(h) Rotational speed demand is lowered.

It is evident from the above statements that a study of this type of array is worthwhile. Presently, efforts are being expended to study the design in more detail in preparation for submitting a realistic feasibility and cost proposal.

E. A. Davidson

V. COMMUNICATION AND RADAR TRACKING ANTENNAS

For some time, several groups in the Laboratory have indicated the need for greater precision in servo-controlled antenna mounts that might be extensively used in the radar and communication research fields. In general, requirements for such mounts have slowly evolved from experience in rather diverse research programs, but they were found adaptable to correlation into a preliminary set of specifications that satisfy a broad spectrum of general research activity. In brief, these requirements encompass the design of a controllable antenna mount that has the power and structural strength to carry parabolic reflectors ranging in size from 28 to 60-feet or even larger diameter, and an associated control system that allows for any conceivable remotely initiated signal directive. A design program has been initiated to provide a universal-type antenna mount that will be suitable for as wide a set of design specifications as possible.

Because of the normal, long waiting period for the design, development and manufacture of controllable antennas, a short-term solution was demanded for several urgently required applications in the Laboratory. Fortunately at this time, a check made into the field of servo-controlled gun mounts revealed that the Navy in its current missile modernization program would be in a position to release some of its well-designed twin 5-inch shipboard gun mounts to Lincoln Laboratory. Foresight of a member in the Navy Bureau of Ordnance and of the Office of Naval Research had realized the potential value of these servo-driven mounts and retained them for future university research programs. Upon application through the Navy liaison office, two Mk 32, 5 inch, 38-caliber gun mounts were soon delivered to Lincoln Laboratory from the Naval Ordnance plant at Pocatello, Idaho. These gun mounts were found to be in almost perfect unused condition, and several more are on order for future use.

Performance details and dimensions of these gun mounts are contained in the Bureau of Internal Publications, O.P. 805 and O.P. 1101. Structurally, the basic controllable gun mount weighs about 25 tons stripped of superfluous armor and equipment, and each of its trunnions is

designed to withstand a 92,000-lb recoil from a gunfire salvo. The servodrive on the gun mount is a Waterbury A-B hydraulic drive with a fixed-stroke hydraulic motor on each axis, including a movable stroke hydraulic pump driven by a constant-speed electric motor and inertia disk. This is the same type of servo system (with its intervening years of improvement since the Mk 32 gun mount was designed) which has been chosen by RCA for the BMEWS tracking antennas. Some salient characteristics of the gun mount servo are:

Maximum speed of "B" end motor	900 rpm
Maximum speed of elevation axis	15°/second
Elevation beam ratio	360/1
Maximum normal torque at "B" end	300 ft-lb (1140 psi)
Maximum torque at blowoff on relief valve at "R" end	400 ft-lb (1525 psi)
Maximum normal torque on elevation axis	108,000 ft-lb
Moment of inertia of DS Kennedy 60-foot dish in elevation	4.7×10^6 ft^2-lb (without conterweights)
Maximum angular acceleration of dish in elevation	40°/second^2
Maximum wind torque on 60-foot solid dish at worst angle and 30-mph wind	72,000 ft-lb

If the extra stabilizing effects of the inertia disk on the electric drive motor is neglected and the output torque is limited by the steady-state horsepower of the electric motor, then the graph shown in Fig. 71-70 can be drawn.

Notice that the inertia disk can naturally provide assistance for short-term-load torque impulses. Also, a higher horsepower electric motor can be inserted to operate the antenna in high winds, since the hydraulic lines can take a continuous 108,000 ft-lb torque load at 1140 psi pressure. Comparable performance figures on the azimuth drive are:

Electric motor	40 hp
Speed of "B" end	0 to 900 rpm
Gear ratio	216/1
Maximum azimuth rate	250/second
Maximum normal "B" end torque	1400 ft-lb (at 1780 psi)
Maximum overload torque	1800 ft-lb (at 1900 psi)

These figures show that the Mk 32 mount has more than ample power to move a 60-foot parabolic dish. A major consideration, however, is the smoothness of tracking with the gun mount servos. This gun mount has been used as a commanded-position unit and experiments will be carried out to determine the characteristics of the gun mount when used in an automatic and tracking servo loop.

Design programs on control consoles, structural modifications and supporting reinforced concrete towers at various operational sites had been under way for some time, pending arrival of the gun mounts from the Navy. A future quarterly progress report will describe these activities in more detail. In order to expedite the complete backup antenna program, the antenna

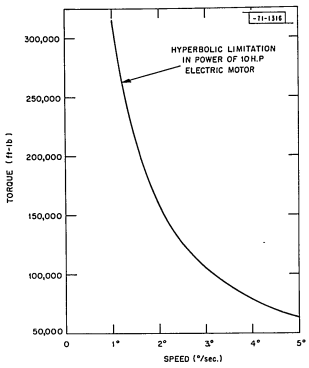

Fig. 71-70. Elevation power capability of Mk 32 5-inch, 38-caliber gun mount.

tracking frame has been under analysis and design by Group 75 (Construction Engineering), and pertinent details are reported herewith.

The design of the antenna support for the Mk 32 gun mount has been evolved with two major considerations: (1) the support should be capable of attaching either a 28-foot or a 60-foot parabolic dish, and (2) the antenna support should be readily mounted on the available gun slides with no structural modification to the gun mount. Structural studies have shown that both of these requirements are attainable.

One major problem in using the twin 5-inch mounts as trackers is that of supporting the reflectors. The plan is to strip the mounts of all elevating gear except the gun slides. Barrels, rammers and other items will have to be removed. The antenna support structure is being designed to attach to the slides. In arriving at this design, several requirements were established:

(a) The gun slides, which are open steel plate boxes, must be stiffened to carry the antenna loads.

(b) The antenna is to be supported at four coplaner points. The structure must maintain the plane surface under loading without assistance from the reflector structure.

(c) The slide stiffening members are to be of steel to eliminate thermal distortion of the slides, trunnions and bearings in the gun mounts.

(d) The support structure is to be made of 6061-T6 aluminum. This will reduce the total inertia of the moving assembly and eliminate thermal distortions between the reflector and support structure

(e) The aluminum members are designed to an allowable stress of 10,000 psi in bending, under loads applied by winds of 120 mph.

(f) The support structure is designed as a space frame with integral outrigger supports: this permits these members to contribute to the over-all structure stiffness.

(g) No provision is made in the design to resist independent operation of the gun slides. The design of the mount is such that independent operation is not possible.

The design is currently in progress.

J. E. Picardi
P. Stetson (Group 75)

VI. SUPPORT AND ROTATION OF LARGE ANTENNA SYSTEMS

During this quarter, the study of large antenna systems continued and the following information was obtained.

A program to determine the amount of retained austenite in one-inch-diameter bearing balls subjected to normal and alternate metallurgical treatment has been initiated. Retained austenite in bearing materials is undesirable for several reasons:

(a) Plastic flow of the stressed material causes retained austenite to decompose into untempered martensite, a hard, brittle composition.

(b) Retained austenite transforms to martensite on aging at room temperature, with similar effects and dimensional instability due to an accompanying volume increase.

(c) Low temperatures in service also cause decomposition of retained austenite with high local stresses and again the resultant dimensional instability.

The program consists of the following phases:

(a) Measure retained austenite and hardness on the surface of nine standard one-inch SAE 52100 bearing balls,

(b) A repetitive refrigerate-bake cycle for three of the balls,
A 450°F temper to three of the balls,
No treatment to remaining three balls, which will serve as the controls,

(c) All balls then ground through an equatorial plane,

(d) Retained austenite and hardness then to be measured as a function of distance along the radius.

A comparison of the average amount of retained austenite in each type of ball will help to confirm the effect of heat treatment on the amount.

It is evident that the rolling element bearing may be approaching the upper limit of fabrication capability; therefore, it is imperative that other methods of supporting and rotating large antenna systems be investigated.

A proposal on a preliminary program for the design and evaluation of fluid bearing types for large antennas has been formulated. The proposed program would contain:

A. Survey

(1) To determine where effort is being spent on similar work, thereby preventing repetition.

(2) To establish such factors as bearing loads, antenna size, environmental conditions, drive and control requirements, manufacturing requirements, life and similar factors related to bearing design.

B. Lubrication Aspects

A comprehensive digital computer and analog field plotter solution to determine hydrostatic pad and bearing configurations will be conducted. Data from this work will be presented in the form of design curves. Hydrodynamic effects may be superimposed on the hydrostatic bearings due to the relative motion of the bearing parts, turbulence and other factors, which will be included in the computer solutions.

C. Structural Aspects

In the design of large hydrostatic bearings, the structural relationship of the bearing parts to the lubricating film is of the utmost importance. Where film thicknesses of 5 mils are considered, large structural deflections have a significant effect on load-carrying capacity and performance of the bearing. The mating-bearing surface can be designed to match when in the loaded position, so that the bearing film thickness is relatively constant. The more complex bearing configurations will be analyzed through the use of computers.

It is also essential that the metallurgical aspects of rolling element bearings be studied for achievement of greater load capacity, life and reliability. A program of study toward this end has been formulated and would start out as follows:

Examine a series of specially treated 52100 steel balls, and balls of other metals such as M2, M50 and 440 C modified. An attempt will be made to instigate catastrophic failure with these balls in a small 4-ball test machine, by running them at extremely heavy loads and at low temperatures. In addition, measurements of load-life relations will be used in an attempt to establish more reliable values of AFBMA load-life formula constants. It is anticipated that these measurements will be tied in with parallel measurements on large-size balls to determine the relationship that might possibly exist between data developed on small bearings and data for larger units.

A part of the program would be devoted to the design and manufacture of a 4-ball tester which will handle large specimens. The machine would be capable of examining test balls from 2 to 8 inches in diameter. An additional phase of the program would comprise:

(1) Placing the 4-ball unit into operation,
(2) Determining those loads which will result in catastrophic failure for various materials,
(3) A cursory determination of the effect of lubricant on ball failures.

S. J. Acquaviva

VII. MASER PROGRAM

In the past, several different maser cavities have been designed and fabricated for Group 37. Currently an L-band traveling-wave maser has been constructed, together with a magnet which has 6 × 30-inch pole faces, as shown in Fig. 71-71. The equivalent length of the maser cavity is 8 feet. The maser is shown assembled and positioned between the magnetic pole faces in

Fig. 71-72, and uses X-band stainless steel waveguide to insulate the body of the maser from room temperature at the mounting flange. The cavity will be tested in liquid helium and the portion of the energy path in the magnetic field is to be filled with sintered ruby. Shorting plungers at the bottom of the assembly are for tuning the four arms of the cavity. An exploded view of the cavity may be seen in Fig. 71-73.

A. M. Rich

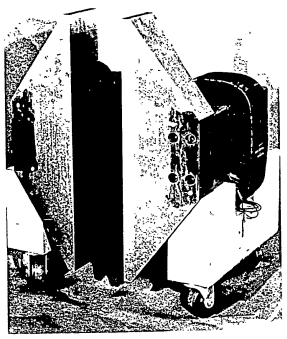

Fig. 71-71. Magnet for L-band traveling-wave maser.

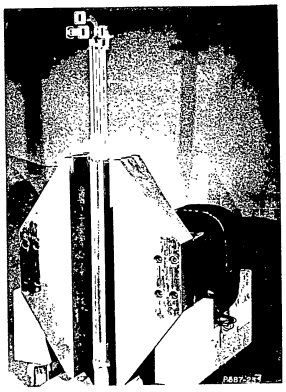

Fig. 71-72. Position of maser cavity in magnetic field.

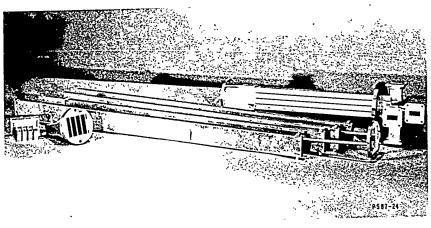

Fig. 71-73. L-band traveling-wave maser components (exploded view).

VIII. MOBILE RADIOMETER PROJECT

The mobile radiometer project reported in the Division 7 Quarterly Progress Report for 15 April 1958 for use in calendar has fallen short due to other pressing programs. Work is progressing, however, at a slow but steady pace. The inside of the 25-foot Fruehoff trailer has been completely insulated and shielded, with 4-inch fiberglass mats used for the insulation and 0.060-inch copper sheet providing the shielding. The latter is expected to eliminate all external noise, and as the receiver is designed to use any one of several maser cavities, internal noise from the electronic equipment will also be held to a minimum. All racks housed in the trailer will be of the Emco console type. The trailer will be air conditioned for equipment temperature control.

As the progress now indicates, completion of the trailer and its associated equipment will be in the Spring of 1959.

A. M. Rich.

IX. MICROWAVE INTERFEROMETER

During this quarter a rather successful test of the microwave interferometer linear measuring system was completed at the subcontractor's facility. Although the device has been tested on previous occasions, repeatability was not satisfactory. This difficulty was traced to physical instability of the target position. Wind tended to move the target to constantly new positions on successive readings. The new test was conducted in a dead calm with all physical dimensions remaining steady.

As shown in Fig. 71-74, the microwave horn at X-band, a ferrite circulator, two 10-db couplers, a ferrite isolator and a crystal detector were mounted on a moveable, calibrated platform which in reality was a milling machine bed fastened to an antenna pedestal. The assembly could be moved in 0.001-inch increments Below the pedestal was located a rack containing an ultrastable oscillator, a transfer oscillator, an electronic counter, a tuned audio amplifier and a phase-sensitive null detector. Outside the rack were the audio oscillator and modulator. Approximately 60 feet away on a wooden tower the neon-glow package containing four NE-2 bulbs was mounted as the target.

The neon bulbs were modulated by the modulator and audio oscillator. The signal reflected from the neon target followed a path through the ferrite circulator, crystal detector amplifier and the phase-sensitive null detector. Frequency was measured with a Hewlett-Packard counter reading to six places, permitting measurement of the distance from source to target to what proved to be an accuracy of 0.001 inch.

The next step will be to better package the equipment for taking static and dynamic measurement of large antennas out in the field. Among other things, it will be necessary to gimbal-mount the horn in order to aim it at various targets which may be placed anywhere on an antenna. Of primary importance is accurately locating the measuring reference plane in the horn and then correlating it to the antenna focal point.

A. M. Rich

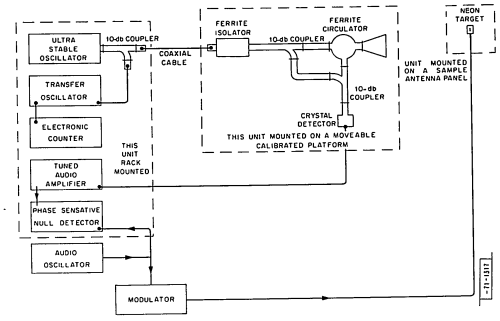

Fig. 71-74. Circuit for operational test of microwave interferometer.

X. DATA GENERATOR FOR THE AN/FPS-70 RADAR

In this quarter the ALRI (airborne long-range inputs) program was used to evaluate data furnished by the airborne 1024 change pulse generator, previously provided by Group 71 After favorable experience was realized with this unit, a second was requested for installation on another airplane which suddenly became available. Seven days after the request was received the new unit was delivered.

The initial components for the 1024 generator were constructed utilizing an existing rack from a radalarm OA-1003/APS-70. This necessitated using an existing gear box which reduced the synchro-motor speed of 207.2X to 1X. An additional gear train was then designed to increase the speed from 1X to 64X. Although the modified units performed satisfactorily, a request was received for a unit affecting improvement over the experimental models. As shown in Figs. 71-75 and 71-76, the new unit now reduces the 207.2X shaft of the selsyn to 1X, making use of the gear train reduction to drive a 16-tooth wheel at 64X. This results in 1024 azimuth pulses per revolution of the antenna, but since the true north reference tooth is on the same wheel, 64 north pulses are generated. Since only one pulse is required, a short time interval switch which remains closed for two degrees at 1X allows only one north pulse through. These prototype units, Fig. 71-77 will replace the experimental models.

Meanwhile, a contract has been let to construct a combination ground coincidence detector and azimuth north data generator. This unit will be servo-controlled to follow the compass under development by the contractor.

A. M. Rich

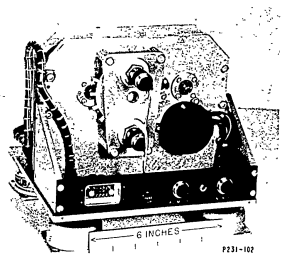

Fig. 71-75. Magnetic pickup heads, switch and data generating wheel.

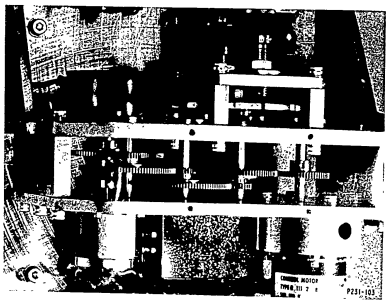

Fig. 71-76. Gear train which reduces 207.2 of motor to 64 for data generating wheel and to 1 for the autosyn and switch.

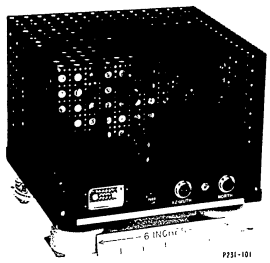

Fig. 71-77. 1024 data generator for APS-70 radar.

XI. CPN-18 FGD GENERATOR

Because of the success achieved in providing data generators for the FPS-3, FPS-20, FPS-8, FPS-6B, SP-1-M, FPS-14 and FPS-70, Group 71 was requested to furnish an FGD generator for the CPN-18. This unit, as in past fine grain generators, utilizes the magnetic field interceptor theory originally incorporated into units for the FPS-3 radar sets. Since an azimuth generator was on hand, only a mount and gear train had to be provided. The finished unit mounts on the side of the pedestal and engages the gear which drives the original equipment data generators. The reason for the change in design was that these radars did not have a 4096 pulse output, which became necessary for Laboratory sites.

A. M. Rich

ELECTRONICS SHOP
GROUP 73

NICHOLS, H. C., *Leader*

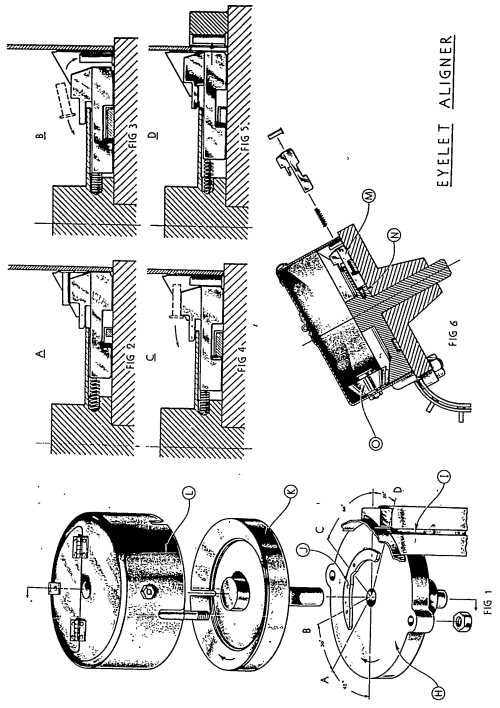

Fig. 73-1. Eyelet aligner used in the production of printed wiring boards.

ELECTRONICS SHOP
GROUP 73

I. INTRODUCTION

Group 73 normally reports its activities in Division 7's Internal Progress Report. The report is designed for internal distribution, and it discusses such topics as work load efforts, trends in work loads, jobs of special interest, and other items that are of interest primarily to Laboratory personnel.

The group's work in fabricating and assembling printed wiring cards has often required the development of special devices to facilitate production. The following article describes the development of an interesting device for aligning eyelets prior to their assembly into printed wiring boards.

II. EYELET ALIGNER

The production of printed wiring boards requires eyelets with lengths greater than their diameters. This presents a problem since the feed mechanisms of conventional eyelet hoppers will not accept these longer eyelets. Thus, the manual hand-swaging method of fastening eyelets had to be used. To eliminate this time-consuming operation, a new-type eyelet aligner was designed and put into operation to allow automatic insertion of long eyelets.

The conventional eyelet aligner consists of a rotary brush with bristle tufts set radially from a hub and contained in a cylindrical housing or hopper assembled on a raceway. This type of feeder effectively performs its functions so long as the diameter of an eyelet is greater than the length and the center of gravity falls within the perimeter of the eyelet flange.

However, with an eyelet having a body diameter of 0.100 inch, a flange diameter of 0.155 inch and a total length of 0.406 inch, the chance of an eyelet being ejected into the raceway with the conventional brush feed is about one in 10,000.

An approach to this problem was to provide positive positioning and ejection for the eyelet at the exit to the raceway. The eyelet could only be allowed to approach the exit with its flange in contact with the surface of the bracket and its body at 90° to that plane. At any other position the eyelet would be rejected and returned to the bulk eyelet mass.

It had been observed that eyelets of this category tend to assume positions parallel to each other when allowed to revolve on a plane in the horizontal. Thus, the elements of a cone moving or rotating below the axis of an eyelet satisfies this requirement if these elements are allowed to come into the horizontal at some place in its cycle.

In Fig. 73-1 (Fig. 1), H is a surfaced bracket, I is a raceway, J is a fixed cam, i.e., attached to the surface of the bracket, and K is a rotor machined to provide a storage for bulk eyelets as well as a conical surface to align them. One or more slots are provided along this surface to accept eyelets when the slot passes through the horizontal plane, the lowest point that an element of the cone passes. L is a housing or a cylindrical hopper to accept bulk eyelets. M is a control device which provides positive positioning of the eyelet. It has radial motion in the slot or slots machined in the conical surface and is spring-loaded by N against the inside wall of the housing. It is drawn toward the hub or the center of the rotor by the fixed cam J.

GROUP 73

At A (Fig. 1) the part M starts to be drawn toward the center of the rotor by means of the cam J. This action provides space for an eyelet body between M and the side wall of the housing. In the following 45° of travel of the rotor, any eyelet (as indicated in Fig. 2) will have taken a position with the flange against the surface of the bracket, and the body will be at 90° to that plane. Again, any eyelet that may have been picked up in the slot with the flange toward the center is rejected and returned to the bulk by the sharp shoulder on part M as shown at B (Fig. 3) and again at C (Fig. 4). The eyelet is ejected into the raceway (Fig. 5) as M is released by the cam J and is actuated by the spring load N.

In Fig. 6, O is a device which tends to assist aligning eyelets, on the surface of the cone, parallel to each other. It is like a miter or bevel gear with tooth sections greatly enlarged and conforming to the plane of the cone. The tooth sections are flexible, complying to misaligned eyelets that may fall onto the surface of the cone. This part has motion; it rotates on the stud that supports it, yet it does not contact the surface of the rotor.

R. D. Thompson

CONSTRUCTION ENGINEERING
GROUP 75

THERIAULT, W. J., *Leader*
MOORE, D. C., *Assistant Leader*

BROWN, M. I.
CLARKE, E. L.
GAUDETTE, E. P.
GECHIJIAN, H. G.
JORDAN, McC.*
PADDLEFORD, J. B.
SCOTT, J. N.
STETSON, P.
WEAVER, W., Jr.*

*Summer staff.

CONSTRUCTION ENGINEERING
GROUP 75

I. GENERAL OPERATIONS

Group effort during the past quarter has been concentrated mainly on preparation of designs and specifications for several additions to the Millstone Hill complex in Westford, Massachusetts, certain modifications to the Laboratory, special system studies, and preliminary structural and electrical work toward adapting surplus Navy twin 5-inch 38-caliber gun mounts to use as supports for tracking antennas, in conjunction with Group 71.

II. MILLSTONE HILL SITE WORK

The Millstone Hill complex includes the AICBM radar and prototype AN/FRC-47 communications sites. The radar work in particular is being expanded to provide assistance in the International Geophysical Year satellite programs and other missile-detection studies. This expansion will involve a number of additions to the present site, including an extension to the existing radar site building, more air-conditioned laboratory space, increased telephone facilities, an auxiliary tower for a beacon antenna, and a change in the access road system to provide a safe intersection with the Lowell-Groton road. Also, a second tower will be constructed to mount an additional tracking antenna for other studies.

A. Building Extension

The present stage of development of the Millstone Hill radar requires the close cooperation of personnel interested in radar transmitters, radar receivers, computers, auroral studies and other fields. This work has developed to the point where additional laboratory and office space is essential for efficient operation. The new addition, a wing 50 feet wide by 80 feet long, will include space for the CG 24 computer, now temporarily installed in the existing building, areas for computer maintenance and auxiliary facilities, a general laboratory area, laboratory space for use with the high-voltage test ring, and additional office space.

1. Design

The new wing will have a rigid frame structure, with corrugated metal siding to match the existing building. The floor, as before, will be a concrete slab on grade. The area under the computer and its auxiliary equipment will be a pit to permit easy installation of air-handling ducts and power and signal cabling. In addition, this type of installation provides for possible changes in equipment layout or interconnection.

2. Shielding

The complete floor area of the building extension will be shielded with a metallic screen placed in the concrete floor, and bonded to the building structure. The interior finish of the building will be aluminum-foil-backed gypsum board, with aluminum screening providing electrical continuity through mechanical connections at the joints. This foil layer will provide a secondary layer of shielding behind the exterior metal walls of the building. The computer area will

be further screened by bronze wire screening on the walls and ceiling, with all joints soldered. This screen will be connected to the building ground at a single point to prevent internal current loops.

3. Electrical Power

Power will be furnished at 120/208 volts 3-phase wye through a spare circuit breaker in the main switchgear. Power cables will be run through an existing spare conduit to the new wing, and then through a new conduit in the attic area to a distribution panelboard in the new general laboratory area. This panelboard will handle lighting and general laboratory power. Power for the computer will be taken from an existing panelboard modified to handle the new current requirement. Power for mechanical equipment will come from spare breakers in the existing mechanical power distribution panelboards. Fluorescent lighting fixtures will match those in the existing building; lighting intensity will be about 35 foot-candles.

4. Heating

In selecting the type of heating system to be used, consideration was first given to an extension of the present steam system. However, new steam mains would be required, as those adjacent to the building extension could not carry the additional load. Also, several new condensate pumps and additional condensate piping would be needed. Instead, the system selected will use a hot-water generator with boiler steam as the heat source, and circulating this water through finned-pipe radiation along the perimeter walls. The existing boiler has sufficient capacity for this additional load, and space is available for the hot-water generator in the boiler room. Based on an interior temperature of 75°F and outside temperature of −10°F, a building heat loss of 300,000 Btu/hour was calculated and a heat exchanger having a capacity of 350,000 Btu/hour was selected. The pneumatic temperature control system will be extended to incorporate the new wing, with separate thermostats and multizone control to allow for differing heat loads in the various areas.

5. Air Conditioning

The relocation of the CG 24 computer necessitates the extension of the present air-conditioning system. In addition to the computer, which is to be cooled by a direct induction of cooled air, general area cooling is required to accommodate the auxiliary equipment. The computer load will be handled by the existing multizone air-handling unit through new ducts run in the equipment pit and up into the computer cabinets. The auxiliary load will be handled by a new air-handling unit installed in the attic area, using the existing refrigeration system as cooling medium.

6. Progress

Design has been completed, proposals received and a requisition written. An order will be placed and construction started in October, and work should be completed early in 1959.

E. L. Clarke
H. G. Gechijian
J. B. Paddleford

B. Propagation Study Laboratory Air Conditioning

The Propagation Study Laboratory area in the existing radar site building at Millstone Hill has an extremely high concentration of electronic equipment which requires cool and relatively constant ambient temperatures to insure component reliability and extend the life of the equipment. The total sensible heat loss from the electronic equipment is about 14 kw. Occupation, lighting and building losses are considerably less. In order to obtain the large amount of sensible cooling required, a unit having a ratio of sensible to total cooling of approximately 90 per cent is required. This is a very high ratio, and no standard package unit with this capacity is available. To expedite delivery and permit more flexibility of use, a package unit having a ratio of 65 per cent and sufficient additional capacity to handle the total sensible heat load is preferable.

Tests showed that the existing refrigeration compressor had ample capacity to handle this additional load. A standard air-handling unit with direct expansion coil was therefore located in the room with refrigerant lines extending through the wall into the equipment room and tying into the existing refrigerant suction and liquid lines.

Room temperature control is maintained through use of a thermostat operating a refrigerant solenoid valve. A pneumatic pressure selector was installed in the existing air-conditioning system to permit a call from any zone-cooling thermostat to start compressor operation.

H. G. Gechijian

C. Telephone Room

Expansion of operations and staff at Millstone Hill will require additional telephone facilities. The existing system can only handle some twenty extensions and will be inadequate for the new extension. It is to be replaced by a 740-E PBX system, with 2-digit dialing and a capacity of about 80 extensions.

The telephone company requires a dust-free room 10 ft^2, 8 feet clear height, with temperature control and convenient access. With a critical space situation already existing in the main building, it was decided that the telephone room would be built in the storage area over the entrance lobby. This location involves problems of floor strength and access which required solution.

The existing storage area was designed for a live load of 60 lb/ft^2. This will be doubled by adding new floor joists. The new room will be of frame construction, with gypsum-board wall and ceiling finish, and an asphalt tile floor.

Personnel access to the room will be provided by a pull-down stairway located in the ceiling of the east-west corridor and just outside the new room. Equipment will be moved in through the storage area from the main bay.

The required temperature control will be provided by a new duct connecting to the existing air-conditioning system.

Fluorescent lights will be used, with an intensity of 35 foot-candles. The fixtures will be mounted to give maximum head room. Power receptacles will be provided for test equipment and tools; these receptacles will be controlled by a switch with pilot light located near the doorway. An empty 3/4-inch EMT conduit will be provided to existing cold water piping for use in

running the system grounding conductor. A 4-inch^2 screen-cover wireway will be run from the existing telephone equipment to the new room to carry the new cables.

Design of this room is complete, and requests for proposals have been issued. Work should be completed during the next quarter.

E. L. Clarke
E. P. Gaudette
H. G. Gechijian

D. Beacon Antenna Tower

Recent emphasis on International Geophysical Year satellite work has required use of the 84-foot reflector with an auxiliary dipole antenna at 108 Mcps for monitoring of satellite telemetry signals. However, no adequate location has been available for permanent installation of a beacon transmitter to test alignment of this dipole antenna.

In order to provide a permanent support for the necessary beacon antennas required for calibrating the reflector, a 180-foot high guyed tower will be constructed near the communications site, approximately 1600 feet from the radar tower. The tower height is necessary to place the beacon antenna location approximately even with the centerline of the radar reflector, due to the slope of the ground.

The tower will have a triangular cross section 15 inches on a side, and be guyed at four levels. The site is on a hillside with extensive ledge outcroppings. The tower foundation and guy anchors will therefore consist of studs and eyebolts grouted into the ledge. Erection of the tower is scheduled for October 1958.

D. C. Moore

E. Access Road Extension

The original road construction consisted of a paved roadway 18 feet wide and approximately 0.8 mile long, running from the "Millstone Hill Road" near the Westford-Groton town line. The Millstone Hill Road is a winding town road connecting with State Route 40, about 12 feet wide, and almost beyond repair. The intersection at Route 40 is on a hill and immediately adjacent to a blind curve over the crest of the hill. This makes the intersection completely blind for a vehicle trying to gain access to the State highway.

The situation was examined by engineers from the State Highway Department, representatives of the Board of Selectmen of Westford, and personnel from Division 1 and Group 75 at Lincoln Laboratory. It was found that the combination of the narrow, winding town road and dangerous intersection was such that the best and safest solution would be to construct a new road, extending the existing site access road directly to Route 40.

The design of the road extension is complete. Following a preliminary traverse between the two roads to obtain necessary grade data, a roadway centerline was selected, with the intersection with Route 40 given primary consideration. This intersection will be located about 155 feet west of the Westford-Groton town line at a point where sight distances of about 500 feet are possible. The alignment is such that the access road will not require any additional landtaking.

Subsoil explorations were made to determine depth of peat in a marsh area along the roadway centerline. These showed that the peat was not excessively deep, and could be removed

easily by common excavating methods. The roadway profile was established at a grade that would reduce the quantity of ledge excavation to a minimum and thus substantially reduce the cost and construction time of the road.

Plans and specifications have been completed. It is hoped that construction can start during the next quarter.

J. B. Paddleford

F. Tracking Antenna Tower

Groups 71 (Design Engineering) and 75 (Construction Engineering) are currently working on a system of modifying surplus Navy twin 5-inch 38-caliber gun mounts into tracking antenna mounts and drives. This work will be reported by Group 71.

One early installation of a "gun-mount tracker" will be at Millstone Hill. This installation will be used for several different projects, supporting antennas up to 60 feet in diameter. The mount will be supported on a cylindrical concrete tower 35 feet high and 12 feet in diameter.

The tower foundation consists of a reinforced concrete mat 10 feet below ground level, and triangular buttresses extending from the mat to ground level. The walls of the tower will be one foot thick, with pipe sleeves and structural inserts provided at convenient locations to carry internal platforms, ladders and cables. A concrete slab at the rear of the tower will support a house containing the electrical controls for the gun-mount drives. Access will be gained by a single door in the front of the tower and by ladders on the inside wall. An inverted gun-mount stand will be cast in the top of the tower to provide support for the modified gun mount. This installation will minimize alignment and machining problems in placing the mechanical equipment. The area surrounding the tower will be graded and fenced for security. In general, the electronic equipment will be housed in trailers parked adjacent to the tower.

Electrical power will be furnished at 480 volts 3-phase delta from a new transformer bank to be added to the existing substation. The power cables will be run underground in conduit from weatherproof outdoor switchgear to the electrical control house at the rear of the tower. This house, of frame construction, will contain the motor-starting contactors for the gun-mount drives and transformers to provide power at 120 volts 3-phase delta and 120/208 volts 3-phase wye for the electronic equipment. A second underground conduit will provide for future control and data cables to the radar site building. Lightning grounds will connect to the existing ground field.

The design has been completed, proposals received and a purchase requisition written. Construction is scheduled to start in October 1958.

E. L. Clarke
E. P. Gaudette

III. LABORATORY WORK

Because of changes in Laboratory programs and development of new equipment, the various laboratory units are continually being modified. These modifications include a revision of air-conditioning requirements for the FSQ-7(XD-1) computer.

A. Addition to Air-Conditioning System, FSQ-7(XD-1) Computer

The replacement of the original 64^2 plane memory with a 256^2 plane memory and auxiliary equipment required modification of the air-conditioning system. The original memory required a dual temperature supply consisting of air at a variable 60°F ± 2° for the vacuum tubes plus air at a constant 75°F for the magnetic core arrays. The new memory requires only a supply of constant temperature air. The original specification from IBM was for a source of 60°F air, based primarily on the availability of this temperature at SAGE production sites. Since the actual requirement is that the equipment be maintained at a constant temperature, the system for the XD-1 was designed on the basis of furnishing a supply of air at 56°F to make the best use of existing equipment.

An air-handling unit consisting of chilled-water cooling coil, fan and high-efficiency filter was installed at ceiling level in the basement of Building F. Preconditioned air is obtained from the air-handling unit furnishing air to the arithmetic frames. This unit has sufficient reserve capacity for the additional load and, like other units which provide air to the computer, supplies air at varying temperatures to its electronic frames to balance the electronic load and maintain a constant room temperature. With air entering the new air-handling unit at 58°F to 62°F, a modulating water valve controls the discharge air to the memory array at 56°F.

The control system is to be maintained at its present level of accuracy while incorporating the new memory into the supervisory alarm system. Taylor Industrial Controls have been specified since their past performance has shown high reliability and accuracy. A new continuous strip recorder will be installed on the supervisory panel, together with various warning systems covering air failure and temperature rise.

The unit is installed and in operation. The temperature control system is incomplete, however, and the system is operating with temporary industrial and commercial controls, pending delivery of the balance of the control elements. Using the temporary controls, temperature variations of one degree plus or minus were recorded. During such periods, tests on the computer showed that results were not adversely affected. The balance of the controls are expected in October, and final installation will be completed by December 1958.

H. G. Gechijian

IV. EQUIPMENT STUDIES

Studies of methods for air-conditioning various computer components and laboratory areas are an important part of the group effort. During the past quarter, in addition to the projects discussed earlier, a study was made to determine how to cool a new airborne data processor.

A. Air Conditioning for Airborne Data Processor

The Systems Design Group is constructing a transistorized airborne data processor to be used as part of the airborne long-range input (ALRI) project undertaken by the Laboratory. Some of the problems of providing cooling for this piece of equipment are obvious, such as size and weight limitations. Others include type of air circuitry to be used, control method and details of the cooling system.

The aircraft industry uses an air cycle system extensively. This type of system involves a high-speed turbine using ram air, and then expanding this air to obtain cooling. Such a system is compact and trouble free, but is not acceptable for the particular use required since the data processor must be capable of ground, as well as in-flight, operation.

Instead, a liquid-vapor-type system with a 28-volt DC motor-driven compressor using refrigerant 12 was selected. Since rapid delivery was required, vendors were contacted for information on presently-developed components. The Stratos Division of the Fairchild Engine and Airplane Corporation furnished drawings of a unit they had made for Bell Telephone Laboratories for a similar application. Investigation showed that this unit could easily be modified for the Laboratory's requirements. However, Fairchild informed us that, because of special components, delivery would require about four to five months. Fortunately, the Bell Telephone Laboratories' need for the original units had ended, and the units had been declared surplus. Arrangements have accordingly been made to obtain these units for the Laboratory.

The total computer heat load is approximately 3 kw, or about 10,000 Btu/hour, with about 2.5 kw due to the power supply and 0.5 kw supplied by the computer proper. The most critical element is the core memory section which must be maintained at a constant temperature of 70°F ± 1/2°.

The air circuiting has been arranged so that the system is a closed loop with two supply circuits and one return line. The main supply circuit feeds the entire top rear of the computer frame, with air flow over all components to the front of the plug-in units. This air, which is still relatively cool, is then directed over the power supplies at the base of the unit and returned to the cooling unit. The second supply circuit furnishes air to the memory core; this air then is exhausted into the main computer air circuit.

The memory core array temperature will be maintained at a constant level by a damper in its air supply line. The damper positioner will be controlled by an electronic temperature-sensing element located at the memory array air discharge. Under ordinary circumstances controlling such a small volume as the array within close limits would impose severe problems. However, since the array will operate effectively in a steady state or constant load condition, it is felt that a proper balance between air supply and ambient temperature can be obtained without too much difficulty.

At present the computer is under construction. No cooling equipment has been received, but it is expected within a month. Project completion is planned for December 1958.

H. G. Gechijian

DEVELOPMENT ENGINEERING
GROUP 76

HANNOOSH, M. M., *Leader*
BAGLEY, D. G., *Assistant Leader*

COHEN, A.
DAVIS, P.
HENSEL, S. L., Jr.
MALTESE, A. W.
MULDOON, R. A.
MURPHY, E. B.
NILO, S. C.
ORABONA, J. F.

DEVELOPMENT ENGINEERING
GROUP 76

I. INTRODUCTION

We have continued to stress the development of metal space-frame radomes and foam radomes. The 150-foot CW-412/FPS(XD-1) metal space-frame radome design was modified to assure its survival capability in winds up to 200 mph. The 68-foot CW-491 foam radome development was accelerated and the design was completed. This radome has spherical panels of polyurethane foam joined together with a similar foam material to achieve a uniform thin shell broad-band radome. Both radomes are being procured by Rome Air Force Depot. The 68-foot FLR-3 rigid radome was structurally tested for RADC. Tests indicate that it satisfies the structural design criteria. Electrical transmission data for metal space-frame radomes has been compiled and plotted for design reference. Wind tunnel data for pressure distribution over spherical radomes has been reduced and plotted in dimensionless form for design reference. An intensive foam material evaluation program is in process. We are accumulating data and information on weathering, electrical properties of foam at elevated temperatures, structural joint efficiency and foaming-in-place techniques.

Other activities include the antenna wind load study. The wind tunnel rotating model of the experimental radar antenna was completed and initial tests were made in the M.I.T. Wright Brothers Wind Tunnel. The model was damaged and is now being rebuilt.

The antenna test range has been approved and funds have been allocated. The specifications are complete and procurement will be initiated. A symposium on rigid radomes was conducted and the Proceedings of the Symposium are now available for distribution. Personnel from military agencies, industrial concerns and academic institutions in the United States and Canada attended the 3-day symposium.

Developments in component miniaturization through the use of printed wiring, plated connections and encapsulation are continuing. The printed-wire memory plane is being developed, and electroforming of complex parts has progressed to the point where this process could be established as a practical and convenient service facility.

II. RADOME DEVELOPMENT

A. The CW-412 150-Foot Metal Space-Frame Radome

1. Introduction

Service test funds have become available, through Cambridge Research Center's Lincoln Project Office, for the purchase of a CW-412 150-foot metal space-frame radome. It is anticipated that the radome will be delivered in September or October of 1959. To determine a method of erection and to evaluate the general design, the radome will be erected at a site near Lincoln Laboratory in November and December 1959.

Work during this quarter centered about the preparation of drawings and specifications for the procurement of the radome. These have been submitted to the Air Materiel Command at Griffiss Air Force Base by the Lincoln Project Office.

An investigation of the structural capability of the Laboratory radome design was conducted to assure compliance with a recent specification in BMEWS (Ballistic Missile Early Warning System) requiring wind pressure loading from 200-mph winds. This is the radome which will be procured with service test funds.

Preparations are being made to make full scale tests on components of the radome, as well as wind tunnel tests of a structural scale model.

2. Electrical Tests of Model Radome

The pattern data obtained for two versions of the trapezoidal hexecontahedron model radomes (Table 76-I) have been reduced with emphasis placed on examining the effect of the model radomes on the antenna side lobes for various antenna-to-radome orientations.

TABLE 76-I
DATA FOR RADOME MODELS EVALUATED

Type of geometry: trapezoidal hexecontahedron
Scale factor: 21:1

	RADOME A		RADOME B	
	Scale Model	Full Size	Scale Model	Full Size
Equatorial diameter	7.2 feet	150 feet	7.2 feet	150 feet
Base diameter	5.7 feet	120 feet	5.7 feet	120 feet
Member diameter	3/16 inch	3-15/16 inches	3/16 inch	3-15/16 inches
Hub diameter	3/4 inch	16 inches	1/2 inch	10-1/2 inches
Antenna diameter	4 feet	84 feet	4 feet	84 feet
Frequency	9250 Mcps	440 Mcps	9250 Mcps	440 Mcps
Transmission loss (one way)	0.6 ±0.1 db		0.6 ±0.1 db	
Average boresight shift	Not measured		0.2 milliradian	

For each radome, a number of principal plane pattern measurements were made so that a representative portion of the radome was sampled. Free space (no radome) pattern measurements were made before and after a given series of measurements with the radome. The angular position and level of each side lobe, within 50° to the left and right of the main beam with the model radomes were tabulated and compared with the applicable no-radome data. For a given polarization and plane, the change in level for a given side lobe as a function of radome positioning was prepared for histogram presentation. The associated free-space side lobe was similarly tabulated. Final grouping was made for side lobes having the same level in free space. The antenna patterns with no radome and the side-lobe grouping used for the model B radome, are shown in Figs. 76-1 through 76-4.

The data presented are a condensed version of the histograms prepared for detailed evaluation. The average change in side-lobe levels for the model radomes are shown in Figs. 76-5 and

76-6. It will be noted that between the 20- to 25-db levels, the radomes have little effect on side-lobe levels for all conditions. These levels correspond to the first two side lobes on either side of the main beam, 1-1 and 2-2.

For horizontal-azimuth and vertical-elevation polarizations, this trend continues to the 30-db level. For the same conditions, side lobes to the 38-db level show increases of 1.5 db. For vertical-azimuth and horizontal-elevation polarizations, increases of 3 to 4.5 db occur for free-space side lobes at the 30- to 38-db levels. The average change and upper and lower limits in side-lobe levels with the radome relative to the average side-lobe levels with no radome are shown in Figs. 76-7 through 76-9. Not included are levels, at either extremity, which occurred less than 2 per cent of the time. It will be noted that, for horizontal-azimuth and vertical-elevation polarizations, the radome performance is very good with maximum increases of only 3 to 4 db occurring at levels between 33 and 38 db. The vertical-azimuth and horizontal-elevation conditions show that the changes are more pronounced, since increases of 7 db can occur at the 30- to 38-db level. The next phase of this program will be to examine the geometrical configuration of the metallic members for the various antenna-to-radome orientations in relation to side-lobe performance, and to determine the member configuration which produces the least change for either polarization.

A. W. Maltese

3 Structural Analysis of CW-412, 150-Foot Radome

A recent specification of radome performance in BMEWS requires the structure to withstand wind pressure loading from 200-mph winds with stresses not to exceed the yield point of the material. The CW-412, 150-foot radome is of proper size for BMEWS and, since its electrical performance is acceptable for BMEWS application, an investigation of the structural performance to assure compliance with the BMEWS specification was accomplished. The following is a report of this investigation. In order to allow direct comparison of the structural performance with other radomes under consideration for BMEWS, the analysis is developed along lines used by the Goodyear Aircraft Corporation.*

In BMEWS the radome will operate in the proximity of a building which may influence the wind forces on the dome. To take this influence into account the following wind force coefficients were assumed in the analysis:

Drag coefficient , $C_D = 0.6$

Lift coefficient , $C_L = 0.9$.

These coefficients are unusually high for a radome structure with the geometric properties of the CW-412. The drag coefficient was taken from "A Study of Aerodynamic Loads on Large Spherical Radomes for Ground Installations," by J. Bezbatchenko, which appears in Volume I of the Proceedings of the Rigid Radome Symposium held at M.I.T. in September 1958. The lift coefficient is significantly greater than that given in the above report.

* Goodyear Aircraft Corporation, "Theory of Spherical Ground Radomes," S69-2 (1 May 1958).

A distribution of wind pressure was assumed in the form

$$C_p = \frac{P - P_\infty}{(1/2)\,\rho V^2} = A + B\cos\xi + C\cos 2\xi \quad ,$$

where P is the pressure at any point defined by the central angle ξ, P_∞ is the free-stream static pressure, and $(1/2)\rho V^2$ is the free-stream dynamic pressure. A, B and C are constant coefficients dependent upon the radome base truncation angle and the drag and lift coefficient parameters. They are given by the system of equations

$$C_D = \frac{B}{3}(2 - 3\cos\psi_b + \cos^3\psi_b)$$

$$C_L = \sin^2\psi_b[-A + C(1 - (1/2)\sin^2\psi_b)] \quad ,$$

where ψ_b is the truncation angle. This system leads to the following values for the CW-412:

$$A = -0.610$$

$$B = 0.510$$

$$C = 1.100 \quad .$$

A plot of the pressure distribution with these values of A, B and C is shown in Fig. 76-10. As shown in the figure, there is some discrepancy between the analytical distribution and that observed in wind tunnel tests. This discrepancy might be reduced by considering additional terms in the analytical distribution.

Calculations of beam-column stresses, following procedures as outlined in the Division 7 Quarterly Progress Report for 15 April 1958, indicate that the yield point is reached in winds of about 208 mph.

Buckling of a column about a minor axis is found to be critical if the effect of the elastic restraint provided by the panel skin is neglected. However, preliminary calculation of the spring constant of the panel skin indicates that the skin will be effective in providing restraint, and therefore must be considered in the column-buckling calculations. When this restraint is taken into account, column buckling is no longer more critical than the yield point stress criterion.

General instability calculations, following procedures outlined in the above-mentioned quarterly progress report, indicate that the major portion of the margin of safety previously allowed has been used. However, it is believed that the criterion used in calculating the general instability by means of an equivalent shell is conservative because proper emphasis was not placed on the bending rigidity of the space-frame construction. This is indicated also by preliminary direct calculations of the buckling of the space frame.

The distributions of stress resultants at the base of the CW-412 radome are shown in Fig. 76-11 and the base geometry is shown in Fig. 76-12. By multiplying the proper stress resultant by a suitable characteristic length determined from the base geometry, the forces in the base fittings are obtained. Characteristic lengths and the resulting forces in the most highly stressed base fittings are given below.

Base Fitting	Characteristic Lengths		Forces in Fittings	
	Shear Stress (inches)	Meridional Stress (inches)	Shear (lb)	Meridional (lb)
P	322	143	349,800	132,100
Q	0	138	0	127,500
R	304	0	330,200	0
S	0	185	0	170,900
T	304	0	330,200	0
U	0	138	0	127,500
V	322	143	349,800	132,100
X	0	101	0	93,300
Y	0	101	0	93,300

Detailed analysis of the stresses at the base of the CW-412 radome, resulting from the above forces, indicates that the radome base design is not critical for BMEWS specifications.

An estimate of the deflections at the equator of a uniform thickness shell with the geometric properties of the CW-412 resulted in the nondimensional plot shown in Fig. 76-13. By using the average extensional rigidity of the CW-412

$$(Eh)_{shell} = \left(\frac{E_a A}{L}\right)_{frame} \cong 5.2 \times 10^5 \text{ lb/inch} \quad ,$$

where E_a is the elastic modulus of the aluminum member, A is the cross-sectional area, L is the characteristic length for an average triangle, it is possible to estimate the deflection of the space frame. For example, the nondimensional radial deflection at the stagnation point is

$$\delta\frac{Eh}{qR^2} = -1.45 \quad ,$$

and at 200 mph

$$\delta = -1.85 \text{ inches} \quad .$$

This estimate may be expected to be low since linearity of the load-deflection process was assumed. Nonlinearity may increase the deflection by a factor of 2 or 3. However, deflections of this order of magnitude are not expected to influence measurably the electrical performance of the CW-412 radome.

On the basis of an analysis as outlined above, it is concluded that the CW-412 radome satisfies the BMEWS structural specifications. In addition, the performance of the structure under load is not expected to influence measurably the electrical performance of the CW-412 radome.

P. Davis
R. A. Muldoon

4. Tests and Mockups of Full Scale Components

a. Sealing Test Mockup

The sealing test mockup for the 150-foot radome was completed. This consisted of a full size panel of 1/8-inch Techwood, three full size beams and hubs of wood, and six short beams all attached to one hub. Actual neoprene panel seals, hub cap seals and beam-hub seals were used. An actual metal hub cap was also obtained. These parts assembled easily and formed a full scale mockup of a panel and all of the parts surrounding one hub. Preliminary water tightness tests indicated that the hub seal and panel seals were satisfactory, but very slight leakage occurred at the beam-hub seal. Parts are being modified now and further tests will be conducted. The typical hub mockup for sealing tests is shown in Figs. 76-14, 76-15 and 76-16. The large panel had been removed prior to this photograph. The one-quarter scale wooden mockup of the base fittings and panels is now being constructed and will be used to check base layout dimensions.

The Niforge Corporation delivered two high-strength aluminum hub castings and a preliminary report of strength characteristics on 27 August 1958. This completed Phase I of their tests; Phases II and III cover similar information on steel and magnesium castings.

The membrane attachment mockup is shown in Figs. 76-17 and 76-18. This consisted of the actual metal cap strips, special nuts, spring clips, bolts, panel edging and aluminum panel sections to simulate the fiberglass panels. These items were mounted to the top of the beam extrusion. The sides and bottom of the beam were completed in wood, and a wooden end fitting and wooden hubs were made. The parts assembled to show a section of beam with panel attached and the beam end-fitting hub joint. Parts of this mockup will be used for structural testing. Two hub caps were fabricated and heat-treated and are now ready for structural testing. The hub cap and seals are shown in Fig. 76-19.

A structural test program for testing the component items will be initiated in the near future

b. Design Changes

As a result of a 200-mph maximum wind condition in BMEWS requirements, it was decided to incorporate additional load-carrying ability in the hub joints to meet the 200-mph wind condition at design yield stress.

The hub joint was modified to a split hub of two aluminum plates 1-3/4 inches thick. The end fitting was changed from aluminum to high-strength steel. The hub bolts and beam bolts were increased in size to carry the additional load. A mockup of this joint is shown in Fig. 76-20. The end-fitting mockup is shown in Fig. 76-21. This change was incorporated prior to delivery of drawings to the Air Force on 29 September 1958.

An improved method was found for determination of wind loads acting on the base fittings. Preliminary analysis has indicated that the base beam members will be increased in wall thickness from one-half to one inch. This change is now in progress.

c. Foundation

A tentative site for erection of the first radome has been selected. The foundation is being designed for a wind loading of 100 mph.

d. Presentation

A design description and cost analysis was presented at Lincoln Laboratory on 4 September 1958. The organizations represented were: BMEWS Project Office of the Air Force, Radio Corporation of America, Goodyear Aircraft Corporation, Lincoln Project Office and M.I.T. Lincoln Laboratory.

L. P. Farnsworth
T. F. King

5. Structural Model Tests

A structural test of the CW-412 150-foot-diameter radome under wind loading or simulated wind loading is both expensive and inconvenient. Preliminary investigation indicated that tests of structural models, on the other hand, are quite feasible. Feasibility was established in studies which considered and proposed solutions for the following problems:

(a) The laws of similarity and prediction which apply to a model of the radome,
(b) The possibility of simulating the structural characteristics of the radome on a small scale, and methods of construction,
(c) Methods of loading the model,
(d) The minimum size of a practical model which will simulate the structure and which can be instrumented with reasonable accuracy,
(e) Required instrumentation and test program,
(f) Accuracy and reliability of the resulting data.

Results of a study by Dynametrics, Incorporated, under contract to Lincoln Laboratory, were reported in their report No. 257-001, "The Feasibility of Investigating a Large Radome by Means of Structural Models and Proposed Methods of Testing." This study corroborated the results of an independent study by Laboratory personnel.

The primary objective for testing a structural model of the CW-412 radome is to prove the structural stability and strength of the radome. A secondary objective is to prove or disprove the validity and accuracy of the methods of analysis To accomplish the primary objective it is necessary to simulate the full scale loading conditions as accurately as possible. This may be accomplished best by testing the radome structural model in a suitable wind tunnel. Instrumentation for: (a) stresses in the radome, (b) deflections and modes of buckling of the radome, and possibly (c) wind pressure distribution on the radome surface will aid in the secondary objective.

Investigation of wind tunnels indicates that the NACA 30 × 60 foot tunnel at Langley Field, Virginia, has a maximum wind speed capability of 118 mph. Although the wind tunnel is physically large enough to accommodate a reasonably large-size structural model, its wind speed capability is limiting. The NACA 40 × 80 foot wind tunnel at Moffett Field, California, has a capability of about 250 mph and appears to be the best suited for the test of large structural models. Informal inquiries regarding wind tunnel time have indicated that the only time available is on a short-term basis between the wind tunnel major projects. This implies that instrumentation must be accomplished without dependence upon wind tunnel personnel and facilities. A formal request is being processed for wind tunnel time on a short-term basis at the NACA 40 × 80 foot wind tunnel.

Drawings of a radome structural model are presently being prepared. The structural model satisfies the laws of similarity and, since it is one-tenth full scale, can be constructed practically. The drawings will be completed during the next quarter at which time bids for model fabrication will be requested.

P. Davis

6. Erection Procedure Studies

Previous quarterly progress reports have evaluated various techniques for erecting a 150-foot radome in an arctic environment. Work during the past quarter has been concerned primarily with erection of the service-test radome on a local site. The procedure developed for this operation is not necessarily designed to resist the severe climatic conditions of the Arctic, but there are indications that it may be feasible to modify the local technique for such use.

The erection of the radome at a local site is based on the "scaffold technique" discussed in the Division 7 Quarterly Progress Reports of 15 April and 15 July 1958. This technique involves erecting a central core of staging and using this as a working platform to provide access to and support of the radome structure as it is assembled. It is similar to the method used for work on interiors of large open areas such as cathedrals and auditoriums. The problems involved in such a method include designing the scaffold to conform to the interior contour of the radome and providing sufficient restraint to tie the entire scaffold assembly into a single structural system. Once this is done, the scaffold provides an excellent means of temporary support for the radome structure in case of bad weather or unforeseen delays. The steps involved in such a procedure are discussed below.

a. Crew Size

In planning the erection procedure, the first decision was the number of men to be used. The radome is geometrically symmetrical in five sectors, and the sector widths are such that each could provide working area for two crews; with three men on the scaffold and two handling material, each crew would have five men, or a total of fifty men. In addition, it would be advisable to have an additional pair of men in each sector to handle changes in the scaffold and hoist rigging as the erection proceeds, to avoid delay in assembly operation. The detailed procedure is based on a maximum crew size of sixty men. It should be noted that this is for maximum efficient speed; for local erection where time may not be the most important factor, the crew size may be scaled down and the time scaled up linearly as conditions warrant.

b. Stockpiling

The first step in any structural erection is to "shake out," or sort, all the various items into stockpiles to minimize working time once the assembly begins. In view of the symmetry of the structure and the crew assignment, it was decided that, for the framed radome, the material should be sorted into stockpiles for each sector; this would minimize handling time and difficulties.

c. Scaffold

In a local environment the erection of the scaffold might precede the stockpiling operations, especially if the scaffold is rented for the operation. The order of these steps will, in a large part, be dependent on the particular circumstances. Erection of the scaffold will probably be

completed before starting radome erection; however, in an arctic environment it may be desirable to erect the scaffold in stages to minimize icing problems. Figure 76-22 shows a typical scaffold arrangement.

d. Radome Framework Assembly

Erection of the framework would commence from the ground up, by fitting each beam into place and bolting it up. Materials would be hoisted into place up the outside of the structure until the equator is passed, and then up open shafts in the scaffold inside the framework. Hoisting rigging would consist of small electric winches and light lines through pulleys mounted ahead of the erection crews. This rigging would be moved as needed by the scaffold maintenance crew. As much preassembly should be done as possible; certainly hubs would be fastened to beams where possible on the ground, and it may prove practicable to bring up complete triangular assemblies in one lift. As the framework erection nears completion, the erection crews may begin to interfere with one another. If so, the surplus crews would be reassigned to begin installation of the membrane.

e. Membrane Attachment

Membrane installation is the most difficult step in the procedure. The individual sheets are large and thin, with no lateral stability. This means that some sort of jig must be developed to hold them in position until they can be fastened to the structure. Present planning envisions an oversize pipe framework mounted on large bicycle-type wheels at the corners. The membrane would be held in position by vice-grip clamps mounted on spring attachments. The jig would be hoisted up over the exterior surface of the radome, with membrane installation working from the ground up. At the working area, the erection crew would use hand-held vacuum clamps to pull the skin into position, and one or two men working in bosun's chairs would install the cap strips.

f. Disassemble Scaffold

The final operation would be to disassemble the staging and remove it through an opening in the base of the radome.

g. Time and Cost Estimates

Preliminary estimates indicate that the time involved in this procedure is between 8500 and 10,000 man-hours, including scaffold work. However, some assumptions have been made concerning working efficiency which can only be tested in the erection operation. A separate estimate of scaffold requirements indicates that the cost of the scaffold for this radome, erected and dismounted once, would be about $124,000. If the scaffold were rented, the cost would be about $29,000.

h. Adaptability to Arctic Environment

Earlier quarterly progress reports (i.e., 15 April and 15 July 1958) noted that there were certain difficulties to be expected in an arctic environment with a scaffold erection system. In general, these would be due to ice accumulations on the scaffold and structure, to wind and cold weather delaying and slowing down work on the scaffold, and to problems involved in hoisting all the material up to position. However, there are certain advantages that may balance these difficulties. First, the scaffold can be made an exceedingly stiff structure by cables and braces, and

so provide a firm restraint for the partially erected structure. Second, even though the scaffold is expensive, the other methods proposed are much more expensive, and in addition will require extensive detailed design and special manufacture. The scaffold is generally standard. Third, the scaffold can be used for other operations and is not limited to this special use.

D.C. Moore (Group 75)

B. The 68-Foot CW-491 Foam Radome

1. Introduction

AFCRC has a requirement for six 68-foot equatorial-diameter radomes for the AN/FPS-30 radar sets to be installed in the Arctic. The electrical requirements for FPS-30 radomes are not so stringent as to dictate the use of foam as the structural material. However, a thin-shell solid-foam radome was recommended since it would satisfy the basic FPS-30 requirements and also provide the opportunity to advance the development of radomes at the same relative cost as other types of structures. Also, it was realized that if foam radomes were obtained for these installations, they would serve as scale models for larger radomes. Thus, the electrical, structural and assembly characteristics of foam radomes can be studied and the feasibility of constructing larger radomes of this type evaluated. The larger radomes, 150 to 300 feet in diameter, may be used for the large tracking systems which have more stringent electrical performance. Radomes smaller than 68 feet in diameter presently perform over the UHF to C-band frequency range. For extremely large sizes it is anticipated that foam radomes will perform with improved electrical performance over all-dielectric space-frame-type radomes. Since the electrical performance of the foam design is considered to be frequency insensitive, it will offer a frequency broad-band standard design through C-band and possibly higher.

Lincoln Laboratory drawings S-8268 and AFCRC Exhibit No. 58-8A have been submitted through the AFCRC Lincoln Project Office to the Air Materiel Command at Griffiss Air Force Base for procurement of six foam radomes. Air Force nomenclature for these radomes is CW-491/FPS. The structure will be built of blocks of polyester polyurethane foam. Considerable effort has been spent on a means of fastening the blocks together to form the radome. Two methods of approach have been investigated; mechanical fastenings and foam welding by foaming the joints of the blocks in place. Since the welding technique appears more promising, the present CW-491 incorporates the foamed joint method of panel attachment. This results in a uniform thin-shell broad-band radome.

The method of erection will depend to some extent on the method of joint attachment. Studies are being conducted on several types of erecting techniques.

S.C. Nilo

2. Electrical Design

The CW-491 radome design is for optimum electrical performance over the UHF to C-band frequency range (300 to 5900 Mcps). The anticipated electrical characteristics of the foam radomes are:

(a) 0.5-db maximum loss in main beam,

(b) Negligible increase over the antenna-pattern free-space side-lobe levels,

(c) Negligible beam distortion, boresight shift (0.5 milliradian maximum) and rate of change of boresight shift.

Stringent electrical performance in boresight shift and boresight shift rate is particularly required in radome designs for projects such as BMEWS and Nike-Zeus. From the electrical point of view the concept utilized in the CW-491 radome is applicable to system requirements irrespective of frequency and boresight requirements.

The resultant radome (68-foot equatorial diameter, 56-foot base diameter and 53-foot 3-inch height) is a continuous and uniform shell of low-loss dielectric material whose properties are not dependent on frequency for performance and offers negligible boresight errors.

S.C. Nilo

3. Geometry

The design is based on the fabrication of cast polyester polyurethane curvilinear square and triangular panels derived by circumscribing and subdividing the small rhombicuboctahedron, a semiregular polyhedron having 18 square faces and 8 triangular faces (Fig. 76-23). The first step in the subdivision of the circumscribed figure is to divide the square faces into four equal spherical quadrilaterals by means of great-circle arcs drawn from the midpoints of the opposite sides. Each of these is then further subdivided into four more parts in such a way that two of them are equal to each other and the other two are mirror images. The triangular faces of the basic polyhedron are divided into nine essentially equilateral spherical triangles; the six meeting at the center are equal and the three at the vertices are equal. Thus, the main portion of the radome can be assembled with five different types of panels.

Since a radome is a truncated sphere, a modification of the regular panels is usually made where they are intersected by the base plane. If this procedure had been followed in this case, nine variations of the five regular panels would have been required for the so-called base panels. Most of these would have been relatively small in comparison with the full size panels, and since it is planned to weld the panel edges of the assembled radome with a foam-in-place technique, more linear feet of panel edges would have been required than with the procedure that was used. With these points in mind, a modification of the circumscribed polyhedron was made below the belt of basic square faces encircling the equator. The vertical great-circle arcs forming the sides of these faces were extended to the base circle. The latter was divided into 32 equal parts and great-circle arcs were drawn from these points to the corresponding lower corners of the first row of regular radome panels. Four different types of these base panels are required, two of them are mirror images of the other two. The base edge of each of these panels is the same, so the problem of securing the radome to its mounting ring is simplified with this modification.

Figure 76-23 summarized the procedure followed in the subdivision, and shows the different types of panels identified by letters. The "L" or "R" following the first letter identifies these panels as being mirror images. A total of 276 panels of 9 different types are required for each 68-foot radome.

J. Orabona

4. Structural Analysis of a 68-Foot Foam Radome

A 68-foot-diameter foam radome has been designed and is currently under procurement. The radome consists of panels which will be welded together by a foam-in-place technique When erected, its structural behavior will be that of a uniform thickness spherical shell with no surface discontinuities except at the base plane.

The anticipated mode of failure of the structure is general instability of the thin spherical shell under external pressure loading. The shell thickness required is obtained from Tsien's* equation for buckling pressure under "dead weight" loading conditions

$$P_{cr} = 0.28\, E\left(\frac{t}{R}\right)^2 \quad ,$$

where P_{cr} is the external buckling pressure, taken here as 20 per cent greater than the dynamic pressure due to 150-mph winds at −10°F at sea level, E is the elastic modulus of the dome material, t the thickness of the shell and R the shell radius.

A characteristic of foam material is that the elastic moduli in compression, tension and flexure are not identical. It is necessary, therefore, to transform the foam shell into a mathematical equivalent which retains invariant the rigidities influencing general instability. This is accomplished by the transformations

$$E_e t_e = E_c t_s$$

$$E_e t_e^3 = E_f t_s^3 \quad ,$$

where the meaning of the subscripts is: e, equivalent; c, compression; f, flexure; and s, shell. These transformations result in an equivalent thickness and modulus of elasticity

$$t_e = t_s \sqrt{\frac{E_f}{E_c}}$$

$$E_e = E_c \sqrt{\frac{E_c}{E_f}}$$

These expressions may be substituted directly into Tsien's buckling criterion resulting in

$$t_s = 1.4056 \frac{R}{(E_c E_f)^{1/4}}$$

The use of commercial brochure data published by the Hooker Chemical Company leads to plots of thickness and weight as functions of foam density (Fig. 76-24). The present design, based on a foam density of 14 pcf, requires a thickness of 4.5 inches and is expected to weigh about 60,000 lb.

Stresses at the radome base may be approximated by using the distribution of stress resultants shown in Fig. 76-11. Material stresses are obtained by dividing the stress resultants by the shell thickness. Stresses in the 68-foot radome resulting from 150-mph winds are rather low; e.g., at about 70° azimuth at the base

$$\sigma_\psi = 52 \text{ psi tension}$$

$$\tau_{\Theta\psi} = 60 \text{ psi shear} \quad .$$

* H.S. Tsien, J. Aeronaut. Sci. 9, 373 (August 1942).

The minimum strength of foam specified was 250 psi. The foam weld joints must be strong enough to sustain combined loads from distributions similar to Fig. 76-11 with reasonable margins of safety.

A first approximation to the bending stresses in the radome shell indicates that the maximum bending stress amounts to about 4 per cent of the maximum membrane stress. Additional bending stresses may be expected as a result of the surface discontinuity at the base of the radome. According to St. Venant's principle these stresses should be localized in a small region at the base. Although no analysis has been attempted, it is believed that the design has an adequate margin of safety in strength to accommodate this localized bending.

P. Davis
J. F. Orabona

5. Mechanical Design

Design was started 28 July 1958 and was completed on schedule 15 September 1958.

The original design was based on the small rhombicuboctahedron panel geometry with a wall thickness of 4-1/2 inches. Mechanical anchor panel fasteners were included to hold the panels in place in winds up to 60 mph. Foam-in-place joints completed the panel joint and provided design capability to withstand 150-mph wind loading. Two 3-foot-diameter aluminum access doors were provided, one at the top and one at the base. A pulley and navigation lights were provided at the top also. An equipment access door was provided at the base by allowing removal of 3 base panels.

In view of advancements in foam-in-place techniques, it was decided to aim for higher electronic capabilities for this radome. On 29 September 1958, it was decided to remove all mechanical panel fasteners and rely solely on the foam-welded joint This redesign was completed 8 October 1958, and drawings were delivered to the Air Force for procurement action.

a. Panel Joint Tests, Embedded Mechanical Fasteners

As part of the initial design a quick but rather extensive test program was undertaken to determine an adequate anchor configuration for the foam panel mechanical joint

The requirements for this joint were to obtain the best load-carrying ability with the smallest over-all length and width dimensions and the smallest cross-sectional area.

The initial family of anchors were designed as straps with various shapes on the section molded into the foam. The strap was selected to dissipate the concentrated load on the joint as gradually as possible into the foam. Panels of 2-3/4 inch thickness were used because molds for panels of this size were available. Tests will be conducted at a later date on the 4-1/2 inch panels with mechanical anchors. Results of these tests and photographs of failed panels are shown in Figs. 76-25 through 76-44 and Table 76-II.

Two conclusions were drawn from the early tests. First the strap was too wide (1-3/8 inch width was chosen, or one-half of the panel thickness). Initial cracking usually occurred directly in line with the anchor, although this was not always the final path of failure. From this observation, the first conclusion was that a circular cross section such as a rod would have an advantage in load-carrying ability over the elongated section of the strap. A disadvantage would be the increase in metallic area for electronic blockage The second conclusion was that failure usually

TABLE 76-II

TENSILE TEST RESULTS OF POLYURETHANE FOAM PANELS WITH METALLIC ANCHORS

Dwg. No Bx-2257-	Title	Average Breaking Load (1), (2)		Foam Test Specimens (3) Average Values				Foam (4) Material	Approximate Joint Efficiency (per cent)	Figure Reference
		12-inch Width 33 in.²	20-inch Width 55 in.²	Density (pcf)	Ultimate Tensile Strength (psi)	Tensile Modulus ($\times 10^{-3}$ psi)	Elongation (per cent)			
57	Strap, flat type		1780 ①	9.5	164			H	19.8	76-25
57	Strap, flat type		2160 ①	12 2	285			H	13 7	76-26
57	Strap, flat type		1610 ①(7)	12 0	262			H	11 2	76-27
58	Strap, large, corrugated	1460 ①						N	14.6 (8)	
59	Strap, small, corrugated	Strap failed								
60	Strap, ribbed type	2150 ①						S	21 5 (8)	76-28
61	Strap, serrated	2070 ①						H	20.7 (8)	76-29
61 (Mod)	Same, 2 inches shorter	2170 ①		15.4	370			H	17.7	
62	Strap, tube end	1800 ①						S	18 0 (8)	76-30
63	Strap, bent with rod	1340 ①	(9)	11 7	375	28 5	1 73	S	10 8	76-31
64	Strap, flat with bow	2565 ①		11 6	290	24.0	1.26	S	26.8	76-32
65	Strap, perforated	1230 ①	(5)					S	12.3 (8)	76-33
66	Strap, flat with column	2100 ①						S	21.0 (8)	76-34
67	Strap, flat with 3 columns	1500 ①						S	15.0 (8)	76-35
81	1-inch bolt with aluminum ball end	4872 ①		12 2	365	25 0	1 72	S	40.4	76-36
82	1-inch bolt with polystyrene ball end	Not tested yet								
	3/4-inch eyebolt	3530 ①			320			S	33 5	
	3/4-inch rod, spherical end	1330 ①	(5)					S	13 3 (8)	76-37
	Strap, wooden ball end	1470 ①	(5)					S	14 7 (8)	76-38
	1-1/2 inch bushing	2230 ①		12.4	300			H	22 3	76-39
	1-1/2 inch bushing and 0 032 Aluminum plates	1560 ①	(6)					N	15 6 (8)	

NOTES (1) Foam panel thickness 2-3/4 inches.
(2) Number in circle refers to number of panels tested.
(3) Tensile specimens tested as shown in Figs. 76-43 and 76-44 on Instron TTC-M1 10,000-lb. tester.
(4) (H) Hooker Chemical Company No. 126 foam (14 pcf nominal).
(N) Nopco Chemical Company B-614SS (14 pcf nominal)
(S) Pittsburgh Plate Glass Selectrofoam 6002, 6003 (14 pcf nominal).
(5) Selectrofoam does not adhere to metal as well as the Hooker 126.
(6) Bushings were not aligned properly and appeared to induce bending
(7) Internal cracks throughout panel.
(8) 300-psi ultimate tensile strength arbitrarily used for panels which did not have tensile test specimens.
(9) Small rod evidently failed first.

occurred at the very end of the anchor at approximately the same breaking load, splitting across the panel. The shape of the strap did not seem to affect the load-carrying ability when the end of the anchor remained in the shape of the strap. These results indicated a stress concentration at the inner end of the anchor. The shapes most likely to minimize this effort would be a spherical, ball end or a circular section.

A standard 3/4-inch-diameter eyebolt was the most readily available item to fit these requirements. The test of this eyebolt realized a 60 per cent increase in strength over the strap-type anchor. By using a 1-inch-diameter rod with a 2-inch-diameter ball end, an even greater increase, up to 100 per cent over the strap-type joint, was realized.

These tests have been conducted to provide information on selecting a shape for the mechanical anchor rather than to obtain exact load-carrying abilities of any one shape. Because of this, testing was limited to one or two panels of each anchor configuration. During the next reporting period tests will be conducted of the more promising configurations in 4-1/2 inch thick test panels.

L. P. Farnsworth
T. F. King

6. Foam-In-Place Panel Weldment Technique

The present concept for erection of the radome is to interconnect the foam panels by temporary mechanical straps. The permanent erection is then effected by removal of straps after panel interweldment. The weldment is made with polyurethane prefoam, deposited as a charge in a submerged elliptical cavity along the panel seam edges. The panel interweldment results from the adhesive bond of cured-foam interfaces between adjoining precast panels.

a. Foaming Equipment

Various automatic metering, mixing and dispensing equipments were evaluated for the foam panel weldment technique study. The equipments investigated were from the Nopco Chemical Company (Nopcometer), Newton Tool and Manufacturing, Martin Sweets, National Aniline, and Minnesota Mining and Manufacturing. Evaluation was made on the basis of ability to deliver metered foam material formulation constituents within panel edge seam cavities under field site erection conditions. Necessary features are: accurate delivery, over a small delivery rate range, below 5 lb/minute of profoam; rugged construction for shipment and handling during erection; long-term maintenance-free reliable operation and cost.

The 3-M Brand Formulator (Mod. A) and Turbulator Gun (consisting of a metering unit modified to handle polyester polyurethane rigid prefoam systems) has been purchased. The mixing head is integral with the spray gun, which is capable of delivering both pour and spray material.

b. Panel Joint Tests (Polyurethane Foam Weldment)

Time has been scheduled (December 1958) in the climatic chamber facility at the Environmental Protection Research Division of the Quartermaster Research and Engineering Command at Natick, for panel weldment studies. As part of the foam weldment technique study, climatic conditions of temperature, humidity and wind velocity will be simulated in the environmental

chamber in order to determine the joint efficiency of various foam formulations, and also to determine the optimum climatic conditions for panel weldment.

In anticipation of receipt of the 3-M unit at Lincoln Laboratory, a total of 17 welded joints is being made, using the 3-M unit and both Scotchfoam I and Pittsburgh Plate Glass 6002-6003 weldments for panel pullout testing.

For this study a total of 34 foam tensile pullout panels were cast by the batch process. They consisted of both one shot and/or prepolymer systems of Hooker 126, Pittsburgh Plate Glass 6002-6003 and Nopco Lockfoam B-614SS polyester polyurethane rigid foams of nominal 14 pcf density. The polyester resin, water, surfactant, catalyst and tolylene diisocyanate or isocyanate-rich prepolymer formulation ingredients were mechanically dispersed by a Hobart mixer.

Various panel edge configurations were considered, such as closed box channel, open V and V notch grooves, and closed elliptical channels. The latter configuration was chosen as the most promising, and accordingly the next phase of the study incorporates the technique of foaming through "pigeon-holes," i.e., depositing within an unexposed recess.

Initial weldment data were obtained on joints welded by a batch operation of pouring foam premix into panel butt joints. Figures 76-45 through 76-48 show welded panels, and Table 76-III

TABLE 76-III
DATA FROM INTERPANEL WELDMENTS

22 × 20 × 2-3/4-Inch Panels
Weld Area = 22 × 2-3/4 Inches (× 1 inch thick)

Panel Nos.	Type of Cure	Fracture Load
3-4	Oven	4810
7-8	Oven	3190*
9-10	Oven	4230*
11-12	Oven	4920*
13-14	Oven	2950*
1-2	Heat lamp	2330

* Fracture did not occur at weld. Therefore, weld strength is higher than these values.

gives the results of preliminary tests of this method of connection. The foam welds were made one inch wide with Hooker 126A foam, which requires a post cure (the same material as the panels). In cases where the curing was done with heat lamps, much lower joint strength resulted. Other foam welds were cured in an oven and these show the highest joint strength values yet obtained. In fact, fractures occurred (with only one exception) not at the joint, but at the end of the panel where the load was applied. To eliminate this condition future tests will be conducted on specimens with a reduced section at the foam weld.

S. C. Nilo

C. Pressure Distribution on Radome Surfaces

A program to measure the distribution of wind pressure around radomes has been undertaken by the M.I.T. Wright Brothers wind tunnel. The distribution of wind pressure around a spherical, smooth-surface, tower-mounted radome has been obtained. The data are reported in the Aerodynamical Laboratory Report No. 963, "Lincoln Laboratory Spherical Radome and Tower." Wind pressure distribution measurements have also been made on a spherical, faceted, tower-mounted radome. These measurements are reported in the Aerodynamical Laboratory Report No. 964, "Lincoln Laboratory Geodesic Radome and Tower."

The radomes tested are 1/24 scale models of 55-foot-diameter radomes. They are made of polished mahogany of 27.5-inch diameter. The distance from the center of the sphere to the top of the base is 5.728 inches. The base is a regular 12-sided prism with a height of 12.0 inches. Photographs of the models are shown in Figs. 76-49 and 76-50.

The models were mounted on the flush floor mount which simulated the ground effect on the radome and permitted forces and moments to be obtained on the mechanical balance system. Pressure taps were installed along two longitudes; one in the center of a base flat, one on the corner of the base. These longitudes were 15° apart. Additional pressure taps were installed at various locations on the faceted model as shown in Fig. 76-51. The distribution of wind pressure was obtained by indexing the model and base on the balance mount through various yaw angles. Results were reduced to coefficient form and tabulated. No plots were included in the reports.

The studies have revealed that the geodesic (faceted) construction does not result in any gross changes in the pressure distribution, only local differences due to change in local geometry. The edges and corners of the geodesic surface produce lower pressures than the pressures on the smooth radome. The fact that lift and drag coefficients are nearly unchanged by the geodesic construction indicates that any large deviation in pressures must occur over small regions.

The results were examined more fully during this quarter by means of detailed plots. Pressure distribution curves for the spherical and faceted radomes drawn along vertical planes through the zenith at various yaw angles are shown in Figs. 76-52 and 76-53. The distributions of pressure along horizontal planes at various elevation angles on both radomes were also plotted. Typical plots are shown in Figs. 76-54 and 76-55. A few plots of the localized pressure variation at the facet edges and corners are shown in Figs. 76-56 and 76-57.

Graphical integration of the pressure curves is planned for the next quarter. This integration will provide a comparison between the pressure loads and the measured resultant air loads. The comparison should establish compatibility between the pressure distribution and the resultant air loads.

An extension of this study, involving consideration of tower height and base angle parameters, is planned. Variations in tower geometry may also be considered. A further generalization of the study will be made to include the pressure distribution around other surfaces of revolution with possible application to radomes.

P. Davis
W. Chafe

D. Structural Load Test of the 68-Foot Radome CW-408/FLR-3

1. Introduction

The structural load test designed to demonstrate the general buckling capability of the CW-408 rigid radome was conducted by Lincoln Laboratory at its test site in Lexington, Massachusetts, by request of RADC. The CW-408 is shown in Fig. 76-58.

2. Description of Test Equipment

Loads were applied at each of 31 joints near the zenith of the dome by means of chains (Fig. 76-59). Each chain was attached inside the hub at the end of the stiffener by means of connecting plates. Only alternate stiffeners were directly loaded by the connecting plate and chain assembly, each joint being loaded by three chains.

The chains were of equal lengths, were connected to the top eye of an eye-and-eye swivel by means of connecting chain links and were assembled in such a way that the resultant force passing through the swivel also passed through, or close to, the apex of the panel group. A pulley block was hooked to the bottom eye of each swivel. An additional 30 pulley blocks were attached by means of individual chains to individual eyebolts on a loading platform, which was suspended by means of a continuous wire rope reaved through the upper 31 and lower 30 pulley blocks. The platform was positioned to converge the 31 resultant forces to the center of the dome.

Suspended from the loading platform by means of a shear pin was a calibrated load cell or tension link made of high-strength steel on which were mounted SR-4 strain gages. The tension link was calibrated in a load-testing machine and the calibration curve is shown in Fig. 76-60. Strains were read on a Baldwin-Lima-Hamilton strain indicator. A 35-ton hydraulic cylinder was used below the load cell to apply the loads. The cylinder was connected by means of a turnbuckle and rod system to an anchor plate embedded in the reinforced concrete foundation. Thus a retraction of the cylinder rod forced the radome down against the reinforced foundation. The assembled test equipment is shown in Fig. 76-59.

3. Test Procedure

Before the test began it was noted that one hub, about midway between the equator and the zenith, was missing. Investigation revealed that the hub which had been provided was not the proper type, did not fit into place and was omitted in the erection. An attempt at loading without the hub in place was made by placing 30,000 lb on the radome in three equal increments. This resulted in some local fractures in the panel skins surrounding the hubless joint. The damage is shown in Figs. 76-61(a) through (d). Testing was halted until the hub provided was machined to size and placed into position. The test resumed with the following loading sequence:

Load No.	Weight Applied (lb)	Load No.	Weight Applied (lb)
1	0 to 30,000	6	30,000 to 40,000
2	30,000 to 0	7	40,000 to 50,000
3	0 to 10,000	8	50,000 to 55,000
4	10,000 to 20,000	9	55,000 to 60,000
5	20,000 to 30,000	10	60,000 to 62,500 to 0

Vertical deflections were measured at each increment of load. The deflection readings were taken at four joints as shown in Fig. 76-62. The motion of tape measures suspended from each of the four joints was obtained with the aid of a leveled transit. The vertical deflections are shown in Figs. 76-63 through 76-66.

The test was concluded abruptly at the 62,500-lb load by a premature failure in the hydraulic cylinder. The failure occurred at a load significantly below the rated capacity of the cylinder. The stripped thread failure of the cylinder rod is shown in Fig. 76-67.

4. Conclusions

The maximum applied load was 62,500 lb and, as shown in Fig. 76-68, the corresponding wind velocity is about 162 mph at −10°F at sea level. The linearity of the load deflection curves indicates that the critical general buckling load had not been approached.

This test has also shown that the removal of a hub from the radome may seriously decrease the radome's structural capability.

P. Davis
R. A. Muldoon

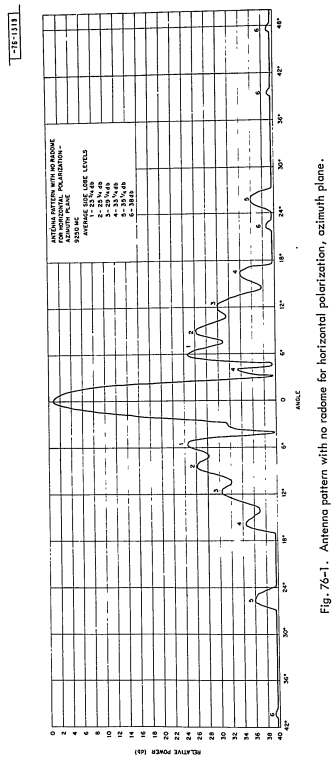

Fig. 76-1. Antenna pattern with no radome for horizontal polarization, azimuth plane.

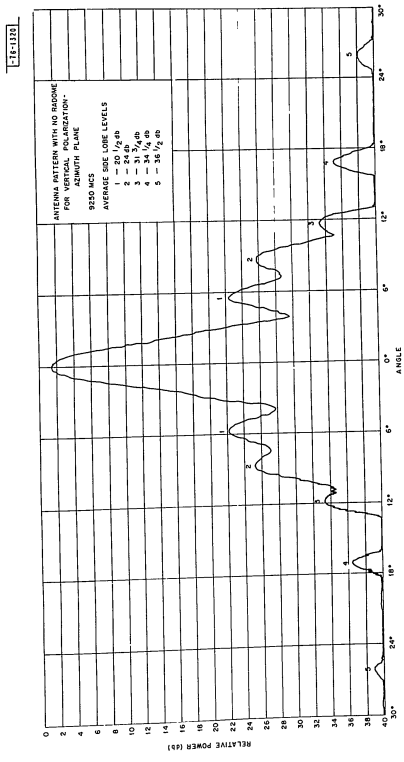

Fig. 76-2. Antenna pattern with no radome for vertical polarization, azimuth plane.

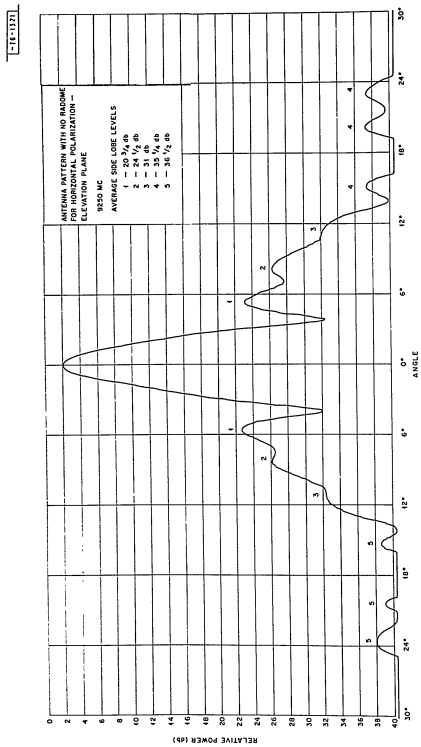

Fig. 76-3. Antenna pattern with no radome for horizontal polarization, elevation plane.

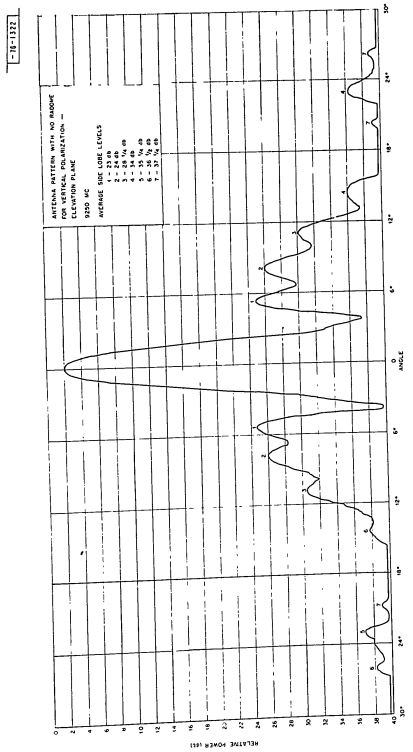

Fig. 76-4. Antenna pattern with no radome for vertical polarization, elevation plane.

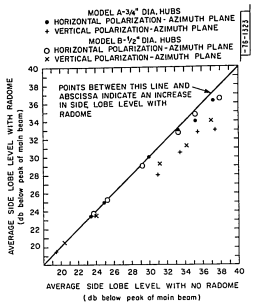

Fig. 76-5. Average change in side-lobe levels for the metal space-frame radome (Mod A, 3/4-inch-diameter hubs).

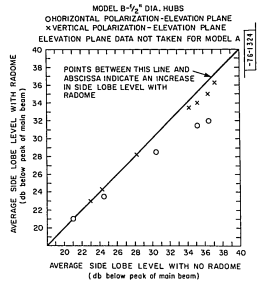

Fig. 76-6. Average change in side-lobe levels for the metal space-frame radome (Mod B, 1/2-inch-diameter hubs).

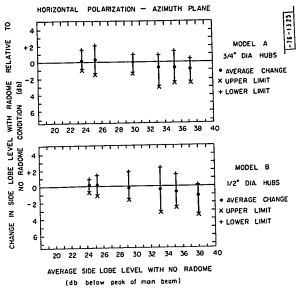

Fig. 76-7. Changes in side-lobe levels for the metal space-frame radomes with horizontal polarization, azimuth plane (Mods A and B).

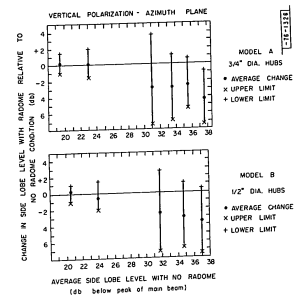

Fig. 76-8. Changes in side-lobe levels for the metal space-frame radomes with vertical polarization, azimuth plane (Mods A and B).

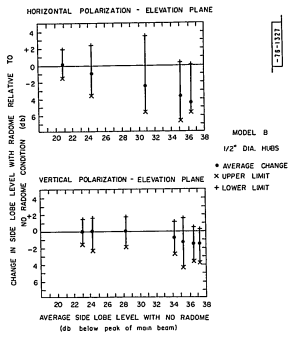

Fig. 76-9. Changes in side-lobe levels for the metal space-frame radomes with horizontal polarization, elevation plane (Mods A and B).

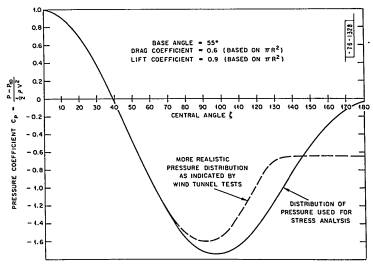

Fig. 76-10. Wind pressure distribution for CW-412 radome analysis.

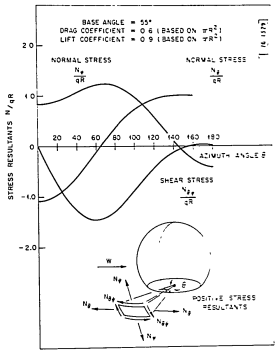

Fig. 76-11. Variation of nondimensional stress resultants with azimuth angle at base of CW-412 radome.

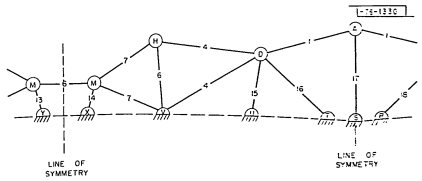

Fig. 76-12. Base geometry of CW-412 radome.

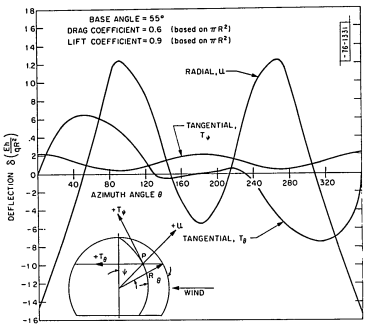

Fig. 76-13. Nondimensional deflection at the equator of radome shell as a function of azimuth angle.

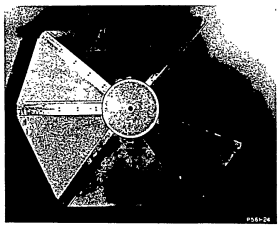

Fig. 76-14. Full scale hub mockup of the CW-412 radome.

Fig. 76-15. Full scale hub mockup (hub cap removed) of the CW-412 radome.

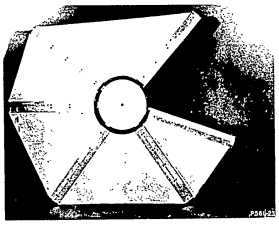

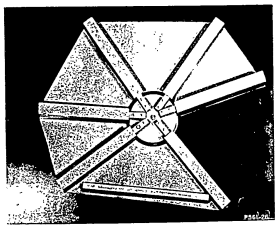

Fig. 76-16. Full scale hub mockup (inside) of CW-412 radome.

Fig. 76-17. Cross section showing beam, membrane and cap strips of the CW-412 radome.

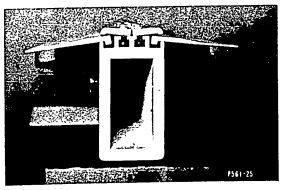

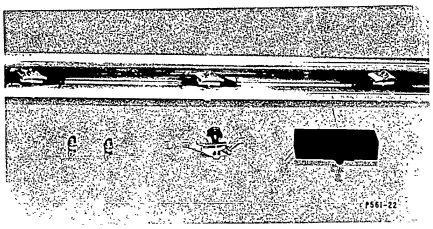

Fig. 76-18. Full scale cap strip of the CW-412 radome.

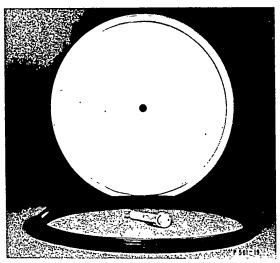

Fig. 76-19. Hub cap and rubber seal for the CW-412 radome.

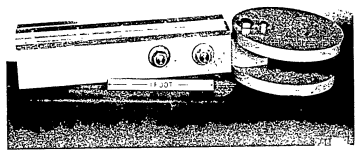

Fig. 76-20. Full scale mockup of beam, end fitting and hub of the CW-412 radome.

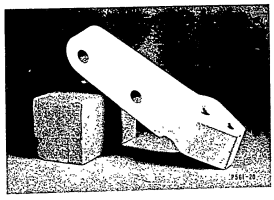

Fig. 76-21. Full scale mockup of end fitting on the CW-412 radome.

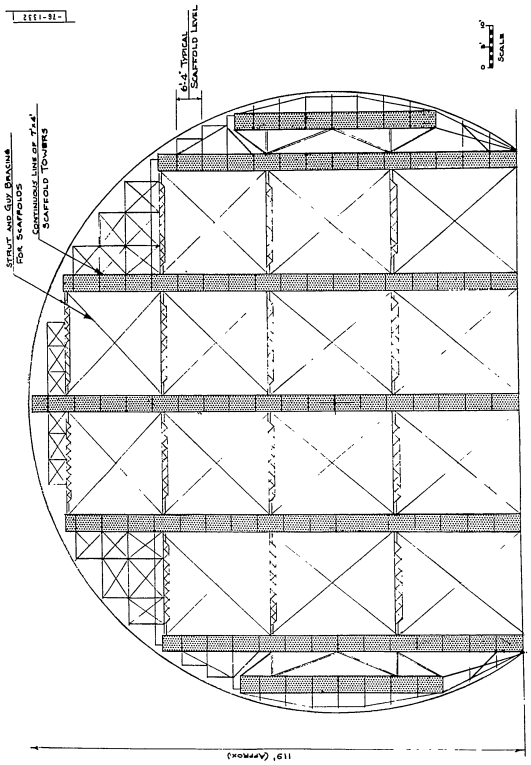

Fig. 76-22. A suggested scaffold arrangement.

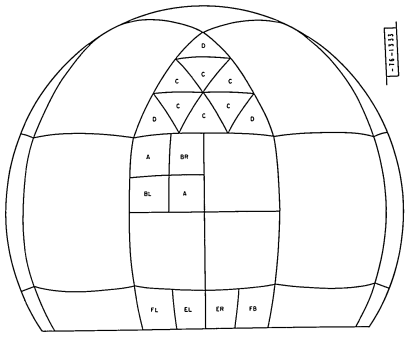

Fig. 76-23. Procedure for subdividing the modified small rhombicuboctahedron.

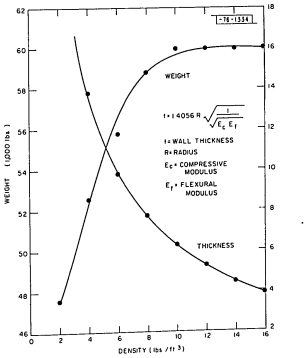

Fig. 76-24. Weight and thickness vs density for the 68-foot radome.

Fig. 76-25. Tensile test of flat-strap metallic anchor in 2-3/4 × 24 × 20-inch Hooker 126 polyurethane foam panel (panel G).

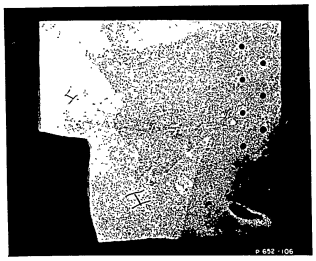

Fig. 76-26. Tensile test of flat-strap metallic anchor in 2-3/4 × 24 × 20-inch Hooker 126 polyurethane foam panel (panel H).

Fig. 76-27. Tensile test of flat-strap metallic anchor in 2-3/4 × 24 × 20-inch Hooker 126 polyurethane foam panel (panel I).

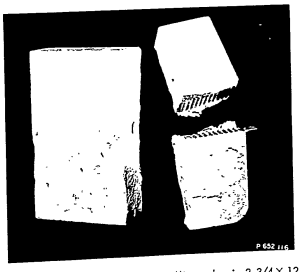

Fig. 76-28. Tensile test of ribbed-strap metallic anchor in 2-3/4 × 12 × 12-inch Selectrofoam polyurethane panel.

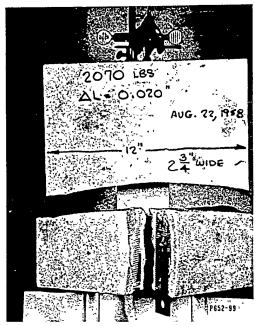

Fig. 76-29. Tensile test of serrated-strap metallic anchor in 2-3/4 X 12 X 12-inch Hooker 126 polyurethane foam panel.

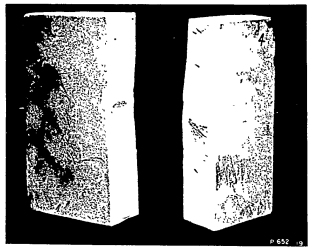

Fig. 76-30. Tensile test of tube-end-strap metallic anchor in 2-3/4 X 12 X 12-inch Selectrofoam polyurethane panel.

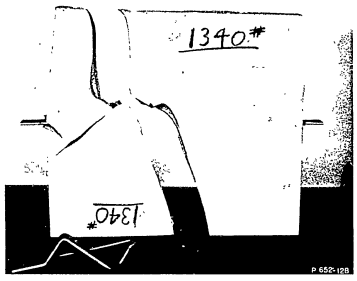

Fig. 76-31. Tensile test of bent-strap-with-rod metallic anchor in 2-3/4 X 12 X 12-inch Selectrofoam polyurethane panel.

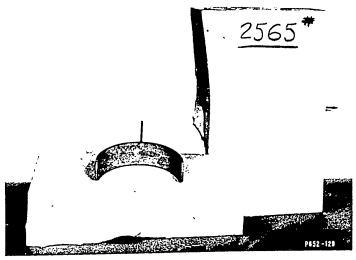

Fig. 76-32. Tensile test of flat-strap-with-bow metallic anchor in 2-3/4 X 12 X 12-inch Selectrofoam polyurethane panel.

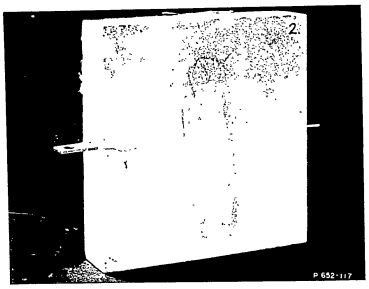

Fig. 76-33. Tensile test of perforated-strap metallic anchor in 2-3/4 X 12 X 12-inch Selectrofoam polyurethane panel.

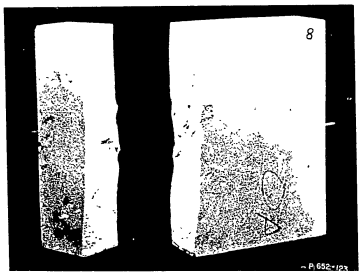

Fig. 76-34. Tensile test of flat-strap-with-column metallic anchor in 2-3/4 X 12 X 12-inch Selectrofoam polyurethane panel.

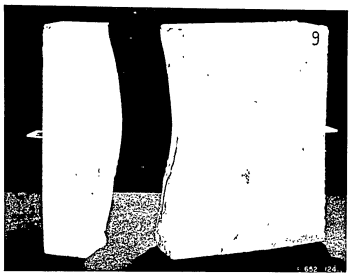

Fig. 76-35. Tensile test of flat-strap-with-3-columns metallic anchor in 2-3/4 X 12 X 12-inch Selectrofoam polyurethane panel.

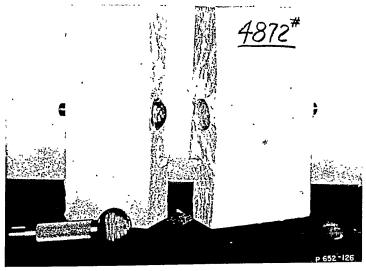

Fig. 76-36. Tensile test of 1-inch-diameter knurled-aluminum bolt with a 2-inch-diameter knurled-aluminum ball-end metallic anchor in 2-3/4 X 12 X 12-inch Selectrofoam polyurethane panel.

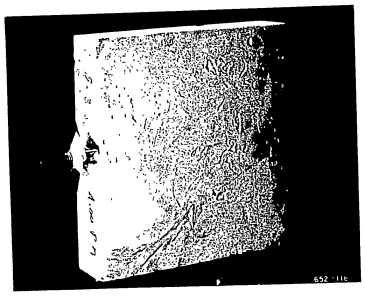

Fig. 76-37. Tensile test of 3/4-inch-diameter steel rod with a spherical-end metallic anchor in 2-3/4 × 12 × 12-inch Selectrofoam polyurethane panel.

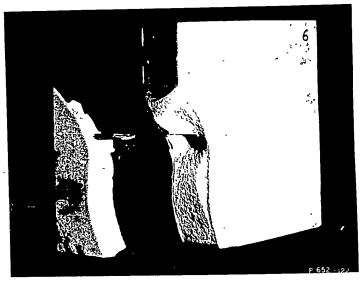

Fig. 76-38. Tensile test of metallic strap with 1-1/2-inch-diameter wooden ball-end anchor in 2-3/4 × 12 × 12-inch Selectrofoam polyurethane panel.

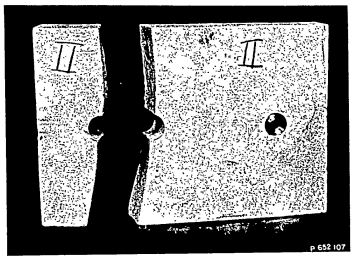

Fig. 76-39. Tensile test of 1-1/2-inch-diameter aluminum bushing in 2-3/4 × 12 × 12-inch Hooker 126 polyurethane foam panel.

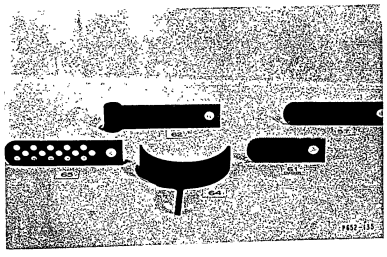

Fig. 76-40. Metallic anchors used as imbedments in polyurethane foam panels: 57, flat strap; 61 (mod), short serrated strap; 62, strap with tube end; 64, flat strap with bow; 65, perforated strap.

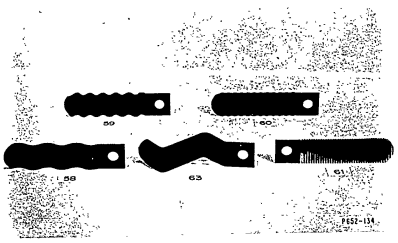

Fig. 76-41. Metallic anchors used as imbedments in polyurethane foam panels: 58, large corrugated strap; 59, small corrugated strap; 60, ribbed strap; 61, serrated strap; 63, bent strap with rod.

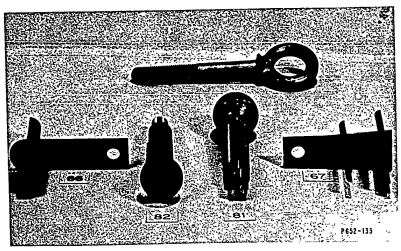

Fig. 76-42. Metallic anchors used as imbedments in polyurethane foam panels, 3/4-inch eyebolt: 66, flat strap with column; 67, flat strap with 3 columns; 81, 1-inch-diameter bolt with 2-inch-diameter ball end; 82, 1-inch-diameter bolt with 1-3/4-inch-diameter plastic ball end.

Fig. 76-43. Instron tester with fixtures for tensile test.

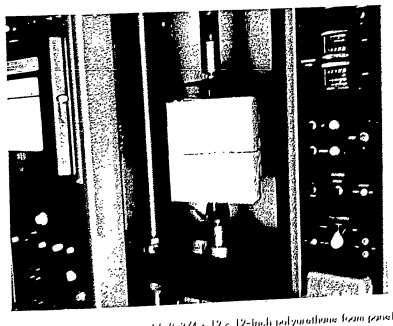

Fig. 76-44. Instron tester with 2-3/4 × 12 × 12-inch polyurethane foam panel after tensile test of metallic anchors.

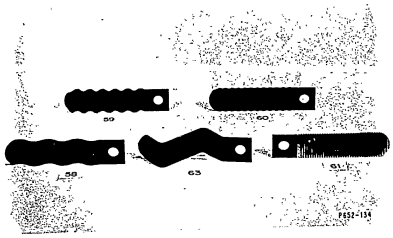

Fig. 76-41. Metallic anchors used as imbedments in polyurethane foam panels: 58, large corrugated strap; 59, small corrugated strap; 60, ribbed strap; 61, serrated strap; 63, bent strap with rod.

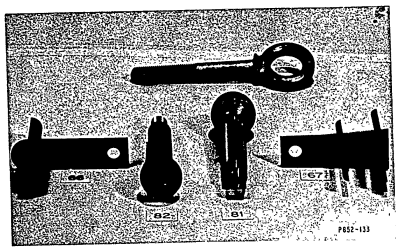

Fig. 76-42. Metallic anchors used as imbedments in polyurethane foam panels, 3/4-inch eyebolt: 66, flat strap with column; 67, flat strap with 3 columns; 81, 1-inch-diameter bolt with 2-inch-diameter ball end; 82, 1-inch-diameter bolt with 1-3/4-inch-diameter plastic ball end.

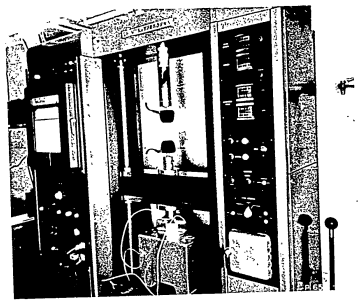

Fig. 76-43. Instron tester with fixtures for tensile test.

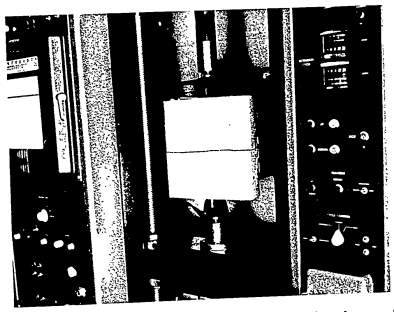

Fig. 76-44. Instron tester with 2-3/4 × 12 × 12-inch polyurethane foam panel after tensile test of metallic anchors.

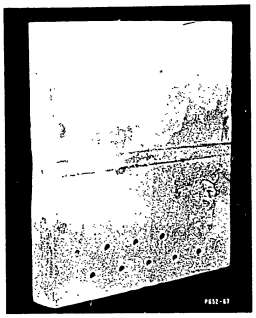

Fig. 76-45. Polyester polyurethane welded joint.

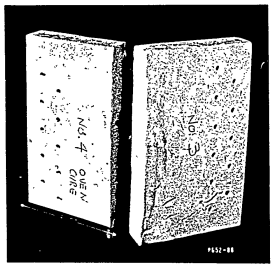

Fig. 76-46. Polyester polyurethane Hooker 126A weld test (Nos. 3 and 4).

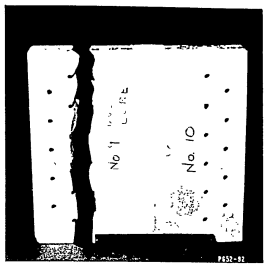

Fig. 76-47. Polyester polyurethane Hooker 126A weld test (Nos. 9 and 10).

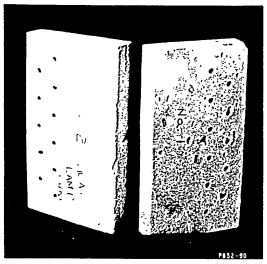

Fig. 76-48. Polyester polyurethane Hooker 126A weld test (Nos. 1 and 2).

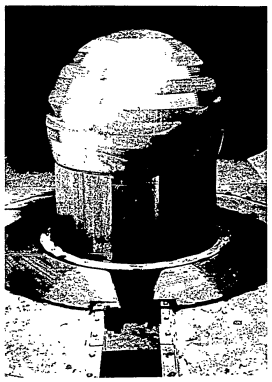

Fig. 76-49. Wind tunnel model of spherical, tower-mounted radome.

Fig. 76-50. Wind tunnel model of spherical, faceted, tower-mounted radome.

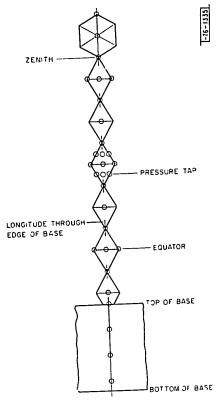

Fig. 76-51. Unwrapped view of location of pressure taps on faceted radome model, showing geometry of surface.

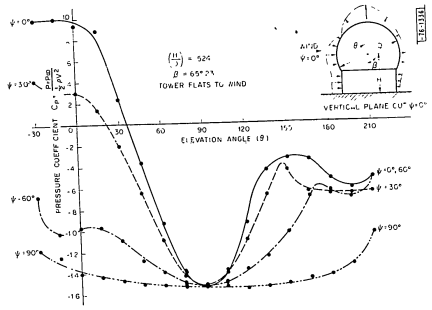

Fig. 76-52. Distribution of wind pressure along vertical plane cuts at various yaw angles through the zenith of the spherical, tower-mounted radome.

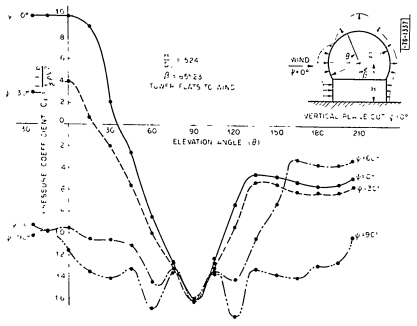

Fig. 76-53. Distribution of wind pressure along vertical plane cuts at various yaw angles through the zenith of the faceted, tower-mounted radome.

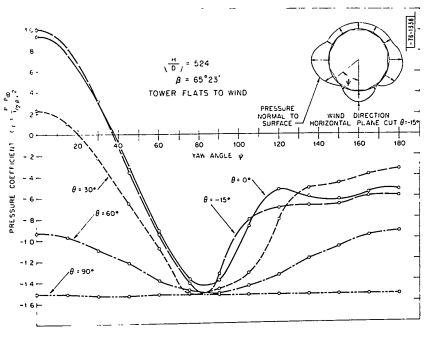

Fig. 76-54. Distribution of wind pressure along horizontal plane cuts at various elevation angles for the spherical, tower-mounted radome.

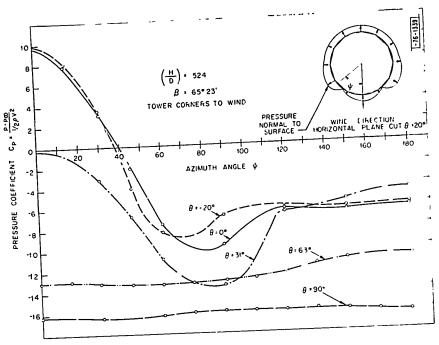

Fig. 76-55. Distribution of wind pressure along horizontal plane cuts at various elevation angles for the spherical, tower-mounted radome.

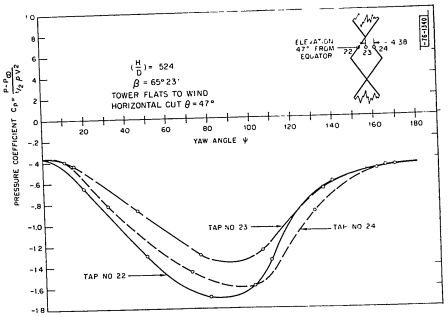

Fig. 76-56. Localized variation in pressure at the facet edges in the faceted, tower-mounted radome along horizontal plane cut at 47° elevation from equator.

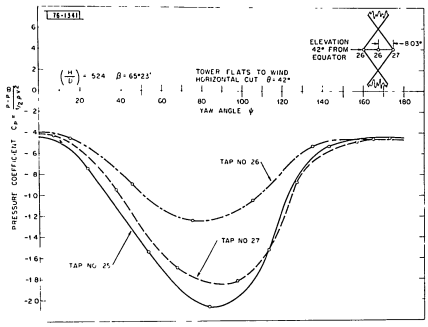

Fig. 76-57. Localized variation in pressure at the facet corners in the faceted, tower-mounted radome along horizontal plane cut at 42° elevation from equator.

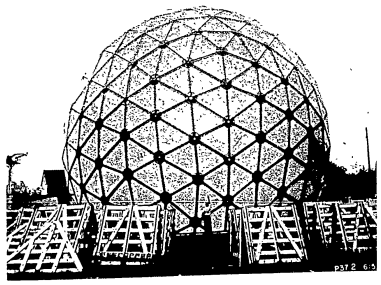

Fig. 76-58. The CW-408 radome.

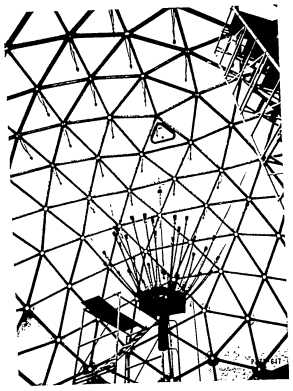

Fig. 76-59. Loading method in structural test of CW-408 radome.

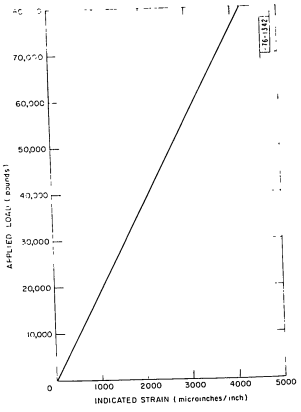

Fig. 76-60. Calibration curve for load cell used in structural load test of CW-408 radome.

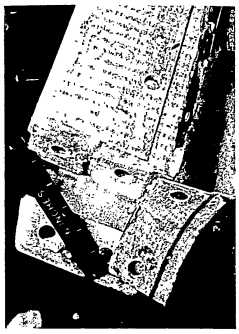

(b)

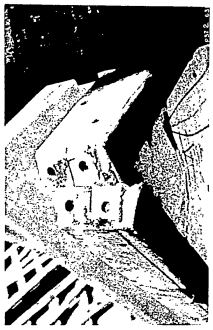

(d)

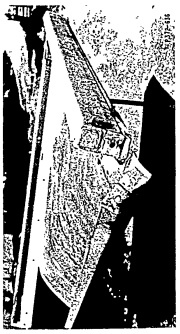

(a)

(c)

Fig. 76-61 (a – d). Panel damage in structural test of CW-408 radome.

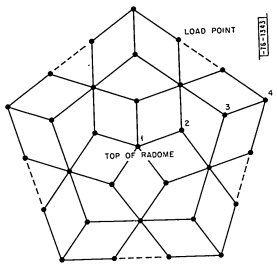

Fig. 76-62. Top section of CW-408 radome showing 31 load points and joints at which vertical deflections were measured.

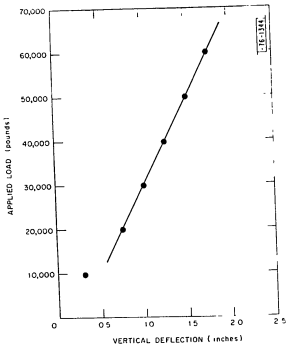

Fig. 76-63. Applied load vs vertical deflection of CW-408 radome, joint No. 1.

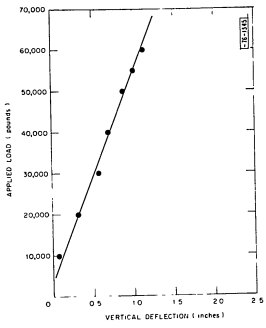

Fig. 76-64. Applied load vs vertical deflection of CW-408 radome, joint No. 2.

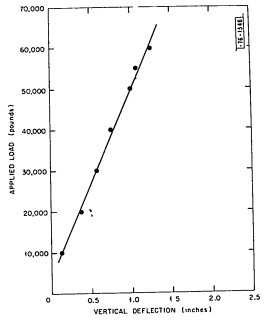

Fig. 76-65. Applied load vs vertical deflection of CW-408 radome, joint No. 3.

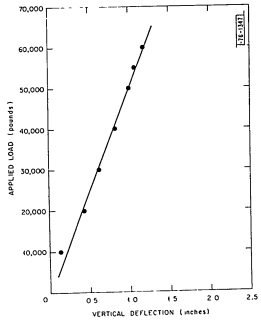

Fig. 76-66. Applied load vs vertical deflection of CW-408 radome, joint No. 4.

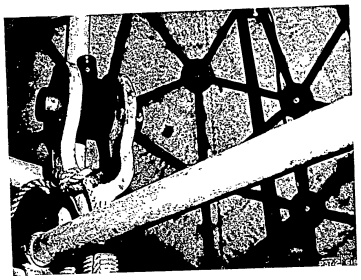

Fig. 76-67. Failed rod of hydraulic cylinder concluding structural test of CW-408 radome.

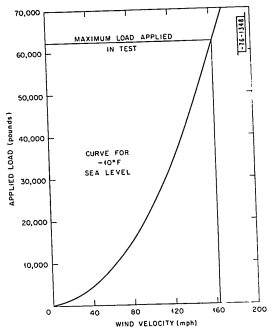

Fig. 76-68. Applied loading vs wind velocity for CW-408 radome.

III. ANTENNA WIND LOAD STUDY

The Wright Brothers wind tunnel at M.I.T. was available during the first two weeks of September for the first series of tests on the 1/24 scale model of the experimental Mk I antenna. Prior to delivery of the model to the wind tunnel, the balance was calibrated at the manufacturer's plant to insure that the strain gages on the load cells were functioning properly. Another calibration was required with the unit mounted in the wind tunnel to check the gains on the Miller recorder that was used for recording the test data.

After calibration, the unit was balanced by rotating the antenna assembly and adding weights where needed to minimize the fluctuations in the recording apparatus. The hub and spider, including the horn, had been statically balanced at the manufacturer's plant before mounting the antenna with its backup structure to the spider. Therefore, balancing the whole assembly was essentially equivalent to balancing the antenna with its backup structure. Figure 76-69 shows the unit as mounted in the wind tunnel. The hydraulic lines to the motor and the wiring from the strain gages do not appear in the photograph because they pass through the tunnel floor directly beneath the mounting location.

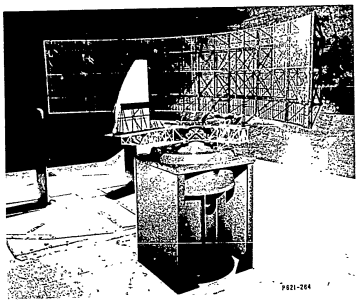

Fig. 76-69. Wind tunnel model of Mk I antenna.

The drive system has provisions for locking the antenna system every 30° in azimuth for taking static data at different wind speeds. Since this method would give no indication as to what is happening between the 30° increments, the test program specified that the model be rotated at a low rotational speed, on the order of 3 rpm, and record data continuously to get a better profile of static loads at all azimuth positions. Dynamic data was to have been obtained at several wind speeds and at various rotational speeds of the model up to 240 rpm.

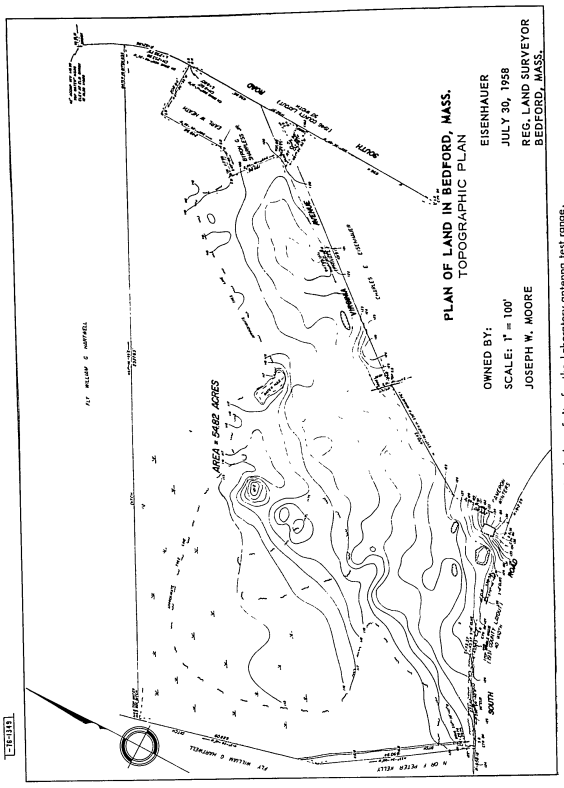

Fig. 76-70. Land plan of site for the Laboratory antenna test range.

The hydraulic power supply system was found to be inadequate for rotating the model at the high and low extremes of rotational speeds. Another power supply which had more capacity than the original equipment, was obtained from the Servomechanisms Laboratory at M.I.T. Unfortunately, in checking out this new unit after it was installed, the antenna system was brought up to a speed of 450 rpm in a relatively short time and was severely damaged, making it necessary to stop the program pending the replacement or repair of the damaged parts. It is expected that this may be accomplished during the next quarter. Meanwhile, a new hydraulic power supply is being procured which will provide the power and control needed for the scope of the testing program.

J. F. Orabona

IV. LINCOLN LABORATORY ANTENNA TEST RANGE

During the quarterly period the necessary Laboratory approvals and funding for the antenna test range were obtained. The specification setting forth its requirements, i.e., site preparations, buildings, equipment and instrumentations, will be sent to outside contractors for bids during the next reporting period.

Property line and topographic surveys have been completed for the test site and are shown in Fig. 76-70. The area involved is about 55 acres in Bedford, Massachusetts, of which about half is wooded. The transmission paths will be located adjacent to Virginia Avenue along the cleared area. The lease for this property has been signed and a study is under way to determine the extent of drainage that will be required to maintain the level of the transmission paths.

A. Cohen
A. W. Maltese

V. MATERIALS TESTING LABORATORY

A. Foam Materials Study

Weather exposure tests are continuing in the Atlas weatherometer. The data from these tests are summarized in Table 76-IV. No significant changes from the results as stated in the previous quarterly progress report were observed. The specimens, which have had a 1000-hour exposure, are undergoing mechanical tests to determine the exposure time vs mechanical strength characteristics.

The dielectric properties of dielectric constant and tan-delta through a temperature range from 77° to 350°F and a frequency range of UHF to K-band are being determined by the Laboratory of Insulation Research. These data are necessary in the application of foam radome designs for high-power systems such as BMEWS The results of this dielectric data investigation at elevated temperature will determine the applicability of present and future polyester foam formulations to high-powered antenna radomes.

S. C. Nilo

B. Printed Wiring

1. Memory Plane

Effort is continuing to develop a suitable printed-wiring technique for making ferrite-core memory planes. It was for this application that the collimated-light printed-wiring technique which has proven successful was developed.

TABLE 76-IV
ACCELERATED WEATHERING BY ATLAS WEATHEROMETER TYPE DMC-H
(102 minutes of light, 18 minutes of light and water)
(black panel temperature 145° to 150°F)

Sample	Description	Density (pcf)	Exposure Time (hours)	Coloration		Remarks
				Original	Final	
1000	Hooker 126A	10.7	1013.4	Pale yellow	Dark brown	
1001	Hooker 126A	26.1	1013.4	Pale yellow	Dark brown	
1002	Hooker 126A	33.8	1013.4	Pale yellow	Dark brown	
1004	Hooker 126A coated: (2 Primer, 3 Radalon)	27.8	1013.4	White	Yellow	
1005	Hooker 126A coated: (2 Primer, 3 Radalon)	34.1	1013.4	White	Yellow	
1014	Styrofoam QI03.21 Hd	4.24	1013.4	White	Dark yellow	Surface erosion
1016	6002 & 6003 sprayed Selectrofoam	8.28	1013.4	White	Mottled brown	Small holes in surface
1017	6002 & 6003 sprayed Selectrofoam	8.24	1013.4	White	Mottled brown	Small holes in surface
1018	6002 & 6003 sprayed Selectrofoam	9.84	1013.4	White	Mottled brown	Small holes in surface
1019	Hooker 126A	12.4	971.4	Pale yellow	Brown	
1020	Hooker 126A	12.4	971.4	Pale yellow	Brown	
1022	Expandable Polystyrene	1.24	874.4	White	Yellow	Surface disintegration
1025	Gliddfoam FR	13.2	854.4	Light	Brown	10 per cent shrinkage

The imbedment of the ferrite cores by phenolic transfer mold was successful only when physical properties of the imbedment material were being considered. However, with more rigorous individual core testing of the prototype 4 × 4 core, significant degradation of response was noted. This has been attributed to nonuniform stress conditions. The phenolic molding powder has about a 3 per cent shrinkage. With the internal diameter of the core clear of resin, this shrinkage around the core is restrained only by the core itself. If the core were to be totally encapsulated, the degradation due to stress would not be so severe.

Experiments are being conducted in which 4 × 4 prototype memory planes are being molded from Thiokol-epoxy resin formulations. A 100 per cent Thiokol formulation was too flexible, although it did not cause any core degradation due to stress. The epoxy content will be increased to determine whether or not a suitable material for imbedment can be produced.

E. B. Murphy

C. Resistance Measurements

A number of electrical resistance measuring tests were performed during the summer months on printed-wiring products and processes. When normal precautionary techniques in etchant immersion, rinsing and defluxing operations were used, resistance values on laminates remained at a reasonable resistance (50,000 megohms) level. Unless the test board showed significant physical degradation, little electrical deterioration resulted from the miscellaneous chemical treatments to which the test specimens were subjected.

The most realistic test seems to be with an ASTM (American Society of Testing Materials) guarded-ring (bull's-eye) pattern. A guarded electrode permits resistance measurements to be made on volume surface resistance and surface resistivity. This latter value includes a volume component. The usual accelerated humidity test requires exposure for 96 hours at 35°C ± 1°C, and 90 per cent rh ± 2 per cent rh.

Two modifications have been suggested by industry which, from a limited number of our tests, appear reasonable. One is to modify the test pattern so that the spacing between the inner and outer electrode would be 1/16 inch rather than 1/8 inch. This would increase the sensitivity of the test. The second modification is to shorten the test period to 24 hours at 50°C ± 1°C and 90 per cent rh ± 2 per cent rh. In fact these modifications caused resistance values to drop to less than one-tenth (70,000 megohms) their original value in the 24-hour period. This indicated that more serious degradation of the boards took place in this period under these conditions than took place in the longer period with milder exposure. The 24-hour test gives the same results as a test of approximately one month's duration under the milder conditions.

E. B. Murphy

D. Plated Connections

We have found that to make a good electrical and mechanical contact between a deposited printed-wiring conductor and an imbedded lead, a thin copper oxide coating is beneficial.

Several attempts to measure the adhesive force of the bond formed by chemically depositing copper on a reduced copper oxide surface have failed, due to tearing of the copper plate when

attempting to peel this plate from the base metal. A suitable test procedure which did not contain any influencing variable was a modified Jacquet method as described by Linford and Wenkateswarlu.* This test was used to evaluate the effect of copper oxide on the bond strength of a nickel electroplate overlay. It consists of plating a copper tab 5 mm wide to a thickness of 80 mils and then peeling.

A majority of our test specimens still broke before peeling; however, one specimen did peel before breaking and was calculated at 592 lb/inch width. These tests were performed on a Tinius Olsen automatic recording tensile tester. Additional tests and comparisons are to be made.

In order to determine the optimum procedure for maximum bond strength, it was desirable to know the thickness of the copper oxide coating. A photomicrograph experiment in which silver paint was used to separate the copper oxide showed nothing that could be measured. Better results were obtained by weighing before and after the oxide formation. The oxide was dissolved in concentrated ammonium chloride and the copper specimen reweighed. Our results indicated that maximum deposit took place in 3 minutes and a thickness of 1.8×10^{-4} cm (70 millionth of an inch) was calculated.

E. Foam Encapsulant with Plated Connection and Printed Wiring

Unless serious consideration is given to expansion coefficients involved in an encapsulated module, using plated connections, failure can occur prematurely as the heat is increased either from operation or environment.

	Expansion Coefficient per °F	
Cu	9×10^{-6}	in/in or cm/cm
Epoxy	60×10^{-6}	
Epoxy resin + 50 per cent filler	$25 \text{ to } 30 \times 10^{-6}$	
Ceramic-fired lava	5×10^{-6}	
XXX P Phenolic laminate	$100 \text{ to } 200 \times 10^{-6}$	
Foams	20×10^{-6}	

A number of foam samples were formulated with a density range from 15 to 40 pcf. Samples of less than 20 pcf operated above 350°F without opening a plated connection.

A module is to be made using ceramics and foams for conventional components. It is hoped that eventually the experience gained with ceramic can be used for the miniaturized component development.

F. Electroforming

Since last March, as a side line activity, a variety of mandrels have been electroformed. Sufficient interest has been generated and the process has proved useful so that a more suitable arrangement is to be made. The machine shop is planning to install an electroforming facility;

* H.B. Linford and A. Wenkateswarlu, Plating 45, 728 (1958).

however, the Materials Testing Laboratory will continue some experiments in order to insure an optimum procedure. The force necessary to separate a stainless steel mandrel and a brass mandrel has been measured. The stainless steel mandrel requires a maximum force of approximately 60 psi of mandrel contact area for separation. This mandrel has been passivated and has received a film of graphite (not visible to the naked eye). If the area is large, and therefore a large force, advantage may be taken of the large difference in heat conductivity between copper and stainless steel. Their expansion coefficients unfortunately are similar but copper can be heated 100 times faster and separation facilitated. With regard to a brass mandrel, no assistance can be expected from either the expansion or conductivity properties. A silver iodide coating on brass, with no graphite treatment, required a force of 750 psi of mandrel contact area to start separation. If graphite is applied, the value is reduced in half to a force of 300 psi of mandrel contact area.

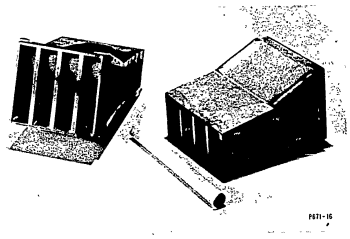

Fig. 76-71. Electroformed waveguide with inserts.

A recent waveguide product to be used in a maser application is shown with inserts electroformed in place (Fig. 76-71). No soldering was required and close tolerance as to their position was readily met.

E. B. Murphy